

2014

New Insights into Fibrous Body Protein Complexes involved in *C elegans* Spermatogenesis

Christopher M. Uyehara
College of William & Mary - Arts & Sciences

Follow this and additional works at: <https://scholarworks.wm.edu/etd>



Part of the [Physiology Commons](#)

Recommended Citation

Uyehara, Christopher M., "New Insights into Fibrous Body Protein Complexes involved in *C elegans* Spermatogenesis" (2014). *Dissertations, Theses, and Masters Projects*. Paper 1539626951.
<https://dx.doi.org/doi:10.21220/s2-cqef-xy58>

This Thesis is brought to you for free and open access by the Theses, Dissertations, & Master Projects at W&M ScholarWorks. It has been accepted for inclusion in Dissertations, Theses, and Masters Projects by an authorized administrator of W&M ScholarWorks. For more information, please contact scholarworks@wm.edu.

New Insights into Fibrous Body Protein Complexes Involved in *C. elegans*
Spermatogenesis

Christopher M. Uyehara

Fairfax, VA

Biology B.S., University of Virginia, 2012

A Thesis presented to the Graduate Faculty
of the College of William and Mary in Candidacy for the Degree of
Master of Science

Department of Biology

The College of William and Mary
August, 2014

APPROVAL PAGE


This Thesis is submitted in partial fulfillment of
the requirements for the degree of

Master of Science

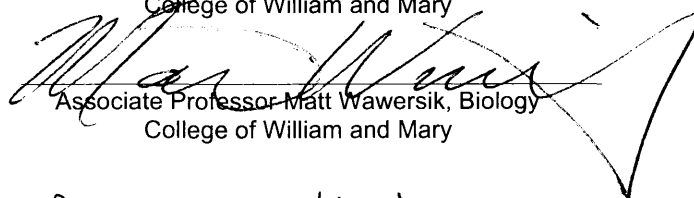


Christopher M Uyehara

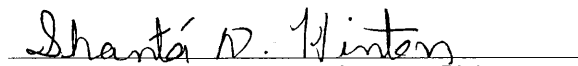
Approved by the Committee, August, 2014



Committee Chair
Professor Diane Shakes, Biology
College of William and Mary



Associate Professor Matt Wawersik, Biology
College of William and Mary



Assistant Professor Shantá Hinton, Biology
College of William and Mary

ABSTRACT

In all multicellular organisms, cells become specialized to perform a variety of functions. In many cases, these functions require specialization of the cytoskeleton to affect the morphology and organization of the cell. To do this, cells use a variety of mechanisms to allow cytoskeletal proteins to form different structures. Developing sperm cells in the nematode *Caenorhabditis elegans* provide an interesting system for these studies because they contain an additional, sperm-specific cytoskeletal protein, the Major Sperm Protein (MSP). During spermatogenesis, MSP exists in three separate forms: a cytosolic form, a highly stable paracrystalline form when in Fibrous Bodies (FBs), and a highly dynamic form when in spermatozoa where its polymerization dynamics drive the extension and retraction of a pseudopod. Although the mechanisms that control MSP dynamics in the pseudopod have been partially characterized, the mechanisms that control FB dynamics are less well understood. Here, we present evidence that the MSP accessory protein MFP2, which was first characterized in the pseudopod of a *C. elegans* relative, *Ascaris suum*, is also present in the FB where completely colocalizes with MSP; this suggests it may play a role in FB development. In addition, we found that the signal intensity of MFP2 drops during spermatid maturation. We quantified this effect to show that this process is perturbed in *gsp-3/4* and *fer-6* mutants. In the former case, the MFP2 signal does not drop as low as in WT, while in the latter case it drops precociously, suggesting that FB breakdown is more complex than previously realized. To investigate MFP2's biochemical properties performed western blots on MFP2 in samples without spermatozoa. Our work suggests that MFP2 may be phosphorylated before its localization to the pseudopod. To gain further insights in FB regulation, we also characterized the phenotypes of four different alleles of the *spe-26* gene, which encodes for a kelch-like protein. Previous work on *spe-26* mutants identified a variety of cell cycle defects, including defects in cytokinesis and chromatin segregation. Our work expanded on these results, and showed that these mutants also contain defects in FB formation and development; FBs in *spe-26* mutants have an expanded length compared to WT, and contain abnormalities in the localization of the FB accessory protein, SPE-7. In addition, we showed that these defects do not correlate directly with the severity of each allele, suggesting that the different alleles of *spe-26* may be affecting different processes in different ways. Overall, this thesis has broadened our understanding of MSP dynamics, which may, in turn provide a model for studying broader mechanisms of cytoskeletal control.

TABLE OF CONTENTS

Acknowledgements	ii
Dedications	iii
List of Tables	iv
List of Figures	v
General Introduction	1
Specific Aims	19
Methods	20
Chapter 1. The MSP Accessory Protein MFP2	28
Chapter 2. FB Defects in Different Alleles of <i>spe-26</i>	70
Bibliography	98

ACKNOWLEDGEMENTS

This writer wishes to express his or her appreciation to Professor Diane Shakes, under whose guidance this investigation was conducted, for his patience, guidance and criticism throughout the investigation. The author is also indebted to Professors Matt Wawersik and Shanta Hinton for their careful reading and criticism of the manuscript.

This Master's Thesis is dedicated to the many thousands of *C. elegans* worms who gave their lives in the service of this thesis.

*"Never in the field of human conflict was so much owed by so many to so few."
-Winston Churchill*

LIST OF TABLES

- | | |
|--|----|
| 1. <i>C. elegans</i> Paralogs to ZK265.2 | 55 |
| 2. Predicted Phospho-Sites on MFP2 | 67 |

LIST OF FIGURES

Introduction:

1. MSP Localization Over the Course of Meiosis 5
2. FB-MO Complexes Contain MSP in a Paracrystalline Form 7
3. SPE-7 Localization Throughout Spermatogenesis 12
4. Factors that Direct MSP Polymerization in *A. suum* 15
5. MFP2's Crystal Structure and Model for Binding MSP 17

Chapter 1:

1. Alignment of the MFP2 Amino Acid Sequence Between Different Species 55
2. A Comparison of the Predicted Structure of MFP2 in *C. elegans* compared to the Crystal Structure of MFP2 in *A. suum* 56
3. Western blot of *fem-3(gf)* and *fem-3(lf)* 57
4. Anti-MFP2 Labeling in WT Sperm Spreads and Negative Controls 58
5. MFP2 Staining in WT 59
6. A Comparison of MFp2 and MSP Localization in WT 60
7. A Comparison of MFP2 and MSP Localization in *C. remanei* 61
8. Deconvolution of MFp2 Aggregates in *C. remanei* 62
9. MFP2 and MSP Localization in *gsp-3/4* Mutants 63
10. MFP2 and MSP Localization in *fer-6(hc6)* Mutants 64
11. Changes in Signal Intensity of MSP and MFP2 Between Mature and Immature Spermatids 65

12. Comparison of MFP2 to MSP Ratios in WT, <i>gsp-3/4</i> and <i>fer-6</i> Mutants	66
13. A Visualization of Predicted Phospho-Sites in Relation to Antibody Binding Site	67
14. Western Blots of MFP2	69
<i>Chapter 2:</i>	
1. WT SPE-7 and MSP Pattern	90
2. SPE-7 and MSP Pattern in <i>spe-26(hc140)</i>	91
3. Comparison of Maximally Sized FBs in Different <i>spe-26</i> Alleles	92
4. A Comparison of Average FB Length Between WT and <i>spe-26</i> Alleles	93
5. Visualization of Novel SPE-7 Patterns in <i>spe-26</i> Mutants	94
6. Terminal Phenotype in <i>spe-26</i> Mutants	95
7. Spermatogenesis in <i>spe-26(it112)</i>	96
8. Spermatogenesis in <i>spe-26(eb8)</i>	97

Introduction: Spermatogenesis in *C. elegans*

Spermatogenesis Overview:

The ability to pass on genes to the next generation is the driving force of evolution. In males, this requires the production of spermatozoa during a process called spermatogenesis. Spermatogenesis is a highly coordinated, multi-step process in which a diploid spermatocyte develops into four, haploid spermatozoa (Chu & Shakes, 2013; L'Hernault, 2006). This process begins with meiosis, in which cells produce a variety of specialized proteins and then divided into haploid spermatids (Kimmins, Kotaja, Davidson, & Sassone-Corsi, 2004). After meiosis, the second stage of spermatogenesis, spermiogenesis, begins. Spermiogenesis involves two broad processes: 1) immotile spermatids undergo cellular morphogenesis into to spermatozoa, and 2) spermatids discard unnecessary proteins and organelles into a residual body structure (Kimmins et al., 2004). In many cases, spermiogenesis is followed by sperm activation in which immotile cells become motile and begin migrating towards the unfertilized oocyte (Chu & Shakes, 2013).

C. elegans as a model for spermatogenesis:

The nematode *Caenorhabditis elegans* is a widely used developmental model; it is an easily manipulable organism with a short generation time, making it ideal for the study of fundamental cellular processes such as spermatogenesis, which occur in both mammals and *C. elegans*. One of the significant advantages of using *C. elegans* as a model for spermatogenesis is that as cells develop from spermatocytes to spermatids, they move proximally along the gonad (Chu & Shakes, 2013). Consequently, when

dissecting male gonads, it is possible to view all of the different cellular stages of spermatogenesis within a single worm (Chu & Shakes, 2013). This allows visualization of changes in protein localization over the course of spermatogenesis without the need for live imaging. In addition, it simplifies mutational analysis, because disruptions in the sequential process of spermatogenesis can be easily studied within a single worm (Kulkarni, Shakes, Guevel, & Smith, 2012).

Although *C. elegans* is used as a model for mammalian spermatogenesis, the two processes differ in several important ways. To begin with, after the completion of the meiotic divisions, mammalian spermatids undergo a final burst of transcription and translation to produce proteins required for cellular morphogenesis (Kimmins et al., 2004). Following this transcriptional event, mammalian sperm cells progressively replace normal histone proteins with highly charged Sperm Nuclear Basic Proteins (SNBPs) that hypercondense chromatin into a transcriptionally inactive form (Sassone-Corsi, 2002). Although these processes occur in *C. elegans*, the order and timing is different. Instead of a final burst of transcription and translation, most transcription is thought to be completed by late prophase of meiosis I (Kulkarni et al., 2012; Shakes et al., 2009a). In addition, translation is completed by the end of the meiotic divisions because ribosomes are discarded into a residual body immediately following Anaphase II (Kulkarni et al., 2012; Shakes et al., 2009a). Furthermore, in mammals cellular morphogenesis is distinct from sperm activation; flagellated cells are created and then remain immotile until a signal from the oocyte induces directed cell migration (Chu & Shakes, 2013). In *C. elegans* hermaphrodites, however, sperm activation does not begin until the spermatids pass from

the ovotestis into the spermatheca (Stanfield & Villeneuve, 2006). At that time, spermatids undergo cellular morphogenesis into spermatozoa (Shakes & Ward, 1989).

In addition to differences in timing, the end product of spermatogenesis, the spermatozoa, differs between *C. elegans* and mammals. In mammals, spermatids differentiate into spermatozoa whose motility is governed by lateral movements of a tubulin-based flagellum that propels the cell forward (Kimmins et al., 2004). In contrast, the motility of *C. elegans* spermatozoa is governed by the extension and retraction of a pseudopod (Sepsenwol, Ris, & Roberts, 1989a). Furthermore, the pseudopod dynamics in *C. elegans* spermatozoa are not dependent on actin dynamics, as might be expected, but, instead, rely on a nematode-specific protein called the Major Sperm Protein (MSP) that acts analogously to actin. (Sepsenwol et al., 1989a).

However, although *C. elegans* spermatogenesis differs from that of mammals in several ways, it nevertheless undergoes the same fundamental processes as mammals. In both *C. elegans* and mammalian spermatogenesis, spermatocytes must enter meiosis, divide to produce haploid spermatids, undergo cellular morphogenesis, discard unnecessary proteins, and then successfully fertilize an oocyte. Consequently, *C. elegans* is an attractive model for studying spermatogenesis as a fundamental biological process.

Spermatogenesis in C. elegans:

In *C. elegans*, the male gonad can be temporally divided into distinct sections that roughly correspond to a temporal progression of cells from mitotically dividing spermatocytes into mature spermatids (Chu & Shakes, 2013). *C. elegans* spermatogenesis begins at the distal tip of the gonad arm where two somatically-derived

distal tip cells (DTC) are located (Kimble & Crittenden, 2005). The DTC extends membranous processes that come into contact with spermatocytes and maintain mitotic proliferation; when cells lose contact with the DTC, they exit meiosis and enter a period of extended prophase (Kimble & Crittenden, 2005).

Prophase in *C. elegans* spermatocytes is particularly important because it is the last stage in which spermatocytes are transcriptionally active to a significant degree (Shakes et al., 2009a). The mechanisms of transcriptional down-regulation in *C. elegans* spermatocytes are still being elucidated; however, there is evidence that they are similar to those used in mammals (Chu et al., 2006). In mammals, transcriptional down-regulation occurs following the meiotic divisions involves the progressive replacement of normal histone proteins with SNBPs, a class of proteins that includes histone variants, protamines, and protamine-like proteins (Govin, Caron, Lestrat, Rousseaux, & Khochbin, 2004).

Although homologs to vertebrate protamines have yet to be identified in *C. elegans*, several proteins that resemble invertebrate protamines have been identified (Chu et al., 2006). These proteins begin associating with sperm chromatin as early as the Pachytene stage of meiosis I. In addition, following diplotene of meiosis I (the disassembly of the synaptonemal complex), *C. elegans* spermatocytes enter an extended phase called Karyosome stage. During the karyosome stage, most, if not all, transcription ceases, and the chromosomes compact into a single mass within the nuclear envelope (Shakes et al., 2009a). At the end of the karyosome stage, *C. elegans* spermatocytes detach from the rachis, a shared syncytium that connects germline cells and developing

gametes. Following budding from the rachis, spermatocytes transition through diakinesis, to Metaphase I (Chu & Shakes, 2013).

At this point, spermatocytes divide meiotically to produce four haploid spermatids (fig. 1). Following the meiotic divisions, spermatids jettison any unnecessary proteins, including the ribosomes, ER, Golgi apparatus, tubulin and actin, into a residual body structure.

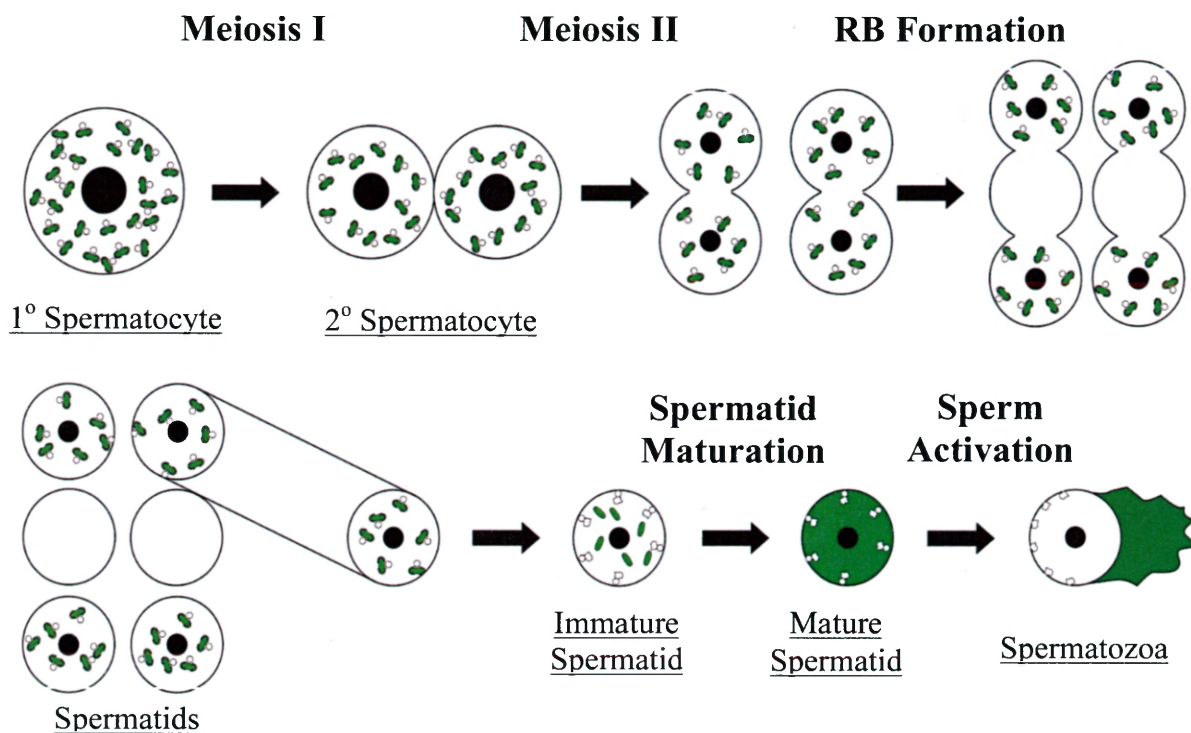


Figure 1: MSP localization over the course of meiosis

FB-MOs are fully formed by the end of meiosis in primary spermatocytes. Over the course of meiosis, FB-MOs are stably transmitted into secondary spermatocytes and then spermatids. During residual body formation, FB-MOs avoid segregation to the developing residual body. In immature spermatids, MOs dissociate from FBs and dock at the edge of the plasma membrane. During spermatid maturation, FBs break down and MSP becomes cytosolic. During sperm activation, MSP polarizes to the developing pseudopod. (Figure adapted from: (Nishimura & L'Hernault, 2010b).

Following their separation from the residual body, spermatids undergo a spermatid maturation phase that produces quiescent spermatids (Messina, 2012). In males, mature spermatids remain inactive until after they are ejected from the males

during mating where they are transferred through the hermaphrodite vulva into the uterus. Once inside, sperm activation occurs, which involves a complex series of events that ultimately leads to the polarization of MSP to the developing pseudopod (Shakes & Ward, 1989). Once the pseudopod has formed, spermatozoa undergo directed cellular migration toward spermatheca where they fertilize oocytes.

Major Sperm Protein (MSP)

The key cytoskeletal protein present in nematode spermatozoa is MSP, which drives the extension and retraction of the pseudopod. Although MSP acts analogously to actin, it shares no homology to actin, or any other mammalian cytoskeletal protein. Instead, MSP is part of the immunoglobulin superfamily and folds into a 14 kDa beta-sandwich structure (Haaf et al., 1996). In solution, MSP monomers naturally associate with one another to form dimers that lack polarity, in a manner similar to the way that intermediate filaments form tetramers that are also non-polar (Haaf et al., 1996). In another similarity to intermediate filaments, MSP does not bind nucleotides. Because of these features, MSP dimers lack both intrinsic polarity and associated motor proteins. One consequence of MSP apolarity is that purified MSP self-assembles *in vitro* into subfilaments that grow bidirectionally at equal rates (del Castillo-Olivares & Smith, 2008).

MSP is highly abundant in spermatids; it comprises ~15% of total protein in mature spermatids and ~40% of soluble protein (Scott, 1996). However, because transcription arrests at the end of prophase, MSP production begins during prophase and it is then present throughout both meiotic divisions, residual body formation and

spermatid maturation. However, although MSP is present, it is not in the same form during each of these processes. Instead, over the course of spermatogenesis, MSP exists in a cytosolic form, a paracrystalline form, and a form that undergoes active polymerization and depolymerization.

At the beginning of spermatogenesis, MSP is translated and exists in its cytosolic form. Translation of MSP occurs over the course of Pachytene, and both immunofluorescence and TEM studies suggest that it is initially unpolymerized (Roberts, Pavalko, & Ward, 1986b). However, this is a transient stage. In response to uncharacterized cues, MSP begins to associate with Membranous Organelles (MOs) (Roberts et al., 1986b). MOs are golgi-derived structures with a broadly defined structure; they contain a head region, an electron dense collar, and a body (fig. 2). When MSP initially associates with MOs, it binds to the body region in an unpolymerized and unstructured form. However, as more MSP binds to the MO body, it begins to polymerize into 4-5 nm spaced subfilaments that densely pack into a paracrystalline inclusion body

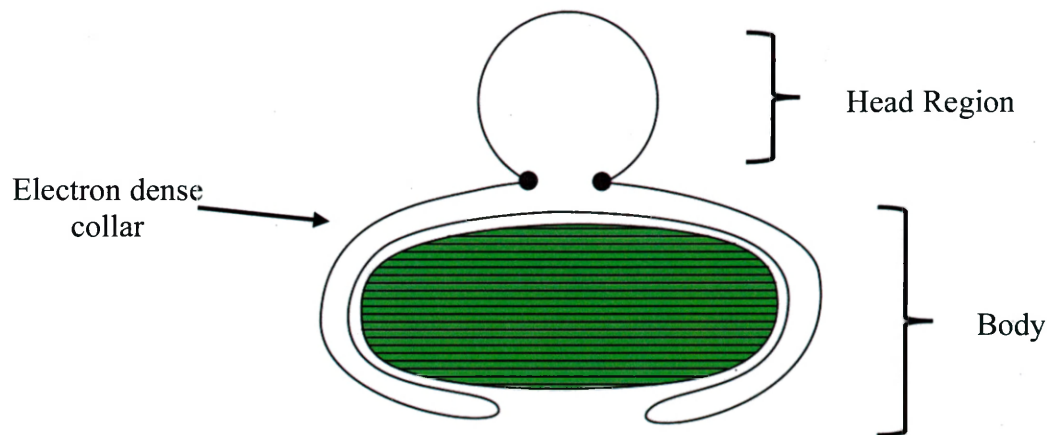


Figure 2: FB-MO complexes contain MSP in a paracrystalline form

FB-MO complexes are composed of an MSP polymerized into tightly backed subfilaments that are arrayed into an oblong-shaped, paracrystalline inclusion body (Roberts et al., 1986b). FBs are bound by golgi-derived MOs which contain a head region, an electron dense collar, and a body that encapsulates the FB.

called a Fibrous Body (FB) (fig. 2a-b) (Roberts et al., 1986b). FB growth occurs throughout prophase, until all MSP is sequestered (Messina, 2012). The completed structure is called an FB-MO complex.

FB-MOs are stably transmitted to dividing cells during meiosis, and are ultimately segregated away from the residual body and into each of the four spermatids (fig. 1). Segregation of FB-MOs is an active process; during Anaphase I and II, they appear to orient towards the poles along their lateral axis, suggesting that FB-MOs may be associating with tubulin spindles through an unknown intermediary. Later, during residual body formation, FB-MOs travel with the chromatin into spermatids, at which point, MOs detach from FBs and dock at the plasma membrane (J. C. Wu et al., 2012). Then, during spermatid maturation, FBs disassemble and MSP becomes cytosolic again.

In addition to its role in driving the motility of spermatozoa, MSP serves as an extracellular signaling molecule in hermaphrodites that acts on oocytes and gonadal sheath cells (Miller et al., 2001). Because spermatozoa do not contain an ER or Golgi apparatus, MSP secretion utilizes a novel system involving the budding off of exosomes (Kosinski, McDonald, Schwartz, Yamamoto, & Greenstein, 2005b). Exosomes are small, bi-layered membranous vesicles that contain MSP sandwiched between the outer and inner layers (Kosinski et al., 2005b). Once secreted, it is hypothesized that exosomes are sufficiently labile structures that they break down in the extracellular space, releasing free MSP capable of binding to extracellular receptors on the oocyte and gonadal sheath cells (Kosinski et al., 2005b; Miller et al., 2001). This process involves MSP binding to two separate receptors; an N-terminal signaling region binds to oocytes receptors and a

C-terminal signaling sequence binds to sheath cell receptors (Miller et al., 2001). Binding of MSP to sheath cells initiates contractile movements that move oocytes into the spermatheca while binding of MSP to oocytes induces meiotic maturation (Kosinski et al., 2005b). The process of MSP secretion process occurs just prior to, or during, sperm activation

Sperm activation is a highly complex process in which multiple events occur simultaneously. An early event in sperm activation is the fusion of MO heads with the plasma membrane, simultaneously changing the composition of the plasma membrane and releasing proteins into the extracellular space (L'Hernault, 2006). This process is required for fertilization; in mutants with defective MOs, spermatids are capable of activating, but incapable of fertilizing (Chatterjee, Richmond, Putiri, Shakes, & Singson, 2005). Concurrent with MO fusion, MSP undergoes a dynamic set of structural changes. Studies in *Ascaris suum*, suggest that this process may begin when MSP associates with the periphery of the cells, and begins polymerizing off MOs, where it forms short, MSP tails (Rodriguez, LeClaire, & Roberts, 2005). Following this, MSP polymerizes into spikes that extend along the outside of the cell. These spikes contain MSP polymerized into parallel fibers, similar to the way MSP is arranged in FBs, though not as ordered (Rodriguez et al., 2005; Shakes & Ward, 1989). However, unlike FBs, MSP spikes are dynamic structures; they are capable of extending and retracting (Rodriguez et al., 2005; Shakes & Ward, 1989). Some spikes also thicken and become webbed (Shakes & Ward, 1989). TEM images of similar structures in *A. suum* suggest that the transition from spikes to webbed structures involves a change in MSP structure from parallel filaments

into a meshwork of MSP (Rodriguez et al., 2005). Sperm activation completes when several blebs join together, forming a pseudopod (Rodriguez et al., 2005).

Ultimately, MSP is organized differently in the pseudopod than in the FBs. Similar to the distinction between MSP in spikes and blebs, the paracrystalline form of MSP found in FBs is comparatively simple when compared to MSP in pseudopod. In the pseudopod, MSP dimers appear to assemble into more complex assemblages (King, Stewart, & Roberts, 1994). *In vitro* studies have used purified MSP and sperm cell extract to mimic *in vivo* conditions and found that MSP assembles into subfilaments, which then coil around one another into filaments (King et al., 1994). In *in vitro* studies, the ends of filaments are often frayed, suggesting that MSP polymerization into subfilaments is the basic unit of MSP polymerization (King et al., 1994). In addition, MSP filaments are also capable of forming larger assemblages. In some cases, 3-5 filaments coil around one another into macrofibers (King et al., 1994). In other cases, filaments network with one another to form fiber complexes (King et al., 1994). In the pseudopod, fiber complexes form at the leading edge of the pseudopod and move proximally along the pseudopod as stable MSP foci (King et al., 1994; Sepsenwol, Ris, & Roberts, 1989b).

Factors that Influence FB Dynamics:

Because MSP forms different structures in different stages of spermatogenesis, it requires a variety of control mechanisms to determine what type of assemblages it forms. In particular, *C. elegans* proteins have been recently identified that are involved in transforming MSP from a cytosolic, unpolymerized form, into the polymerized, paracrystalline array found in FBs. One of these proteins is SPE-7 which is hypothesized

to act as a scaffolding protein for MSP (Messina, 2012; Presler, 2010). SPE-7 is a nematode-specific protein with little homology outside of related nematodes. SPE-7 was initially identified in a genetic screen for mutant worms that were defective in spermatogenesis. Worms with a null mutation in the *spe-7* are infertile and contain primary spermatocytes that have arrested in Anaphase I (Presler, 2010). When the MSP localization pattern was visualized in arrested spermatocytes, it was discovered that they showed defects in FB formation. Instead of assembling into oblong (spindle-shaped) structures, MSP remained diffuse throughout the cytoplasm (Messina, 2012).

Messina characterized the wild type localization pattern of SPE-7, and discovered that it plays a critical role in FB assembly and that its subcellular distribution changes during the course of meiosis. In wild type cells, MSP is translated early in meiotic prophase and is initially cytosolic. SPE-7 translation occurs during Pachytene, where it is first observed in small aggregates, called pre-FB structures, which initially associate with MOs and grow over the course of Pachytene (Messina, 2012) (fig. 3). These pre-FBs are hypothesized to form nuclei that bind MSP, increasing the local concentration sufficiently to allow it polymerize into an FB (Messina, 2012). However, although Messina illustrated that SPE-7 initially colocalizes with MSP in diplotene, the two patterns diverge over the course of meiosis (Messina, 2012). As meiosis progresses, SPE-7 clusters into four groups around the edge of the FB, during which time the FB changes shape from a spherical structure, in diplotene, to a lengthened rod in Anaphase II (Messina, 2012). In the rod-shaped FBs, SPE-7 localizes only at the distal tips (Messina, 2012).

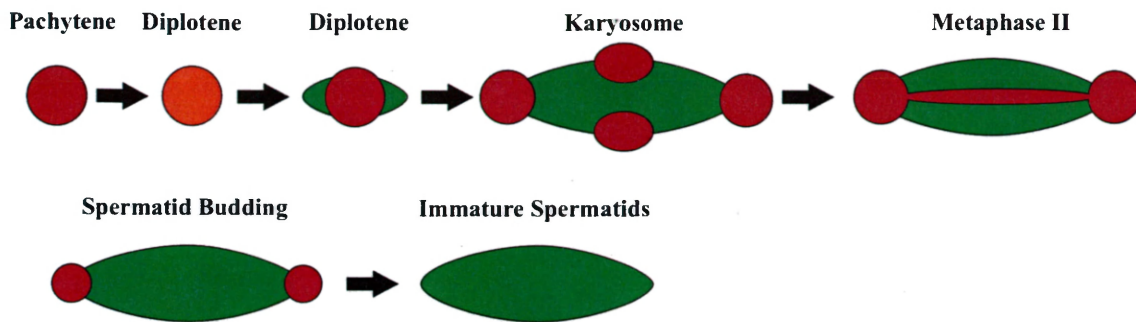


Figure 3: SPE-7 localization throughout spermatogenesis

In Pachytene of meiotic prophase, SPE-7 (red) self-aggregates into small structures. MSP (green) associates with these structures during Diplotene, and the two appear to colocalize. As FBs grow, SPE-7 initially remains centrally located, but eventually forms four points on the developing FB. During the meiotic divisions, SPE-7 becomes progressively more distal on the FBs. During spermatid budding, SPE-7 is only located on the distal tips and has begun to be degraded. By the end of spermatid budding, SPE-7 is completely degraded. Figure adapted from: (Messina, 2012)

In addition to its localization with MOs prior to FB formation, further evidence suggests that SPE-7 may be playing a scaffolding role because it is a putative Intrinsically Unstructured Protein (IUP). IUPs are defined as proteins with large regions of disordered loops (>50 amino acids) (Dyson & Wright, 2005). These loops form in the absence of amino acid interactions that promote the formation of alpha helices and beta pleated sheets. Although IUPs do not completely lack structure, they often have minimal intrinsic structure (Dyson & Wright, 2005). Furthermore, many IUPs form complex structures when they are associated with protein complexes. In these cases, unstructured regions allow sufficient flexibility to bind multiple proteins in a complex (Dyson & Wright, 2005). One possibility is that the unstructured regions of SPE-7 may act in a similar fashion by providing sufficient flexibility for SPE-7 to bind multiple MSP dimers, allowing them to polymerize into FBs.

Although SPE-7 is an important regulator of FB formation, other factors are clearly involved in this process. For instance, *spe-6* plays critical roles throughout

spermatogenesis, including during FB formation. *spe-6* encodes a homolog of casein kinase I in which multiple mutational alleles have been isolated (Muhlrad & Ward, 2002; Varkey, Jansma, Minniti, & Ward, 1993b). The most severe *spe-6* allele, *hc49*, is thought to be a null allele (Varkey et al., 1993b). Similar to a SPE-7 mutant, the *spe-6 (hc49)* null allele exhibits a meiotic arrest as primary spermatocytes (Varkey et al., 1993b). In addition, arrested cells exhibit diffuse MSP staining, suggesting that *spe-6 (hc49)* primary arrest may be analogous to the SPE-7 mutant arrest (Messina, 2012). However, though similar, the two mutants are not identical because *spe-6 (hc49)* mutants contain SPE-7. In these mutants, SPE-7 forms pre-FB structures that grow larger than in WT, but MSP never associates with them (Messina, 2012). This suggests that SPE-7 alone is incapable of forming FB structures, and, instead, the process of FB formation requires multiple factors. In addition, because kinases often act as molecular switches, it is possible that FB formation is actively switched on by SPE-6.

Although SPE-7 and SPE-6 are both required for FB formation, multiple lines of evidence suggest that there are more factors that influence FBs than have been elucidated. For instance, although SPE-6 is required for FB formation, there is no evidence that SPE-7 itself is phosphorylated, implying that SPE-6 is likely acting on a different protein that directly or indirectly interacts with SPE-7 (Messina, 2012). In addition, after meiosis and spermatid budding, SPE-7 is degraded, and FBs typically persist for a short period of time before breaking down. However, FB breakdown is apparently an active process because multiple mutants have been identified that exhibit persistent FB-like structures (Nishimura & L'Hernault, 2010a; Ward, Argon, & Nelson, 1981; J. Wu et al., 2012). In one case, spermatids of a double mutant of the PP1 phosphatases *gsp-3* and *gsp-4* exhibit

partial FB breakdown and are capable of forming only short, blunted pseudopods (J. Wu et al., 2012). Overall, the proteins and events required to transform newly synthesized cytosolic MSP into paracrystalline MSP (FBs) and back to cytosolic MSP (mature spermatids) are only beginning to be uncovered.

Factors that Influence MSP Dynamics in the Pseudopod:

After MSP goes cytosolic in mature spermatids, it undergoes a final structural rearrangement during sperm activation. More specifically, it localizes to the pseudopod where its directed polymerization and depolymerization drives the extension and retraction of the pseudopod. To operate in this fashion, MSP requires a variety of accessory proteins that enhance polymerization at the distal end of the pseudopod and depolymerization at the proximal end. Although the process of directed MSP polymerization is poorly understood in *C. elegans*, this system has been better characterized in a related, biochemically amenable species, *A. suum*. In *A. suum*, directed MSP polymerization in the pseudopod is dependent on MSP Polymerizing Organizing Protein (MPOP), a 48 kDa integral membrane protein that localizes to the plasma membrane (LeClaire, Stewart, & Roberts, 2003) (fig. 4). Though it localizes throughout the plasma membrane, MPOP is differentially phosphorylated at the leading edge of the pseudopod by an unidentified protein tyrosine kinase, resulting in a polarized pattern (LeClaire et al., 2003). Phosphorylated MPOP, in turn recruits a casein kinase I homolog MSP Polymerizing-Activating Kinase (MPAK) to the leading edge of the pseudopod (Yi, Buttery, Stewart, & Roberts, 2007b). MPAK enhances MSP polymerization by phosphorylating the MSP Fibrous Protein 2 (MFP2) which has been shown to enhance

MSP polymerization (Yi et al., 2007b). In addition, three other *Ascaris* proteins have been found to alter MSP dynamics in the pseudopod. A homolog of the phosphatase PP2A localizes to the proximal end of the pseudopod and dephosphorylates the MSP binding protein, MFP3 (Yi et al., 2009a). When dephosphorylated, MFP3 releases from MSP fibers, which then show increased retraction, suggesting that phosphorylated MFP3 stabilizes MSP fibers (Yi et al., 2009a). Lastly, a third MSP binding protein, MFP1 localizes to the distal end of the pseudopod and slows fiber growth (Buttery, Ekman, Seavy, Stewart, & Roberts, 2003b).

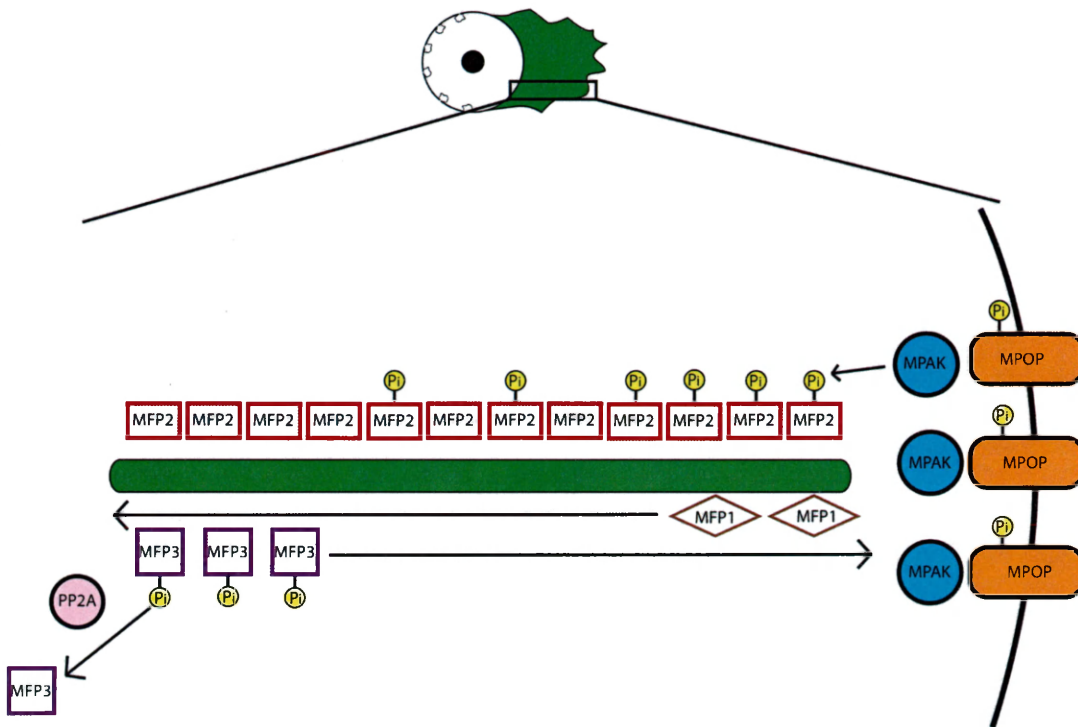


Figure 4: Factors that direct MSP polymerization in *A. suum*.

In the spermatozoa of *A. suum*, the integral membrane protein MPOP is present along the entirety of the plasma membrane but is differentially phosphorylated at the leading edge of the pseudopod. Phosphorylated MPOP binds MPAK and differentially localizes it the leading edge. MPAK phosphorylates MFP2, an MSP accessory protein that associates along the length of an MSP fiber (seen in **green**). Phosphorylated MFP2 enhances MSP polymerization. MFP1 also associates along the length of MSP fibers and is thought to act antagonistically to MFP2, slowing MSP polymerization. Lastly, phosphorylated MFP3 stabilizes MSP fibers, but MFP3 is dephosphorylated at the proximal end of the pseudopod by PP2A phosphatases, causing MFP3 to release from MSP fibers, destabilizing them.

Although the mechanisms of MSP fiber assembly and disassembly in *A. suum* have been partially characterized, *C. elegans* homologs of most of these key proteins have yet to be identified and/or studied. However, there is evidence to suggest that similar mechanisms may be involved. For instance, sperm activation and MSP polymerization in *C. elegans* appears to be dependent on the PP1A phosphatases GSP-3 and GSP-4 (J. Wu et al., 2012). In mature spermatozoa, these proteins localize with MSP in the pseudopod, though they are shifted away from the leading edge of the pseudopod and extender further into the cell body and thus may serve an analogous function to PP2A in *A. suum* (J. Wu et al., 2012). In addition, MSP polymerization within the pseudopod may also be influenced by the aforementioned SPE-6; not only is it a CK1 homolog that may serve an analogous function to MPAK, but one special class of *spe-6* alleles produce spermatids that precociously form pseudopods in the absence of the normal activation factors (Muhlrad & Ward, 2002). Lastly, homologs to MFP1, MFP3 and MFP2 have been identified in *C. elegans* suggesting, that many of the basic mechanisms are likely conserved (Buttery, Ekman, Seavy, Stewart, & Roberts, 2003a; Yi et al., 2009b).

MFP2 as an MSP Regulator

In this study, I report the identification and initial characterization of a *C. elegans* homolog to the *Ascaris* MFP2 protein. In *Ascaris*, MFP2 binds along the length of MSP fibers, but enhances polymerization only at the growing end (Yi et al., 2007b). This effect is thought to be mediated by the differential phosphorylation of MFP2, such that MFP2 exhibits a gradient of phosphorylation, with phosphorylated MFP2 concentrated at the

distal, growing end of the fiber (Yi et al., 2007b). In addition, the crystal structure of MSP has been solved and suggests a mechanism for how MFP2 enhances MSP polymerization (fig. 5) (Grant, Buttery, Ekman, Roberts, & Stewart, 2005a). MSP is a globular protein with two distinct domains connected by an unstructured, flexible linker region (Grant et al., 2005a). The angle that the two domains form is $\sim 100^\circ$, which is approximately the same angle that two MSP dimers meet at when they are arrayed in subfilaments (Grant et al., 2005a). This suggests a straightforward model in which MFP2's domains orient MSP dimers into the correct conformation for polymerization (Grant et al., 2005a). Alternatively, MFP2 may bind MSP filaments and recruit binding partners that enhance MSP polymerization, or it may enhance polymerization through a third, unknown mechanism (Grant et al., 2005a).

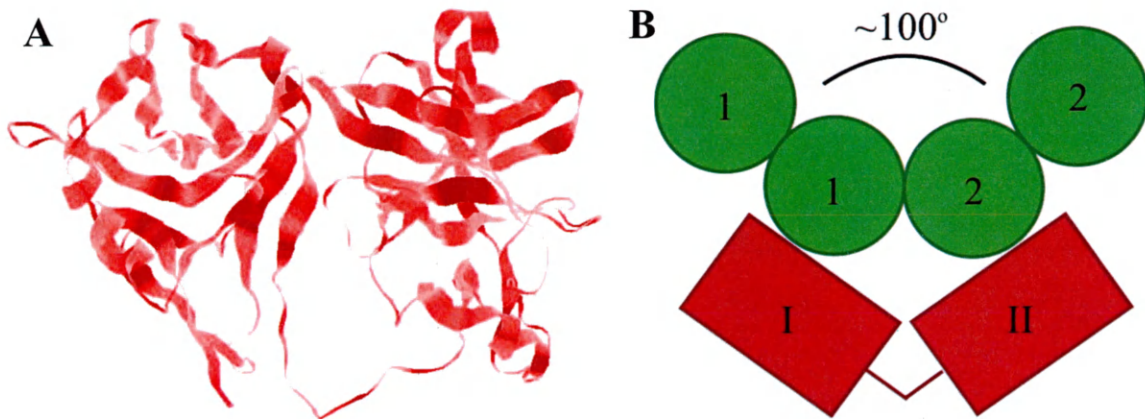


Figure 5: MFP2's crystal structure and model for binding MSP

a) I-TASSER model of MFP2 that shows a high degree of structural conservation between the predicted, *C. elegans* structure and the known crystal structure of *A. suum* (Roy, Kucukural, & Zhang, 2010; Zhang, 2008). In both proteins, MFP2's contains two domains connected by a flexible linker region that meet at an $\sim 100^\circ$ angle (Grant, Buttery, Ekman, Roberts, & Stewart, 2005b). b) This suggests that MFP2 (red) may bind two MSP dimers (green, labeled 1 and 2), orienting them for polymerization (Figure modified from: (Grant et al., 2005b).

Unanswered Questions:

Although some of the proteins and mechanisms that influence MSP dynamics in the FBs and in the pseudopod have been identified, much of this system remains to be elucidated. The recent discovery that proteins such as SPE-6 (CK1) and GSP-3/4 (PP1 Phosphatases) regulate both FB dynamics and pseudopod suggests that these two systems are interrelated. However, it is still unclear to what extent regulatory mechanisms that govern pseudopod dynamics overlap with mechanisms that govern FBs. The MSP accessory protein MFP2 is particularly well suited for such studies, because it is evolutionarily conserved and has a clear *C. elegans* homolog.

In addition, although FBs are large macromolecular complexes, they appear to be have consistent shapes and morphologies, suggesting a mechanism for regulating FB size and morphology. However, differences in size and morphology have not been closely examined in *C. elegans*, and it remains unclear whether FB size has physical constraints, or whether this controlled through some other mechanism.

Specific Aims of Thesis:

The primary objective of this thesis is to further our understanding of the regulation of FB dynamics. To do this, we have utilized a two-pronged approach. The first part of this thesis involves studying a specific MSP accessory protein, MFP2, in both *C. elegans* and *C. remanei*. Prior to this study, the function of MFP2 had only been studied in the context of MSP based cell motility. Using immunofluorescence, we explore the localization pattern of the *Caenorhabditis* homolog throughout all stages of spermatogenesis. In addition, we use various spermatogenesis-defective mutants to gain insight into how misregulation of spermatogenesis affects MFP2. Lastly, we utilize a variety of techniques to probe the biochemistry of MFP2.

The second part of this thesis involves studying various alleles of the *spe-26* gene, which exhibit FB misregulation. These alleles show errors in FB size and morphology that vary between alleles. Using immunofluorescence, as well as image analysis software, we have characterized these differences qualitatively and quantitatively. In addition, we have also analyzed how the localization pattern of SPE-7 is altered in these abnormally large and persistent FBs.

Methods

Microscopy and Image Analysis

Fluorescence and DIC microscopy were performed using an Olympus BX60 fluorescence microscope equipped with an EXi Aqua Camera. Some images were enhanced with Adobe Photoshop (version no. 12.0.4) or iVision. Intensity analyses were performed using iVision on native 14-bit iVision image files and then converted into 8-bit images post-analysis. For length measurements, images were analyzed in iVision on native files. For multi-dimensional imaging, z-axis stacks were taken using a z-axis stage controller at 0.2 μm intervals. For deconvolution, images were run through MicroTome deconvolution software.

Intensity analysis for MFP2 and MSP were performed on spermatids. The MFP2 image was segmented into circular segments whose size was based on the diameter of a typical immature spermatid. Only spermatids that appeared to be in focus were measured. Following image segmentation, segments were copied from the MFP2 image to the MSP image. Mean intensity values were then extracted and used for graphing and data analysis.

For FB measurement, black and white MSP images were used. Cells that contained tightly condensed chromatin were chosen for FB measurement. Only FBs that appeared parallel to the focal plane were chosen, which was determined by examining FB morphology. FB lengths were measured and compiled.

Strains and Genetics

C. elegans worm strains used were obtained from the *Caenorhabditis Genetics*

Center (GGC). Strains used include: CB1489 *him-8 (e1489)*, BA606 *spe-6 (hc49) unc-25 (e156)*; *eDp6*, JK816 *fem-3(q20)*, RV120 *spe-44(ok1400) dpy-20(e1282)/let-92(s677) unc-22(s7)*, EM464 *C. remanei ssp. vulgaris*, BA6 *fer-6(hc6)*, BA793 *spe-26(hc138) dpy-13(e184)*, BA825 *spe-26(hc140) dpy-20(e1282)/+*, BA837 *spe-26(it112)*, SL305 *spe-26(eb8) IV/nT1 [unc-?(n754) let-?]*, XC26 *gsp-3(tm1647) gsp-4(y418)/hT2[bli-4(e937) let-?(q782) qIs48]*; *him-8(e1489)* from Diana Chu; RV120 *spe-44(ok1400) dpy-20(e1282)/let-92(s677) unc-22(s7)* from Harold Smith.

Worm Growth and Sample Preparation

In order to grow worms for western blots and IPs, worms were grown using two conditions. For large-scale preparation, worms were grown on 5-10 100mm MYOB plates enriched for peptone (Church, Guan, & Lambie, 1995). 100 mm plates were seeded with ~3 ml of NA-22 *E. coli* and allowed to grow overnight at 37°C. In order to time-sync worm populations, adult populations of worms were washed with M9 buffer (22 mM KH₂PO₄; 42 mM Na₂HPO₄; 86 mM NaCl; 1 mM MgSO₄) into 15 ml conical tubes and then centrifuged for 1-2 min until a pellet formed. The supernatant was aspirated off and the worms were treated with a bleach solution (1:4 Chlorox bleach:0.625 M KOH) for 5 minutes. The solution was pelleted again and washed with 4-5 ml of M9. Embryos were then plated onto unseeded MYOB plates, left at RT overnight and then transferred to 15-20 NA-22 plates. When they had reached adulthood, the worms were washed with M9 to remove any bacterial contamination and then washed into 1.5 ml centrifuge tubes, frozen in liquid nitrogen, and stored at -80°C

For small-scale preparations, worms were grown on 2-3 X 35 mm MYOB plates seeded with OP-50 *E. coli*. In order to time-synch, worm populations were bleached and then embryos were plated onto unseeded MYOB plates. For sample collections of males, 200-300 L4 males were placed on seeded 5 X 35 mm MYOB plates and then allowed to grow to adulthood. Worms were then picked into ~15 μ L M9 buffer supplemented with Roche Protease Inhibitors, snap-frozen in liquid N₂ and then stored at -80°C.

In order to grow worms for immunofluorescence, worm strains were maintained using previously described methods (Brenner, 1974). All worms were initially grown on 35 mm MYOB plates seeded with OP-50. For WT controls in *C. elegans*, *him-8* worms were used. For WT controls in *C. remanei*, was used. In both cases, adult males and hermaphrodites or females were plated and allowed to lay eggs. After 24 hours, the P₀ generation was transferred to new plates. 36-48 hours later, the F1 generation was dissected. For temperature sensitive strains, worms were grown at 16°C. Every 24 hours, P₀ worms were transferred to new plates and the old plates were moved to 25°C. After 36-48 hours, the F1 generation was dissected.

Immunostaining

Immunostaining was performed by first picking 7-10 worms onto un-seeded agar plate. Worms were then picked onto a plus-charged Colorfrost slide with 5-7 μ L Edgars Buffer (60 mM NaCl; 32 mM KCl; 3 mM Na₂HPO₄; 2 mM MgCl₂; 2 mM CaCl₂; 5 mM HEPES; 0.2% glucose; pH 7.2). When working with *C. elegans*, Edgar's buffer was supplemented with 1X levamisole. For activation studies, the buffer was supplemented with Pronase E (Sigma Aldrich). After dissecting worms, a 24X40 mm cover slip with

four dots of silicone grease was applied to the slide. The slide was then placed in liquid nitrogen. To fix the tissue, the slides were removed from liquid nitrogen, the coverslips were removed and the slides placed in methanol pre-chilled to -20°C and stored at -20°C for at least 24hours.

After 24 hours, slides were removed from -20°C and rehydrated using three, consecutive 5 min. washes in 1X PBS. Slides were then incubated for 20-40 minutes in blocking solution (PBS with 0.04% NaN_3 ; 0.1% Tween; 0.5% BSA). Following this, a primary dilution of antibody in antibody buffer (PBS with 0.04% NaN_3 ; 3% BSA) was applied, and the slides were incubated in in a humidity chamber inside a light-impenetrant drawer. Slides were then washed in PBS, a secondary antibody was applied, and the slides were returned to the humidity chamber and drawer. Following secondary incubation, the slides were washed again and then a mixture of 1 $\mu\text{g}/\text{ml}$ DAPI in Fluorogel with DABCO (Electron Microscopy Sciences, Cat#: 17985-02) was applied. 24X24 mm coverslips were applied and the slides were placed at 4°C overnight. The slides were then removed and sealed with nail polish.

Western Blotting

For western blotting, samples were aliquoted and mixed with an equal quantity of 2X Bio-Rad laemelli sample buffer that had been pre-heated to 95°C . In the case of samples stored at -80°C , heated sample buffer was applied without thawing samples first. After addition of sample buffer, samples were heated at 95°C for 5 minutes and then spun at 15,000 rcf for 3 min.

SDS-PAGE was performed using Bio-Rad Mini-Protein TGX pre-cast tris-glycine gels. Experiments were performed using either Bio-Rad Any kD gels or 10% gels. In all cases, each gel lane was loaded with 20 μ L of sample or 6 μ L of Precision Plus Protein Kaleidoscope protein standards. Gels were run at 100V or 150V for 60-120 minutes. Proteins were then transferred to PVDF membrane by semi-dry transfer for 30 minutes at 19V. After transfer, the membranes were transferred to a blocking solution (4% Carnation Instant Milk:TBST (w/v)) overnight at 4°C on a rocker.

For immunostaining, blots were removed from 4°C and a dilution of primary antibody in blocking solution was applied. The blots were then incubated at RT on a shaker for 1.5 – 2 hrs. Following this, the blots were washed and a secondary antibody was applied and allowed to incubate. Approximately, 30 minutes before the end of the secondary incubation, ECL (enhanced chemiluminescence) reagents were removed from 4°C and allowed to warm to RT. For visualization, approximately 1ml of ECL was applied to the blots and allowed to incubate for 5 minutes. Following this, bands were visualized using X-Ray film.

Antibodies

For immunostaining against MFP2, the affinity purified antibody bl3086 (Yenzyme) was used. Bl3086 is a rabbit polyclonal antibody generated against amino acids 92-108 of the MFP2 protein. The bl3086 antibody was stored at -80°C for long-term storage. For regular use, aliquots were either stored at 4°C or were thawed from -80°C. For immunofluorescence, slides were incubated with a 1:150 dilution of primary antibody stored in the 4°C in antibody buffer for 1.5-2 hrs and then a secondary antibody

was applied prepared from a glycerol stock. Following secondary incubation, slides were washed for 1 minute in 1X PBS and then dipped in DI water. For immunostaining of western blots, blots were incubated with a 1:5000 dilution of primary antibody in blocking solution for 2 hours. Then blots were washed 6X15 min in 1XTBST

For immunostaining against MSP, we used either the affinity purified antibody 4A5 (DSHB, (Kosinski, McDonald, Schwartz, Yamamoto, & Greenstein, 2005a) or the affinity purified antibody 4D5. 4A5 and 4D5 are mouse monoclonal antibodies generated against amino acids 106-121, a conserved C-terminal domain. Both antibodies were stored at -80°C for long-term storage. For regular use, 1:1 mixtures antibody and glycerol were prepared and stored at -20°C. For immunofluorescence with 4A5, slides were incubated with a 1:150 dilution of the glycerol stock of primary antibody in antibody buffer was used. For immunofluorescence with 4D5, a 1:20 stock of primary antibody was prepared in antibody buffer. Following this, slides were incubated with 1:120 dilution of the 4°C primary antibody in antibody buffer, creating an effective dilution of 1:2400. Slides were incubated for 1.5-2 hrs and then a secondary antibody was applied. Following secondary incubation, slides were washed for 1 minute in 1X PBS and then dipped in DI water. For immunostaining of western blots, blots were incubated with a 1:10,000 dilution of primary antibody in blocking solution for 2 hours. Then, blots were washed 6 X 15 min in 1 X TBST.

For immunofluorescence of polyclonal antibodies, an affinity purified goat polyclonal antibody used (Jackson ImmunoResearch). The goat anti-rabbit antibody was a TRITC conjugated antibody generated against the Fc region of rabbit IgG. For regular use, aliquots were mixed with 50% glycerol and stored at -20°C. For staining, slides were

incubated with a 1:400 dilution of the glycerol stock of secondary antibody in antibody buffer for 1.5-2 hrs.

For immunofluorescence of monoclonal antibodies, an affinity purified goat anti-mouse polyclonal antibody was used (Jackson ImmunoResearch). The goat anti-mouse antibody was a Dylight 488 conjugated antibody generated against the conserved Fc region of mouse IgG. For regular use, aliquots were mixed with 50% glycerol and stored at -20°C. For staining, slides were incubated with a 1:150 dilution of the glycerol stock of secondary antibody in antibody buffer for 1.5-2 hrs.

For immunostaining of western blots of polyclonal antibodies, an affinity purified goat polyclonal antibody was used. The goat anti-rabbit antibody was an HRP conjugated antibody generated against the Fc region of rabbit IgG. Aliquots were stored at -80°C and periodically thawed and stored at 4°C. Staining was performed using a 1:10000 dilution of secondary antibody in blocking solution.

Bioinformatics

For bioinformatics analyses, we used the *A. suum* protein sequences for: MFP2a (Accession no. AAP94886) as well as the *C. elegans* protein sequences for: ZK265.3 (Accession no. NP_492244), C04G2.9 (Accession no. NP_501838), Y69E1A.2 (Accession no. NP_502039), Y59E9A1.2 (Accession no. NP_001023536); and the *C. remanei* protein sequences for: CRE_29401 (Accession no. XP_003087592), CRE_03809 (Accession no. XP_003111326). We also used the crystal structure for MFP2a (Protein Data Bank 2BJQ).

To create a predicted structure for ZK265.3, we used the I-TASSER program (Roy et al., 2010; Zhang, 2008). For the prediction of phosphorylation sites, we used NetPhos 2.0 and Phosida (Blom, Gammeltoft, & Brunak, 1999; Gnad et al., 2007).

Chapter 1: The MSP Accessory Protein MFP2

Introduction

Depending on their function, cells can exhibit different levels of structural dynamism. In some situations, cytoskeleton elements can assemble into packed, parallel structures that exhibit dynamic stability (Revenu, Athman, Robine, & Louvard, 2004). In other situations, however, cells like macrophages project contain dynamic filopodia and lamellopodia that extend and retract to allow directed motility (Pollard, Blanchoin, & Mullins, 2000). In all cases, however, the structural dynamism of the cells is determined by networks of cytoskeletal proteins. In addition to determining cellular morphology, cytoskeletal proteins also support organelles and aid in intracellular transport; both of which require differing levels of polymerization and depolymerization to function correctly. Consequently, cells need to be able to regulate cytoskeletal assemblages to create both highly dynamic structures, which rapidly vary their length, and highly stable structures, that have relatively consistent lengths (Pollard et al., 2000; Revenu et al., 2004).

The stability of cytoskeletal assemblages is regulated by three broad mechanisms. The first mechanism involves direct, post-translational modification of cytoskeletal proteins (Omary, Ku, Tao, Toivola, & Liao, 2006). Alternatively, rather than being modified directly, cytoskeletal assemblages can have different accessory proteins, like the Arp-2/4 complex, that either locally alter polymerization dynamics, or alter general stability (Pollard et al., 2000; Revenu et al., 2004). Lastly, accessory proteins can themselves be post-translationally modified, to alter either their effect on cytoskeletal proteins or their ability to bind (Pollard et al., 2000).

The cytoskeleton of most animal cells is composed some combination of the following cytoskeletal elements: microfilaments, microtubules and intermediate filaments, and their respective regulatory proteins. However, the nematode *Caenorhabditis elegans* contains an additional cytoskeletal protein called Major Sperm Protein (MSP). MSP is a nematode-specific cytoskeletal protein that functions in the pseudopod of spermatozoa (Sepsenwol et al., 1989a). Over the course of spermatogenesis, MSP exists in three separate forms. When it is initially synthesized during the Pachytene stage of meiotic prophase, MSP exists as unpolymerized dimers and is cytosolic (Messina, 2012; Roberts et al., 1986b). By late Prophase of meiosis I, MSP polymerizes into an assemblage of tightly packed filaments called a Fibrous Body (FB) that appear to have to stable morphology (Messina, 2012; Roberts et al., 1986b). Shortly after the completion of meiosis, FBs breakdown and MSP becomes cytosolic again (Messina, 2012). Lastly, during sperm activation, MSP localizes to the pseudopod, where it is highly dynamic; its rapid polymerization and depolymerization drive the extension and retraction of the pseudopod (Sepsenwol et al., 1989a). Consequently, over the course of spermatogenesis, MSP exists in an inactive, cytosolic state, a relatively stable, packed filament state, and a dynamic state. As result, MSP is an attractive model for studying the changes required to dramatically alter the properties of cytoskeletal assemblages.

The dynamic form of MSP found in the pseudopod has been extensively studied. These studies have identified a number of MSP accessory proteins that can enhance MSP polymerization and depolymerization both *in vivo* and *in vitro* (Buttery et al., 2003b; J. C. Wu et al., 2012). One these accessory proteins, MFP2, was identified and studied in *Ascaris suum*, a relative of *C. elegans* (Buttery et al., 2003b). These studies revealed that

that MFP2 is capable of binding and enhancing MSP polymerization *in vitro* (Grant et al., 2005b). In addition, MFP2 is phosphorylated at the growing edge of an MSP filament (Yi, Buttery, Stewart, & Roberts, 2007a). These analyses, however, pertain to MFP2's properties in the pseudopod; the localization and function of MFP2 earlier in meiosis, when MSP is cytosolic or in FBs, has not been studied.

Here, we present evidence that MFP2 co-localizes with MSP during all or most stages of spermatogenesis in both *C. elegans* and a relative, *C. remanei*. We also characterize the pattern of MFP2 localization in a variety of mutants in which MSP localization is perturbed, and perform image analysis to explore potential changes in MFP2's structural conformation. Finally, we explore the phosphorylation state of MFP2 in an attempt to determine if there are any differences between MFP2 over the course of meiosis, as its localization pattern changes.

Results

Identification and Sequence Analysis of MFP2 homologs in C. elegans and C. remanei

In order to determine the extent to which MFP2 is conserved between *A. suum* and *C. elegans*, we did a BLASTp search on the primary amino acid sequence of MFP2a in *A. suum*. We found a highly conserved homolog in *C. elegans*, ZK265.3, which had a 99% query coverage, and an E-value of $6e^{-125}$ (Figure 1). For this reason, ZK265.3 shall be hereafter referred to as MFP2. Because *A. suum* and *C. elegans* are related on sequence level approximately to the same extent as human and sea urchin, the high degree of sequence conservation suggested that MFP2 is likely playing the same role in *C. elegans* as it is in *A. suum* (Kiontke & Fitch, 2005).

To further identify homologs in other species of nematodes, we did a BLASTp search on ZK265.3. This located a number of homologs to the *C. elegans* MFP2 protein within different species of nematodes that were both within and without the *Caenorhabditis* clade. This search also showed that although there were homologs to MFP2 in multiple different species of nematodes, there were none in species outside of the nematode Phylum (data not shown). In addition, we also discovered a number of paralogs to the *C. elegans* MFP2 protein that showed significant sequence divergence, similar to what has been shown in *A. suum* (Table 1). Notably, these data showed that *Ascaris* MFP2a is more similar to the *C. elegans* ZK265.3 gene than ZK265.3 is to its *C. elegans* paralogs. Conversely these *C. elegans* paralogs are more similar to the *Ascaris* genes MFP2b and MFP2c (data not shown).

Within the *Caenorhabditis* group, we were particularly interested in the conserved homolog that was identified in *Caenorhabditis remanei*. Although morphologically quite

similar, *C. remanei* is a species that is approximately as related to *C. elegans* as a human is to a mouse (Kiontke & Fitch, 2005). In addition, *C. remanei* differs from *C. elegans* in its reproductive strategy; unlike *C. elegans*, *C. remanei* is a male-female species whose males produce spermatocytes and spermatids that are morphologically similar but substantially larger than in *C. elegans*. Consequently, we hoped that studies on the *C. remanei* homolog would allow us to study MFP2 in more detail within these larger cells, as well as determine the extent to which its properties appeared to be conserved in a species that was of intermediate relatedness between *C. elegans* and *A. suum*.

Although there were homologs to MFP2 in *C. remanei*, we were surprised to discover that there was not a single protein that had coverage over the entire protein. Instead, the BLASTp search identified two homologs of MFP2; one sequence (CRE_03809) covered the first 254 amino acids, and the second (CRE_29401) covered the last 128 amino acids, overlapping in the middle of the protein. Further analysis of the MFP2 sequences present in the NCBI database, determined that one of these protein sequences is only a predicted sequence, partially confirmed by microarray experiments. The second sequence was also a predicted sequence with microarray evidence, but was also based on cDNA sequences that were obtained. Combining these two sequences predicted a three-exon protein in the same pattern as the *C. elegans* protein. Based on this evidence, we think it is likely that the multiple MFP2 sequences identified in *C. remanei* are erroneous, and that, instead, it is one protein. Furthermore we are reporting our results to Wormbase as they suggest a new linkage between previously unlinked contigs in the *C. remanei* genome project.

Lastly, in order to determine whether or not it was feasible to study the *C. remanei* homolog, we aligned the hybrid full-length *C. remanei* peptide sequence to the *C. elegans* ZK265.3 sequence and specifically compared the region of the peptide sequence which we had generated our anti-ZK265.3 antibody against (Figure 1 – boxed region). Within this region, the *C. remanei* sequence was almost identical; it contained only a single amino acid substitution that changed an isoleucine to a valine, which are chemically similar. From this, we predicted that that MFP2 (ZK265.3) antibody would work in both *C. elegans* and *C. remanei*.

The MFP2 structure in A. suum is predicted to be conserved in C. elegans.

To ensure that changes in the MFP2 sequence between *A. suum* and *C. elegans* were insignificant, we used I-TASSER to predict the structure of the MFP2 protein in *C. elegans* (figure 2). I-TASSER predicts protein structures by mapping amino acid sequences onto proteins with known crystal structures. I-TASSER predicted a structure that was primarily based on the known *A. suum* crystal structure. In addition, I-TASSER provides a C-Score that ranges from -5 (low confidence) to 2 (high confidence) and correlates with the probability that the predicted structure is correct. The C- score value I-TASSER provided for the MFP2 model was 1.68, suggesting that the predicted structure is accurate, or mostly accurate.

The MFP2 antibody specifically targets MFP2.

In order to determine whether the MFP2 antibody correctly tagged MFP2, we prepared whole worm lysate from temperature-sensitive alleles of *fem-3(q20gf)* and *fem-*

3(*lf*) worms that had been grown at the restrictive temperature. FEM-3 is a protein involved in sex determination and germline specification in *C. elegans*. In restrictively grown *fem-3 (q20gf)* worms, hermaphrodites develop normal feminine somatic tissue, and begin to produce sperm correctly, but do not undergo the switch to oocyte production. Consequently, they will continue to produce spermatids. In addition, because they are somatically feminine, they are not equipped to mate with other hermaphrodites/females, nor do they produce signals that normally induce spermatids to differentiate into spermatozoa. As a result, over time, they accumulate spermatids. *fem-3 (lf)* mutants, on the other hand, develop as females; their somatic tissue is feminine, and they only produce oocytes. Any sperm-specific genes, such as MFP2, are not produced in *fem-3 (lf)* worms except in the small number of males that naturally occur in the population.

Western blots of *fem-3 (q20gf)* revealed a band at ~37 kDa that was not present in *fem-3 (lf)* samples (figure 3). This is consistent with the predicted MW of MFP2 based on its primary amino acid sequence. In addition, we also observed a number of bands that were present in both samples, which are likely non-specific because MFP2 is not predicted to be present in oocytes. Similarly, there were also bands present in *fem-g(q20gf)* that were not present in *fem-3 (lf)*. However, none of these bands was close to the molecular weight of MFP2, so we concluded that they were non-specific, as well.

The MFP2 antibody has a distinct pattern from negative controls.

To determine the specificity of our anti-MFP2 antibody for use in immunofluorescence, we labeled WT worms with anti-MFP2 antibody and compared

them to secondary-only controls. This allowed us to determine which patterns were specific to MFP2, and which patterns were due to non-specific binding of our secondary (figure 4). When performing controls, we kept all antibody conditions the same and used the same exposure times. Our results showed that labeling by the Anti-Rabbit TRITC secondary antibody produced relatively dim images compared to the labeling that included the primary antibody, suggesting that the secondary antibody contributed relatively little to non-specific labeling.

In addition, to further ensure that MFP2 labeling was specific to MFP2, we used *spe-44 (ok1400)* mutants as a negative control because microarray data suggests that MFP2 expression is down-regulated in *spe-44 (ok1400)* mutants (Kulkarni et al., 2012). *spe-44* encodes a transcription factor that is expressed in a spermatogenesis-specific manner and is itself required for the expression of nearly one third of *C. elegans* spermatogenesis-enriched genes (Kulkarni et al., 2012). Spermatocytes lacking SPE-44 (*spe-44(ok1400)*) fail to assemble fibrous bodies, but do detach from the rachis and initiate the meiotic divisions before arresting in M-phase (Kulkarni et al., 2012).

By comparing MFP2 labeling in WT and *spe-44 (ok1400)* to secondary-only controls, we determined that the MFP2 antibody appears to bind MFP2, but also binds non-specifically to proteins that do not appear to be sperm-specific. The MFP2 antibody brightly labels MFP2 throughout meiosis in WT. In addition, in WT and *spe-44* mutants, but not secondary-only controls, we observed punctate staining that localized to the plasma membrane in both somatic and gonadal tissue (figure 4). Because this staining was present in somatic tissue, and was absent when the primary antibody was omitted, we concluded that this was non-specific staining from the primary antibody itself.

MFP2 localizes to oblong-shaped structures.

We carefully analyzed MFP2's pattern to determine its localization pattern throughout spermatogenesis (figure 5). Due to the non-specific labeling of the plasma membrane, the early MFP2 pattern is ambiguous; the labeling is bright throughout the gonad and, consequently, we did not observe a clear beginning to the MFP2 signal that would signify the start of MFP2 translation. However, following approximately the Karyosome stage of meiosis, we were able to determine that MFP2 appears to localize to discrete, oblong structures that resemble Fibrous Bodies (FBs). Consistent with this hypothesis was the observation that MFP2 localized to structures that appeared to lengthen during Karyosome stage.

Following the end of the meiotic divisions, MFP2 persists in structures for a short time in immature spermatids, before becoming diffuse in mature spermatids. Concurrent with MFP2's change to a diffuse pattern, we observed a significant drop in the signal intensity of MFP2. This change in intensity was severe enough that it is indistinguishable from background labeling in the gonad. However, following sperm activation, MFP2 polarizes to the pseudopod and appears to become brighter again. The detection of MFP2 within the pseudopods indicates that the protein itself is not completely degraded since spermatids lack ribosomes and are thus incapable of synthesizing new MFP2.

MFP2 colocalizes with MSP throughout meiotic divisions

Because MFP2 appears to localize to the FBs during meiosis, we wanted to examine the extent to which it colocalized with MSP. To check for colocalization, we

labeled wildtype worms with anti-MFP2 and anti-MSP antibody and visualized them together (figure 6). In wildtype cells undergoing meiosis, MFP2 colocalizes with MSP in FBs. In addition, this colocalization appears to be perfect; the MFP2 pattern completely overlaps with MSP in the FB and extends no further. After the completion of the meiotic divisions, MSP and MFP2 stains become diffuse at the same time.

Intriguingly, we also observed differences between MSP and MFP2's signal intensity during spermatid maturation. While the signal intensity of MFP2 drops significantly at the end of the meiotic divisions, the MSP signal stays the same (figure 5). Consequently, when mature and immature spermatids are exposed in the same field, the MFP2 signal dominates in the immature spermatids, while the MSP signal dominates in the mature spermatids. We have observed this change in signal strength consistently in WT and it appears to occur concurrently with FB breakdown during spermatid maturation.

Following the meiotic divisions, both MFP2 and MSP localize to the pseudopod. Consistent with the observation in *A. suum* that MFP2 localizes along the entire length of the MSP fibers *in vivo*, we observed MFP2 colocalization with MSP throughout the pseudopod and there was no region of the pseudopod where either was present in the absence of the other (figure 5).

MFP2 colocalizes with MSP in the C. elegans relative C. remanei

Although it was apparent that MFP2 colocalizes with MSP in *C. elegans*, we wanted to know if there was evidence that this pattern could apply to related species of nematodes. *C. remanei* was an ideal candidate for this experiment for several reasons. To

begin with, our antibody recognition site was highly conserved in *C. remanei*, and it was probable that we would be able to visualize MFP2's pattern with the same degree of precision as in *C. elegans*. Furthermore, unlike *C. elegans*, *C. remanei* is a male-female species, and, consequently, has been subjected to strong sperm competition selection pressures that have led to the evolution of larger sperm cells than in *C. elegans*. As a result, although *C. remanei* sperm utilize MSP for locomotion, their sperm is significantly larger than in *C. elegans*. We hoped that the larger sperm size would allow us to visualize MFP2's pattern more clearly.

The results of this study showed that, as in *C. elegans*, MFP2 in *C. remanei* colocalizes with MSP throughout the meiotic divisions (figure 7) and also colocalizes with MSP in the pseudopod. In contrast to our *C. elegans* results, however, MFP2 also appears to form structures or aggregates in many mature spermatids that are distinct from fibrous bodies. In other spermatids, both MFP2 and MSP distribute throughout the cytoplasm (figure 7 and 8). The temporal progression, however, remains unclear. We are uncertain if MFP2 localizes to aggregates prior to becoming cytosolic, or whether it aggregates after becoming cytosolic.

In order to investigate the aggregation of MFP2 more carefully, we took a multi-dimensional image of MFP2 aggregates and then ran a deconvolution algorithm (figure 8). This revealed that MFP2 aggregates do not appear to be regular structures, like FBs, but are instead rough accretions of MFP2. Furthermore, there does not appear to be subcellular localization pattern; instead MFP2 aggregates throughout spermatids. However, though MFP2 forms aggregates, it does not seem likely that a well-conserved protein would spontaneously form aggregates in the absence of additional amino acid

changes. For this reason, the most likely explanation is that MFP2 is binding to existing structures in the spermatids, though the identity of these structures is unknown.

MFP2 localizes with MSP in gsp-3/4 mutants

Although MFP2 colocalizes with MSP in wildtype *C. elegans* worms, we were curious to determine how the localization of MFP2 might be affected in spermatogenesis-defective mutants with defects in fibrous body disassembly. Of particular interest to us were mutants defective in the PP1 phosphatases, GSP-3 and GSP-4 (J. Wu et al., 2012). GSP-3 and GSP-4 are a pair of PP1 phosphatases that are thought to play multiple roles throughout spermatogenesis (J. Wu et al., 2012). Mutants defective in GSP-3/4 produce spermatids with abnormal or no chromatin and persistent MSP structures (Messina, 2012; J. Wu et al., 2012). MSP structures in *gsp-3/4* mutants appear to be morphologically distinct from FBs, though it is unclear what accounts for this difference (unpublished data). In addition, although *gsp-3/4* mutants are incapable of fertilization, their spermatids are capable of activating and forming spermatozoa. However, though these spermatozoa form pseudopods with polarized MSP, they retain distinct MSP structures within their cell bodies, suggesting that some portion of the MSP structures fail to breakdown correctly (J. Wu et al., 2012).

We were curious whether MFP2 had a preferential affinity for either the MSP in structures, or the cytosolic MSP. To examine this, we labeled both MSP and MFP2 in non-celibate *gsp-3/4* mutants (figure 9). Our analysis revealed that MFP2 localized with MSP in the persistent FB-like structures that exist in *gsp-3/4* mutants. In addition, we also observed that, in activated spermatozoa, MFP2 was clearly present in both the pseudopod

and the FB-like structures suggesting that, like MSP, some portion of MFP2 was releasing from the FBs (Compare figures 9 and 6).

In addition, we also observed an odd effect in the relative MFP2-MSP signal strength. While in WT, MFP2 appears bright relative to MSP in immature spermatids and dim in mature spermatids, the spermatids in *gsp-3/4* mutants exhibited a range of shades. Immature spermatids that had just completed the meiotic divisions appeared to have the highest MFP2 to MSP ratio, but the rest of the spermatids were heterogeneous. Lastly, in some cases, we observed some cells with a very high MFP2 to MSP ratio, although the nature of this staining is anomalous.

MFP2 colocalizes with MSP in fer-6 (hc6) mutants.

Because MFP2 localizes with MSP in *gsp-3/4* mutants, we were curious whether it would also colocalize with MSP in *fer-6 (hc6)* mutants. Although the identity of the protein that *fer-6* encodes is unknown, the *fer-6 (hc6)* allele has been partially characterized. These mutants contain abnormalities in pseudopod formation and FB breakdown; they often contain persistent FBs, or larger inclusion bodies thought to be made up of paracrystalline MSP (Ward et al., 1981)s. However, unlike *gsp-3/4* mutants, some spermatids contain cytosolic MSP and are capable of forming a pseudopod (Ward et al., 1981). Consequently, we were curious whether, like *gsp-3/4* mutants, MFP2 would closely colocalize and follow MSP in *fer-6 (hc6)* mutants. In addition we also wanted to know whether there were any abnormalities in the MFP2 to MSP intensity change observed in WT.

We labeled *fer-6* mutants with both MFP2 and MSP (figure 10). In these mutants, MFP2 colocalizes with MSP in FBs. In addition, we also observed an abnormally high number of spermatids with MSP structures in them, suggesting that the process of FB breakdown may be prolonged in *fer-6* mutants. Furthermore, the MSP structures did not appear to be as regularly structured as in WT and appeared similar to the persistent MSP structures in *gsp-3/4* mutants. However, unlike *gsp-3/4* mutants, we do not believe these structures to be completely persistent because we observed a number of spermatids with cytosolic MSP. These spermatids tended to be located at the most proximal end of the gonad, suggesting a temporal relationship.

The MFP2 to MSP signal intensity change was also abnormal in *fer-6* mutants. Unlike WT, there did not appear to be a sharp delineation between immature and mature spermatids. Instead, the MFP2 signal appeared to get dimmer while MFP2 was still localized to structures.

Quantification of the MFP2 to MSP ratio reveals patterns in WT, fer-6 and gsp-3/4

Although we had previously observed that the MFP2 to MSP signal ratio appeared to drop in WT and that this process appeared perturbed in *gsp-3/4* and *fer-6* mutants, we wanted to quantify this effect. Using sperm spread preparations from seven WT worms, we took images with both MFP2 and MSP. We then measured the mean intensities of both immature and mature spermatids across a consistent area that was determined by the size of immature spermatids. Lastly, we compared the signal intensities in immature spermatids and mature spermatids for both MSP and MFP2 and graphed the result (figure 11). This analysis revealed that the average MFP2 signal

consistently dropped during the process of the spermatid maturation; the average fold-decrease in signal intensity was 2.95 ± 0.317 . Surprisingly, however, we also discovered that the MSP signal did not decrease during spermatid maturation; the average change in signal intensity was 0.97 ± 0.116 . Consequently, it appears that changes in the MFP2 to MSP signal intensity can be primarily attributed to changes in the MFP2 signal. It further implies that the ratio of MFP2 to MSP, however, can be used as a control for any random changes in the signal intensity within an image.

Having established the MFP2 to MSP signal ratio changes during spermatid maturation in wildtype males, we repeated our analysis on *gsp-3/4* and *fer-6 (hc6)* mutants, taking care to include spermatids that had just budded off the residual body. Although the numerical data cannot be directly compared to WT we observed differences in the patterns between all three data sets (figure 12).

In *gsp-3/4* mutants, the MFP2 to MSP signal ratio did not appear to have a sharp delineation between immature and mature spermatids. Instead, there appeared to be a range of values, though immature spermatids that had just budded still appeared to have the highest values. In *fer-6 (hc6)* mutants, on the other hand, there was distinct gap in the data. Spermatids that had just budded appeared to have the highest values. All other spermatids, however, appeared to have similar values. This was surprising because most of those spermatids appeared to contain MSP structures. However, it appears that in *fer-6* mutants the MFP2 to MSP ratio drops off normally, even as MSP persists in structures.

Bioinformatics identifies putative phosphorylation residues on MFP2

Because MFP2 is known to be phosphorylated in *A. suum* by the ser/thr kinase MPAK, we wanted to know if there were any putative phosphorylation sites on MFP2 and where they were located (Yi et al., 2007a). In order to do this, we utilized two different phospho-site predictors, NetPhos and Phosida (Table 2A and 2B) (Blom et al., 1999; Gnad et al., 2007). Each program uses different databases and methodology to predict potential phospho-sites. Both programs produced a list of predicted phospho-sites. Interestingly, all of the sites that were predicted by NetPhos were also present on the Phosida, though their scores were different in each case. Because each program used different methodology to predict phospho-sites, we think that sites that overlap between the two programs are more likely to represent actual phospho-sites.

Based on these predictions, we also decided to explore the hypothesis that changes in phosphorylation status could explain the signal changes that occur to MFP2 during FB breakdown. One hypothesis is that phosphorylation of one or multiple amino acids interfere with antibody binding. However, the absence of any serine, threonine and tyrosines inside the antibody-binding site meant that we could rule out the possibility of direct interference of antigen recognition by phosphorylated residues. The possibility remained, however, that the phosphorylation of nearby amino acids could sterically hinder binding of our antibody.

In order to investigate this possibility, we took the predicted phospho-sites that overlapped between Phosida and NetPhos and mapped them to the predicted structure of MFP2 produced by I-TASSER (figure 13) (Roy et al., 2010; Zhang, 2008). This mapping revealed that most sites were not close to the antibody-binding site. The closest site, Ser8, could potentially interfere with antibody binding, but it seems unlikely.

Consequently, we conclude that if changes in MFP2 signal are due to differences in its phosphorylation state, then this effect is due to phosphorylation of a residue that did not overlap between the Phosida and NetPhos lists, indirect steric hindrance caused by changes in protein folding induced by phosphorylation, or changes in the binding of an unidentified accessory protein that is affecting the antibody-antigen interaction.

MFP2 contains a doublet in western blot samples

In order to more directly investigate the phosphorylation status of MFP2, we produced high quantities of *fem-3 (q20gf)* worms that were prepared for western blots. These samples revealed that MFP2 appears to naturally form a doublet, which may be indicative of post-translation modification (figure 14). The second band appears to run just beneath the first band. In order to examine this band more closely, we decided to optimize the gel for separation of the doublet by running samples on a 10% gel long enough that several lower MW standards were run off the gel. This produced a much greater separation of the bands.

Over the course of multiple preparations of *fem-3 (q20gf)* worms, we observed that the higher MW band was consistently more abundant than the lower MW band. In addition, because we were using *fem-3 (q20gf)* worms, which do not produce spermatozoa, we know that the doublet is present either in meiotic cells, in spermatids, or both (figure 14). However, we do not yet know if this doublet is the result of a phosphorylation event, or if it is the result of another post-translational modification or cross-reaction between another protein.

Discussion and Future Directions:

Previous studies in *Ascaris* identified the MSP accessory protein MFP2 as a regulated enhancer of MSP polymerization in crawling spermatozoa (Buttery et al., 2003b; Grant et al., 2005b; Yi et al., 2007a). This study is the first to investigate MFP2 dynamics throughout spermatogenesis and in the genetically tractable system of *C. elegans*. Using a combination of bioinformatics, immunofluorescence, image analysis and biochemistry, we have explored the stage-specific properties of MFP2 throughout spermatogenesis in both *C. elegans* and *C. remanei*. Our studies suggest that the MFP2 protein is conserved at both an amino acid and structural level in multiple species of nematodes. Furthermore, we have characterized the localization pattern of MFP2 and shown that it colocalizes with MSP throughout all stages of spermatogenesis in *C. elegans* and *C. remanei*. During spermatogenesis, MFP2 colocalizes with MSP along the length of fibrous bodies (FBs). During spermatid maturation in *C. elegans*, the MFP2 pattern becomes diffuse. In contrast, MFP2 within the mature spermatids of *C. remanei* appears to exist in separate aggregates. Nevertheless, in both *C. elegans* and *C. remanei* spermatozoa, MFP2 ultimately localizes with MSP in the pseudopod. In addition, image analysis of wildtype mature and immature spermatids revealed that the process of spermatid maturation involves a predictable drop in the average MFP2 signal intensity that likely corresponds to a change in the conformation of MFP2. This change, however, is perturbed in *gsp-3/4* and *fer-6 (hc6)* mutants; in the former case, there was a range of intensities while in the latter case the signal drop appeared to occur precociously because MSP was still polymerized into structures. Lastly, both bioinformatics and western blots suggest that MFP2 may be phosphorylated prior to its localization to the pseudopod.

Overall, this work has identified MFP2 as a key MSP accessory protein and provides the first direct link between MSP organization in the pseudopod and MSP organization in FBs.

MFP2 conservation between different species suggests that it has an important role

Previous work in *A. suum* showed that MFP2 associates with MSP fibers in the pseudopod of spermatozoa (Buttery et al., 2003a). In addition, *in vitro* work showed that, in the presence of sperm cell extract, it was capable of enhancing MSP polymerization. Based on the crystal structure of MFP2, a model was proposed whereby MFP2's interaction with MSP was analogous to the interaction of formins with actin (Grant et al., 2005a). In this model, MFP2 enhanced MSP polymerization by binding MSP dimers and positioning them for incorporation into a growing MSP filament (Grant et al., 2005a). Once incorporated, the authors also proposed that MFP2 may serve a stabilizing effect (Grant et al., 2005a).

Our initial bioinformatics work supported this model. We used BLAST searches and the I-TASSER program to show that both the MFP2 primary amino acid sequence and the predicted structure were conserved between different species of nematodes. This high level of amino acid conservation along the entire length of MFP2 in multiple nematode species, supports the hypothesis that MFP2's primary function is structural in nature. Furthermore, since the linker region that joins adjacent MFP2 domains is thought to be relatively inflexible, the ability of MFP2 to bind MSP subfilaments would be predicted to require a high degree of structural conservation. Conversely, if MFP2 was

functioning catalytically, we might expect high levels of amino and an structural conservation to be limited to the binding, catalytic and regulatory sites

MFP2's localizes to FBs and may play a role in their development

Because FBs are thought to be primarily composed of MSP, we compared the MFP2 and MSP localization patterns throughout spermatogenesis. This data showed that MFP2 and MSP colocalize on FBs in both *C. elegans* and *C. remanei*. In addition, this colocalization was precise; MFP2 localized with MSP along the entire length of the FB and there did not appear to be regions of the FB where MFP2 was not present. Based on its localization with MSP in the pseudopod, the most likely explanation is that MFP2 in the FBs is associated with MSP in the same manner as in the pseudopod. In the absence of direct evidence, the simplest model is therefore that that MFP2 directly binds MSP subfilaments in both cases. However, because MSP is arrayed in a paracrystalline in FBs, it remains unclear whether or not MFP2 is associated throughout the body of the FB, or whether it is located predominantly on the outside of the FBs.

Regardless of its actual localization within the FB, though, MFP2's colocalization of MSP in the FBs and the pseudopod has implications for understanding how MSP is controlled. Although previous work has identified other MSP accessory proteins that are present in the pseudopod, such as GSP-3/4 and SPE-6, they do not localize to the FBs. In addition, the only other protein known to colocalize with MSP in the FB, SPE-7, is not present in the pseudopod. Consequently, MFP2's presence in the FBs is the first direct relationship between the molecular machinery that controls MSP in the FBs and the pseudopod.

In spite of this, it is unclear to what extent MFP2 is functionally active when it is associated with FBs. In the pseudopod, MFP2's enhances MSP polymerization (Grant et al., 2005b). However, once FBs are formed, their lengths appear to be stable, and, thus, not actively polymerizing (Messina, 2012). Consequently, two immediate hypotheses present themselves for MFP2's localization to FBs. The first is that MFP2 is playing an active role in promoting FB formation in the same way that it enhances MSP polymerization in the pseudopod. In this case, MFP2's function during FB assembly would be essentially the same as its function in building subfilaments within the pseudopod, and it would be expected to have the same biochemical properties. In this model, however, it is unclear what protein would serve the role of MPAK, which phosphorylates MFP2 only at the leading edge of the pseudopod. Furthermore, since elongation of FBs is thought to occur at both ends, any associated kinase would have to function at both ends of the FB.

In an alternative model MFP2 may play no structural role in FB assembly. Instead, MSP and MFP2 colocalize to the FBs to prevent them from interfering with actin and tubulin mediated functions during the meiotic divisions and to facilitate their segregation to the spermatids during the budding division

Testing these two hypotheses should be relatively straightforward. In the former model, MFP2 plays an active and necessary role in FB formation, while in the latter model it is only functionally active in the pseudopod. As a result, knocking out or knocking down MFP2 would result in different phenotypes depending on which model is correct. If MFP2 is required for correct FB formation, we would hypothesize that loss of MFP2 would cause defects in FB formation, potentially by preventing or slowing their

assembly. This could result in either an early arrest phenotype similar to *spe-44* mutants, or else an extension of FB growth into Metaphase I or later. If, on the other hand, MFP2 is not required for FB formation, we would hypothesize that FB formation would proceed normally, but that there would be later defects in spermatozoa motility. These experiments could be accomplished using either RNAi knockdown or CRISPR-Cas knockouts of the gene that encodes MFP2.

In addition to its localization to FBs during meiosis, we also observed that MSP became cytosolic in mature spermatids of *C. elegans*. This is interesting because the model for MFP2 function suggests that the stabilization effect that MFP2 has on MSP subfilaments requires it to bind MSP tetramers. However, cytosolic MSP is thought to exist in a dimerized form. Consequently, it is unknown whether or not cytosolic MFP2 is associated with MSP dimers, or whether it is not bound to MSP at all. The easiest way to test this hypothesis would be to perform co-immunoprecipitations and attempt to pull down MSP in populations with an abundance of mature spermatids. These experiments were attempted, however they have proven unsuccessful due, apparently, to the poor affinity of the MFP2 antibody to MFP2 protein (data not shown).

Lastly, although MFP2 appears to become cytosolic in mature spermatids of *C. elegans*, we did not observe this in mature spermatids of *C. remanei*. Instead, MFP2 appeared to form aggregates in mature spermatids of *C. remanei*. However, it remains unclear what MFP2 is associated with in *C. remanei*.

The intensity of MFP2's signal drops in mature spermatozoa

When MFP2 becomes cytosolic in mature spermatids, we observed that the average MFP2 signal intensity dropped over the course of spermatid maturation. This signal change was regular and consistent, and, in WT, was always temporally correlated with FB breakdown and MSP becoming cytosolic. Visually, the signal intensity appeared to increase again in the pseudopods but we do not yet have direct quantitative data confirming this observation. Consequently, we think the most likely explanation is that the signal intensity change that MFP2 undergoes over the course of spermatid maturation likely corresponds to a change in the affinity of our antibody for MFP2. If this is the case, then the change in signal intensity we observe is a proxy for the change in MFP2 conformation that occurs when MFP2 becomes cytosolic. Because our data shows that MFP2 has multiple predicted phosphorylation sites, one form of MFP2, either modified or unmodified, may have greater affinity for our primary antibody. An alternative hypothesis, however, is that MFP2 is being degraded over the course of spermatid maturation. If that is the case, then the drop in signal intensity is due to a change in absolute protein level.

In order to distinguish between these hypotheses, we will need to perform western blots on aged *C. elegans* worm samples and compare them to a protein present in mature spermatids that remains constant such as MSP or SPE-6. If MFP2 protein levels do not drop during spermatid maturation, then the ratio of MFP2 to the second protein should not change over time in aged worm samples. If, on the other hand, MFP2 is degraded, then SPE-6 or MSP levels should increase relative to MFP2 as the worms accumulate spermatids. However, we favor the former hypothesis based on the difficulty of pulling down MFP2 in our immunoprecipitation experiments. Because our lysis protocol does

not denature proteins, it is expected that a problem with antibody-antigen interactions would occur in IPs.

In order to better understand the change in MFP2 signal intensity, as well as MFP2 localization in general, we looked at both *gsp-3/4* and *fer-6 (hc6)* mutants. In *gsp-3/4* mutants, FBs form and correctly partition in FBs. However, the process of spermatid maturation is disrupted. In *gsp-3/4* spermatids, some MSP appears to remain in structures, while some MSP becomes cytosolic and is later capable of polarizing to a shortened pseudopod. This creates a heterogeneous population of spermatids made up of young spermatids that have just completed meiosis and have FBs with normal morphology, older spermatids in which some MSP is cytosolic while some remains in structures, and an activated population of spermatids/spermatozoa in which MSP is both polarized into a pseudopod and present in MSP structures.

When we examined MFP2's localization in *gsp-3/4* mutants, we observed that MFP2 appears to colocalize with MSP in these structures. In addition, we noticed that in activated spermatozoa, some MFP2 localized with MSP in the pseudopod, while some remained associated with the structures in the cell body. This suggests that MFP2 exists in the same heterogeneous state as MSP itself; some of it remains associated with FBs, while some becomes diffuse with MSP and capable of ultimately polarizing to the pseudopod.

Furthermore, we observed abnormalities in the MFP2 to MSP signal ratio in *gsp-3/4* mutants; the MFP2 to MSP signal appears to form a range of values within the image. The MFP2 signal did not appear to ever get as low as it did in WT. If a change in MFP2 signal intensity is indeed due to a change in MFP2's structural conformation, then this

data could be explained by the heterogeneous population of MFP2 in the spermatids. If the MFP2 that remains associated with MSP structures is brighter than the MFP2 that becomes cytosolic, then we would expect the average intensity to be in the mid-range. Alternatively, if the change in MFP2 signal intensity is due to MFP2 degradation, then it means that in *gsp-3/4* mutants less MFP2 is degraded than in WT.

In addition to *gsp-3/4* mutants, we also wanted to examine *fer-6 (hc6)* mutants, which are defective in an unknown gene. *fer-6 (hc6)* mutants are described as having persistent FBs, though not to the same extent as *gsp-3/4* mutants, because we have observed numerous occasions where MSP is cytosolic (data not shown). When we looked at these mutants, we observed MSP structures in the spermatids that were morphologically distinct from FBs. However, it was unclear to what extent they differed from the MSP structures in *gsp-3/4* mutants. In addition, we also observed that MFP2 appeared to colocalize with these structures, though they appeared dimmer. To our surprise, when we quantified this effect, we noted that the MFP2 to MSP signal ratio in spermatids with persistent MSP structures was the same as the MFP2 to MSP ratio in mature spermatids. This suggests that the process of spermatid maturation, as it relates to MFP2, is not intrinsically tied to MSP becoming cytosolic. Instead, relating back to the proposed explanations for the MFP2 signal drop, the potential explanations for this effect are that MFP2 is being degraded even though MSP structures persist, MFP2 is switching conformation while associated with MSP, or else the vast majority of MFP2 becoming cytosolic and a small quantity remaining associated with the MSP structures.

One model that would explain the difference between WT, *gsp-3/4* and *fer-6 (hc6)* is that the process of spermatid maturation is extended in *fer-6 (hc6)*, *gsp-3/4*, or

both. Consequently, steps that occur virtually simultaneously during normal spermatid maturation may be asynchronous in *fer-6 (hc6)* and *gsp-3/4*.

Bioinformatics and western blots suggest that MFP2 is phosphorylated

Previous *in vitro* experiments on MFP2 showed that it was phosphorylated by the S/T kinase MPAK on an unknown amino acid residue. Phosphorylated MFP2 exists as a gradient down the length of a growing MSP subfilament with the highest concentration present at the polymerizing end. We attempted to explore the possibility of MFP2 phosphorylation using bioinformatics and western blots to determine if MFP2 is phosphorylated earlier in spermatogenesis, and whether this phosphorylation could account for the changes in the MFP2 signal intensity that occur during spermatid maturation.

Using two different programs, we identified putative phosphorylation sites for MFP2. When mapped to an I-TASSER predicted model for MFP2, most of these phosphorylation sites did not map close enough to interfere with antibody-antigen binding. The closest site, however, may be close enough to account for this effect, but the data is inconclusive. A second possibility is that phosphorylation of MFP2 induces a conformational change that allows increased or decreased antibody access.

However, when we performed a western blot on MFP2, we observed two bands that potentially represent a phosphorylated and non-phosphorylated form of MFP2. In addition, these experiments were performed on *fem-3 (q20gf)* mutants, which do not produce spermatozoa. Consequently, if the doublet we observed on the western blot does

indeed represent a phosphorylated residue, then it would be present either when MFP2 associated with FBs, or when it is cytosolic.

In order to test this effect, we first intend to run aged MFP2 samples on a phosphogel, which should separate out phosphorylated bands. We could confirm this effect by treatment of our samples with phosphatases to determine whether or not bands disappear. Once we have identified the phosphorylated band, we could determine at what stage the phosphorylated form appears by performing western blots on aged *fem-3 (q20gf)* samples, which progressively accumulate spermatids, and compare the relative abundances of MFP2 and MSP.

One hypothesis is that the phosphorylated form of MFP2 is present in FBs, but not spermatids, which would be consistent with previous data on MFP2 that showed that it was phosphorylated when associated with MSP. A second hypothesis, however, is that MFP2 is phosphorylated when cytosolic, in which case, it would likely be phosphorylated at a different site in mature spermatids than in the pseudopod. The latter hypothesis could be tested using either mass spectrometry or site-directed mutagenesis of predicted phosphorylation residues in conjunction with western blots.

Figures

<i>A. suum</i> (MFP2a)	1	MTT-KEFEDTWAYNTIGSPFPDNPVRVKGQQNMYVALWYKFG
<i>C. elegans</i>	1	MP--VAKEDSWAFQPIGSPFPEAPVRVNPQNNQYVALWYKHG
<i>C. remanei</i>	1	MPVaVAKEDSWAFQPIGSPFPEAPIRVNPQNNQYVALWYKHG
<i>A. suum</i> (MFP2a)	42	KPIHGRAWNDNGNVECSFPYNKVELTGARDLGGQIQILTATE
<i>C. elegans</i>	41	KPIHGRAWNDNGVVECSFPYNKAELKGKLDLGGQIQIL----
<i>C. remanei</i>	43	KPIHGRAWNDNGVVECSFPYNKAELKGKQDLGGQIQIL----
<i>A. suum</i> (MFP2a)	84	QDPTEQFKKTGFWEWRPYKDRVNDQ--LLQLVRCGQSTPVI
<i>C. elegans</i>	79	-QYKGDYNSLGYWYEWLPLKQRHENNEGIREIVRCGNSVPVL
<i>C. remanei</i>	81	-QYKGDYNSLGYWYEWLPLKQRHENNEGIVREIVRCGNSVPVL
<i>A. suum</i> (MFP2a)	124	MKTKDGGKDLLGYIDMSTEVAAVGVSGKSEQVAGGPIQDMLVL
<i>C. elegans</i>	120	AKLKDGTDKLGFLLDLNTEVALFSNAGTTEKYEGGATANFMTI
<i>C. remanei</i>	122	AKLKDGTDKLGYLDELNTEIALFSNGGTEKFEFGGATANFMTI
<i>A. suum</i> (MFP2a)	166	FRNVKAPPKGIKIYDDTWLCLKYRDPFPAakNPIAAGGRKVK
<i>C. elegans</i>	162	FRNLRPPTGLKVYDDLWYDLRYGDNFPS--NAVPADGRALN
<i>C. remanei</i>	164	FRNLRPPTGLKVYDDLWYDLRYGDTFPS--NAVPADGRALN
<i>A. suum</i> (MFP2a)	208	SDDGTEMfQYVALWYKHGQPVFGRAYPDSADKTLANFGWGGQ
<i>C. elegans</i>	202	TETGPHM-QYVALWYKHGD PVFGRSYPSSAGKTMAHFGKNNQ
<i>C. remanei</i>	204	TETGPHM-QYVALWYKHGD PVFGRAYPNSAGKTNAHFGKNNQ
<i>A. suum</i> (MFP2a)	250	ENAGAEIGSFHMLVVPDPDILGFYKWIPIYKEAKAGGpFKPL
<i>C. elegans</i>	243	ENAGPEVGSMLLTVPEASCMGLEYKWMPLSEGKSSG-WTTV
<i>C. remanei</i>	245	ESAGPEVGSPLLTVPEASCMGLEYKWMPLAEGKSSG-WTVV
<i>A. suum</i> (MFP2a)	292	HVGECTPCLLKDANGTERLGNLHMGMEKATAGLAGKDSAVSG
<i>C. elegans</i>	284	HIGNSAPCILKDDKGLEVLGNLDLTIEKASAGYGGKEKIMTG
<i>C. remanei</i>		HIGNAAPCILKDEKGLEVLGNLDLTIEKASAGYGGKEKIISSG
<i>A. suum</i> (MFP2a)	334	PAVGDFLVLCRN---
<i>C. elegans</i>	326	AAVAKLKVLFKRRLA
<i>C. remanei</i>		GAVAALKVLFKRRLA

Table 1: *C. elegans* paralogs to ZK265.3

Species	Protein	E-value	Identity
<i>C. elegans</i>	ZK265.3	0.0	0.0
<i>C. elegans</i>	KO8F8.5	9e-79	42%
<i>C. elegans</i>	Y69E1A.2	1e-78	42%
<i>C. elegans</i>	Y59E9AL.2	3e-77	41%
<i>C. elegans</i>	ZK546.7	2e-62	39%
<i>A. suum</i>	MFP2a	6e-125	56%

Figure 1: Alignment of the MFP2 amino acid sequence between different species

The primary amino acid sequences of MFP2 proteins in *A. suum*, *C. elegans* and *C. remanei*. Amino acids are colored for identity, so that residues in red represent conservation between all three proteins, residues in blue represent residues conserved between *C. elegans* and *C. remanei*, and similar amino acids are colored green. The antibody binding site is boxed in green.

(Table 1) *C. elegans* contains paralogs to ZK265.3 that share less similarity to the *A. suum* MFP2 protein.

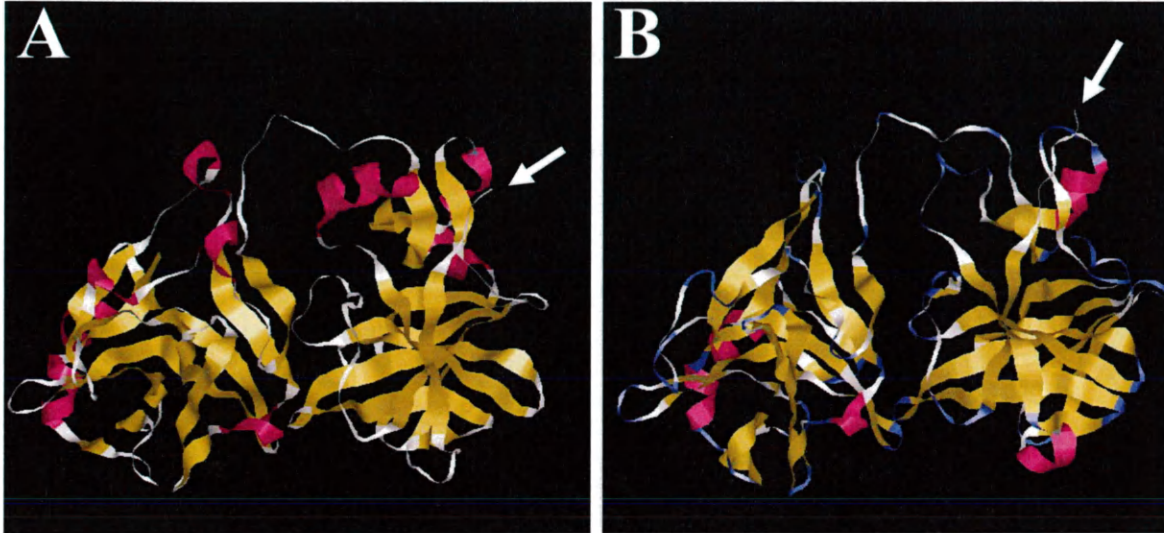


Figure 2: A comparison of the predicted structure of MFP2 in *C. elegans* compared to the crystal structure of MFP2 in *A. suum*

Ribbon views of the (B) crystal structure of MFP2 in *A. suum* shows that it is similar to the (A) I-TASSER predicted structure of ZK265.3 in *C. elegans*. Arrows show the C-termini of both proteins. Alpha helices are in red and beta sheets are in yellow.

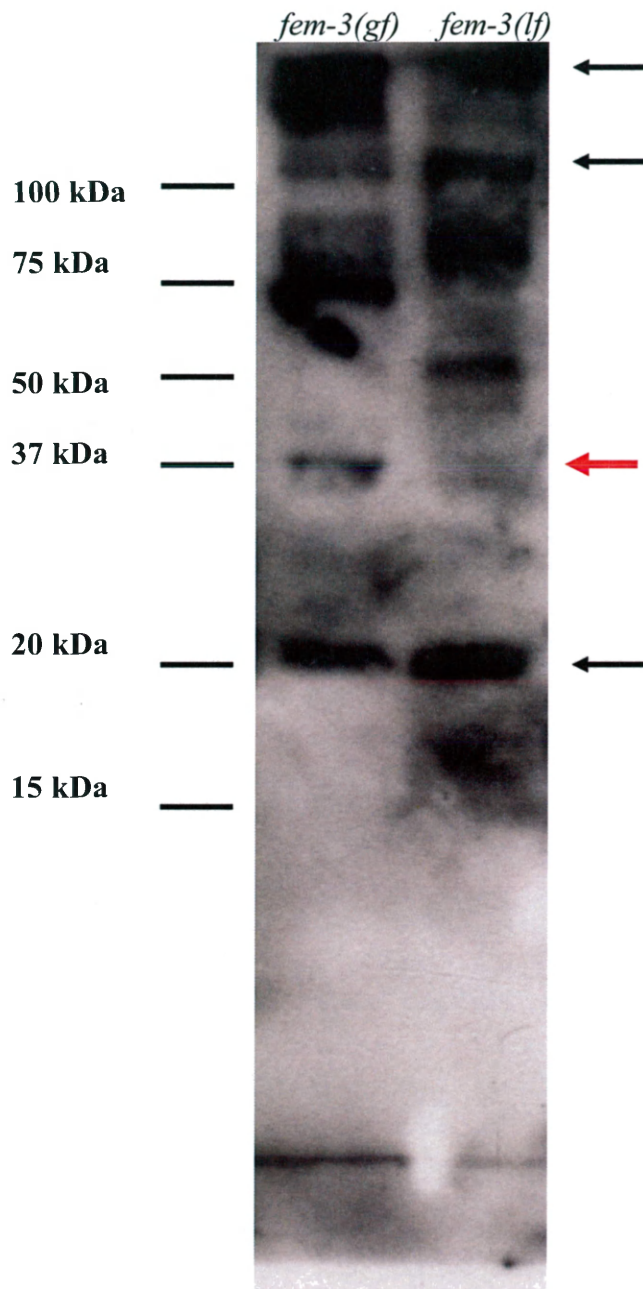


Figure 3: Western blot of *fem-3* (gf) and *fem-3* (lf).

Western blot of with *fem-3* (gf) and *fem-3* (lf) labeled with anti-MFP2 antibody. A visible band is present at ~37 kDa (red arrow) that is absent in *fem-3* (lf) samples. A number of other bands (arrows) are present in both samples and are likely non-specific.

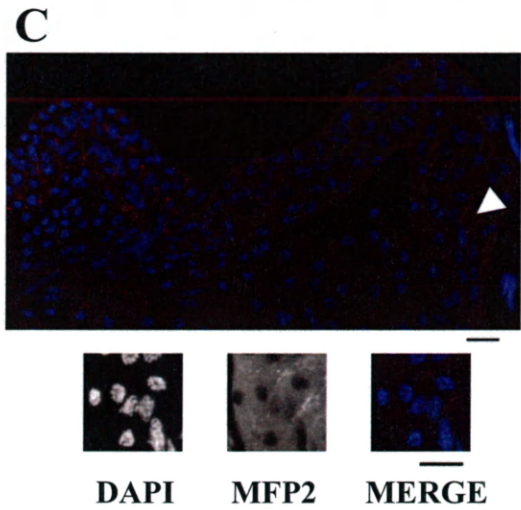
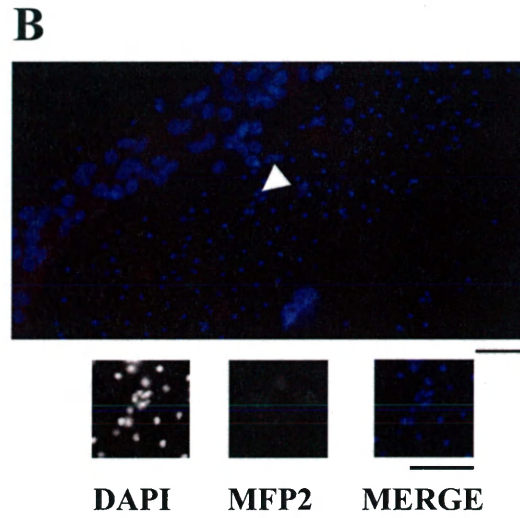
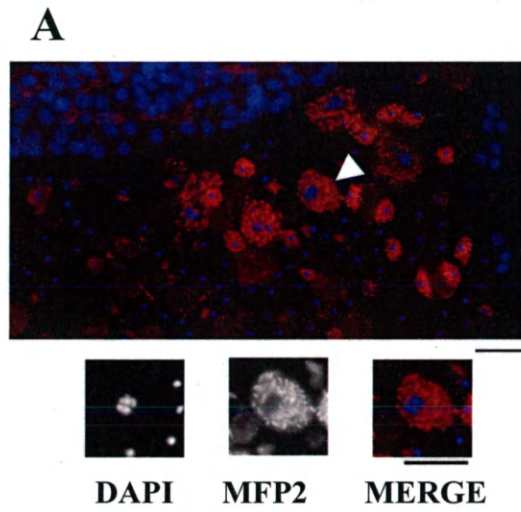


Figure 4: Anti-MFP2 labeling in WT sperm spreads and negative controls.

(A) Immunofluorescence using anti-MFP2 primary antibody and a TRITC secondary (red) of WT. (B) As a negative control, only the secondary antibody was applied to the slide. (C) As an additional control, anti-MFP2 primary antibody and a TRITC secondary (red) were incubated with *spe-44* mutants. Representative cells have been enlarged and placed below each figure, with arrows denoting their original location. Scale bars are 10 μ m.

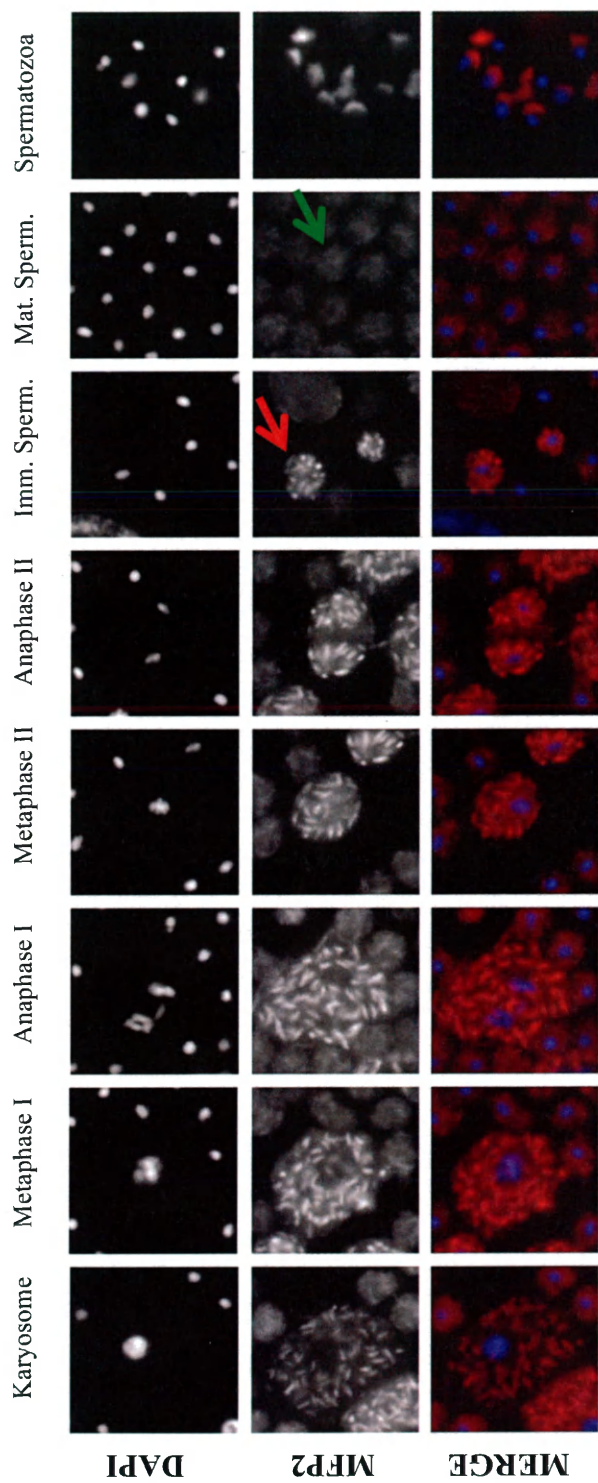


Figure 5: MFP2 staining in WT.

Labeling MFP2 (red) and DAPI show that MFP2 appears to localize to FBs throughout both meiotic divisions. In immature spermatids (imm. sperm.), MFP2 persists in structures (red arrow) before becoming diffuse (green arrow). In spermatozoa, it localizes to the pseudopod. Scale bars are 10µm.

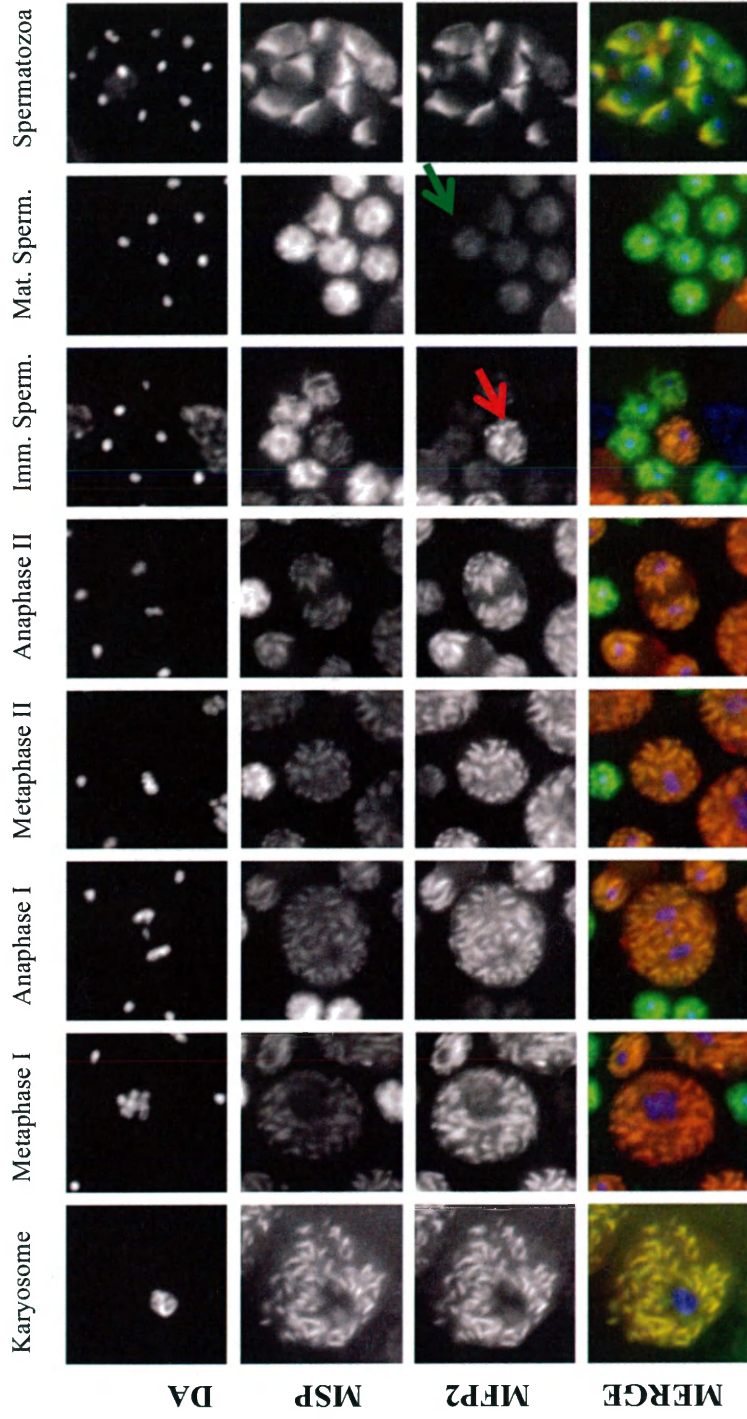


Figure 6: A comparison of MFP2 and MSP localization in WT.

Panel of images from different cell stages labeled with MSP (green) and MFP2 (red) showing perfect colocalization. In immature spermatids (red arrow), the MFP2 signal is bright while in mature spermatids (green arrow) the signal is dimmer. In spermatozoa, MFP2 and MSP colocalizes to the pseudopod and overlaps completely. Scale bars are 10µm.

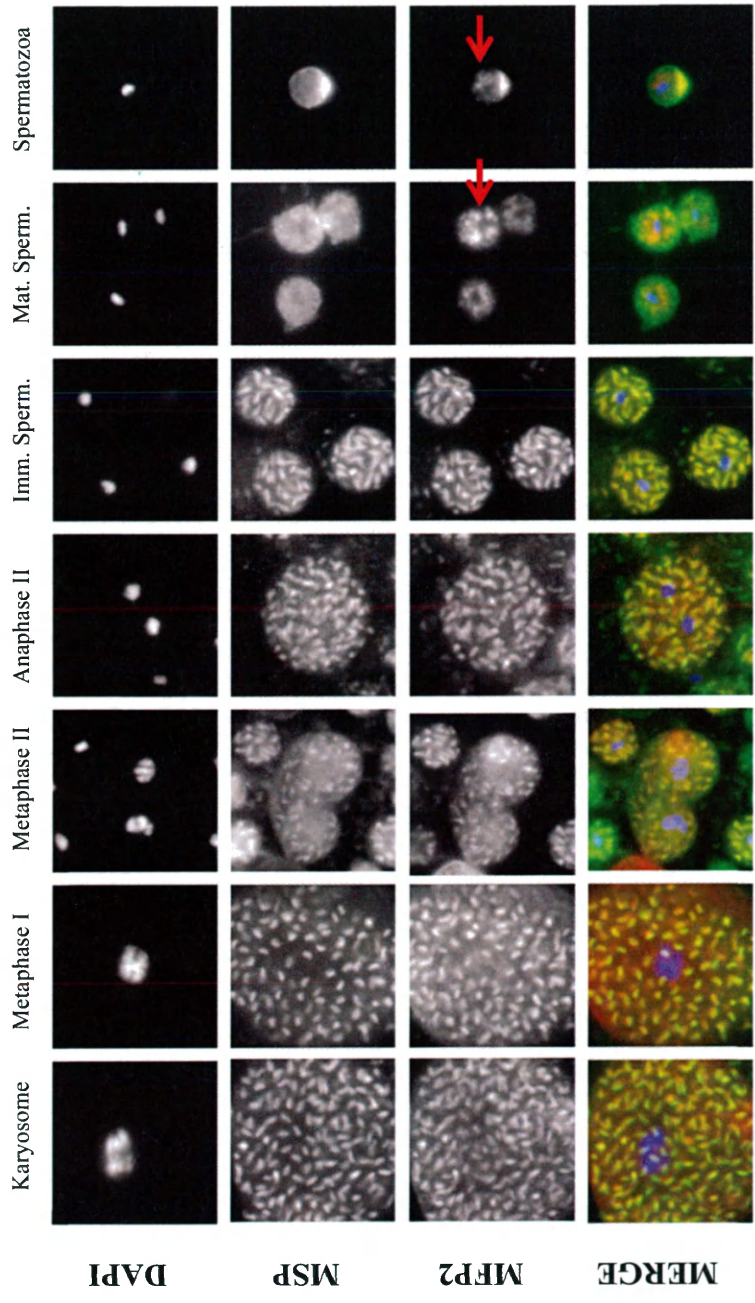


Figure 7: A comparison of MFP2 and MSP localization in *C. remanei*
 Labeled MSP (green) and MFP2 (red) colocalize in *C. remanei* throughout meiosis. In mature spermatids, MFP2 forms aggregates (arrow) that may persist in spermatozoa (arrow)

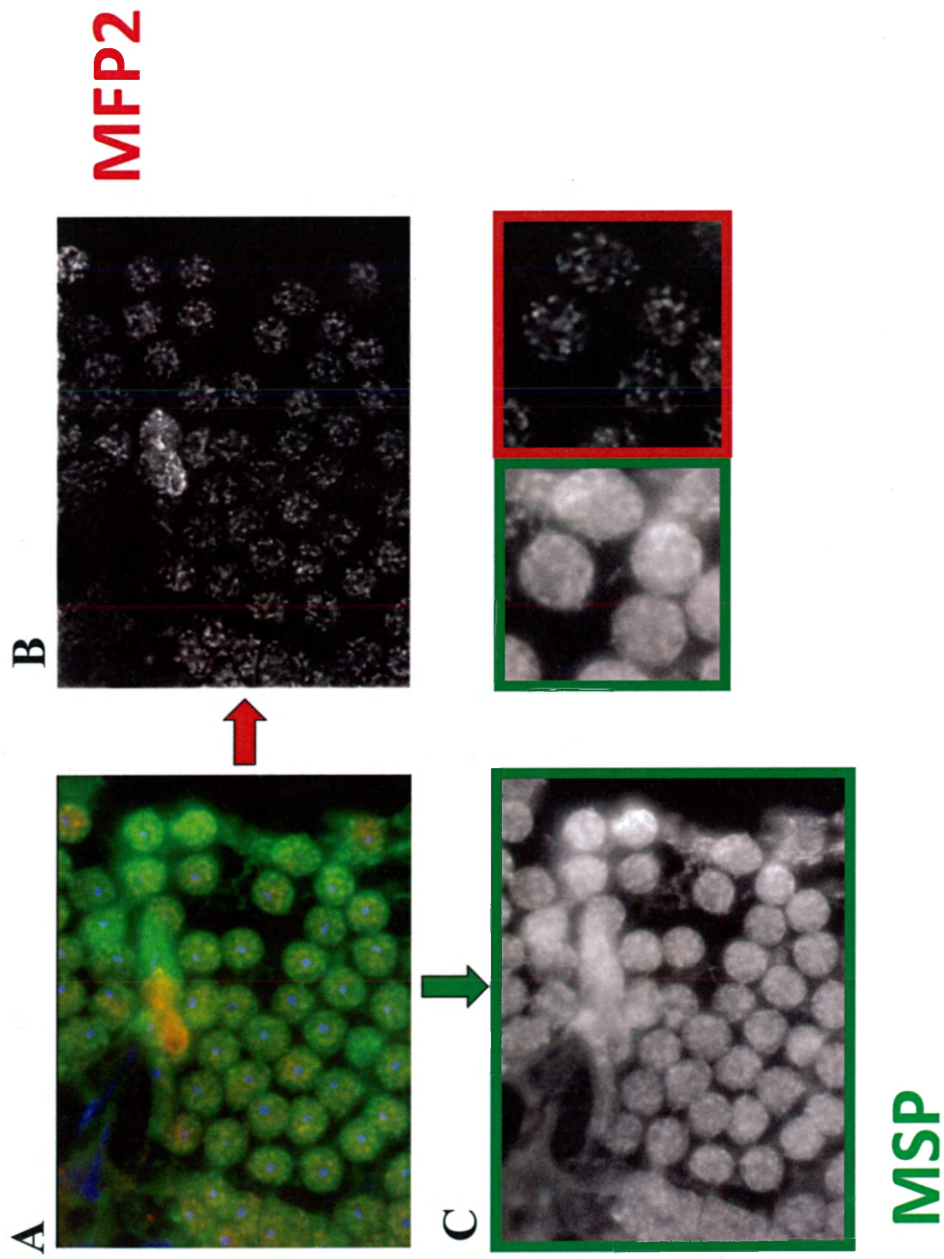


Figure 8: Deconvolution of MFP2 aggregates in *C. remanei*
 (A) MFP2 and MSP localization in spermatids in *C. remanei*. (B) deconvolution of MFP2 reveals that MFP2 forms irregular aggregates in spermatids, even while (C) MSP remains cytoplasmic.

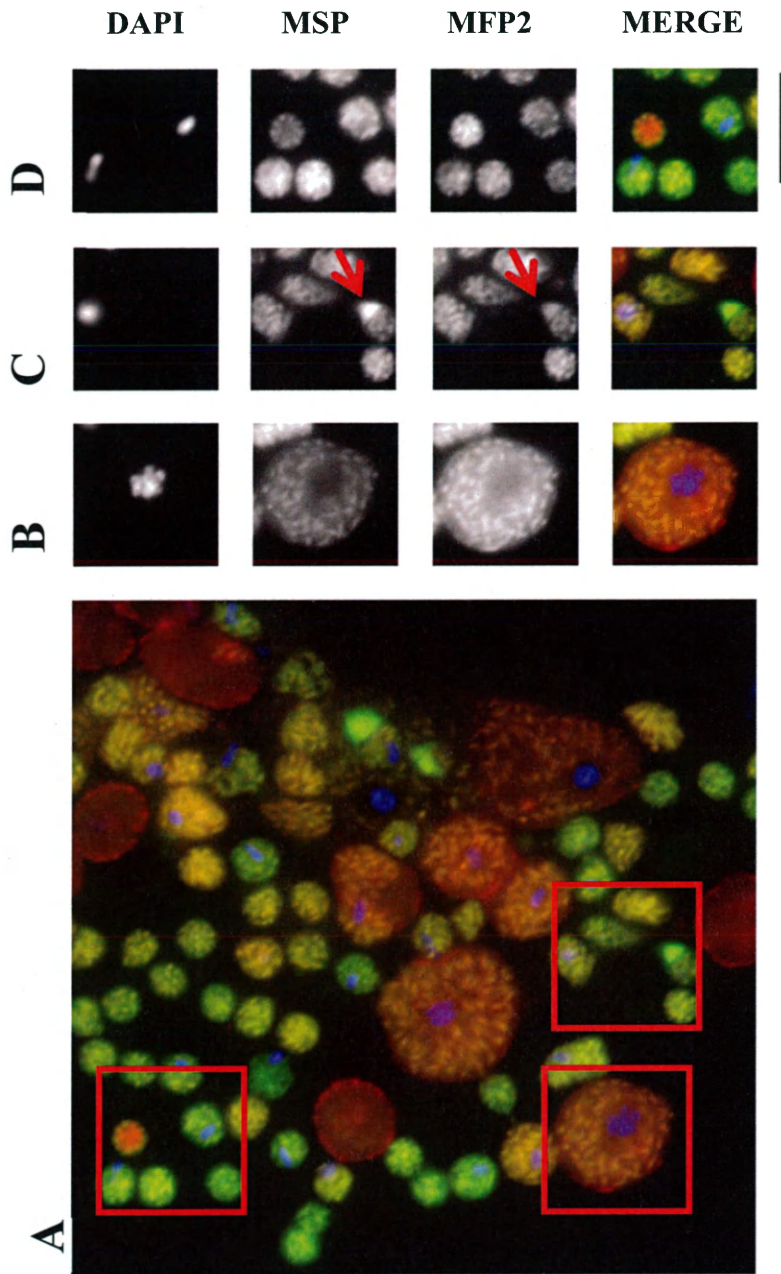


Figure 9: MFP2 and MSP localization in *gsp-3/4* mutants.
 (A) MFP2 and MSP colocalizes during meiosis. Representative cells are boxed in red and (B-D) are offset. (B) MSP and MFP2 colocalizes normal during meiosis I and II. (C) In cases where spermatids have activated, MFP2 localizes to both the pseudopod (arrow) and remains associated with the persistent MSP structures. (D) The MFP2 to MSP ratio does not appear consistent in spermatids. Scale bars are 10µm.

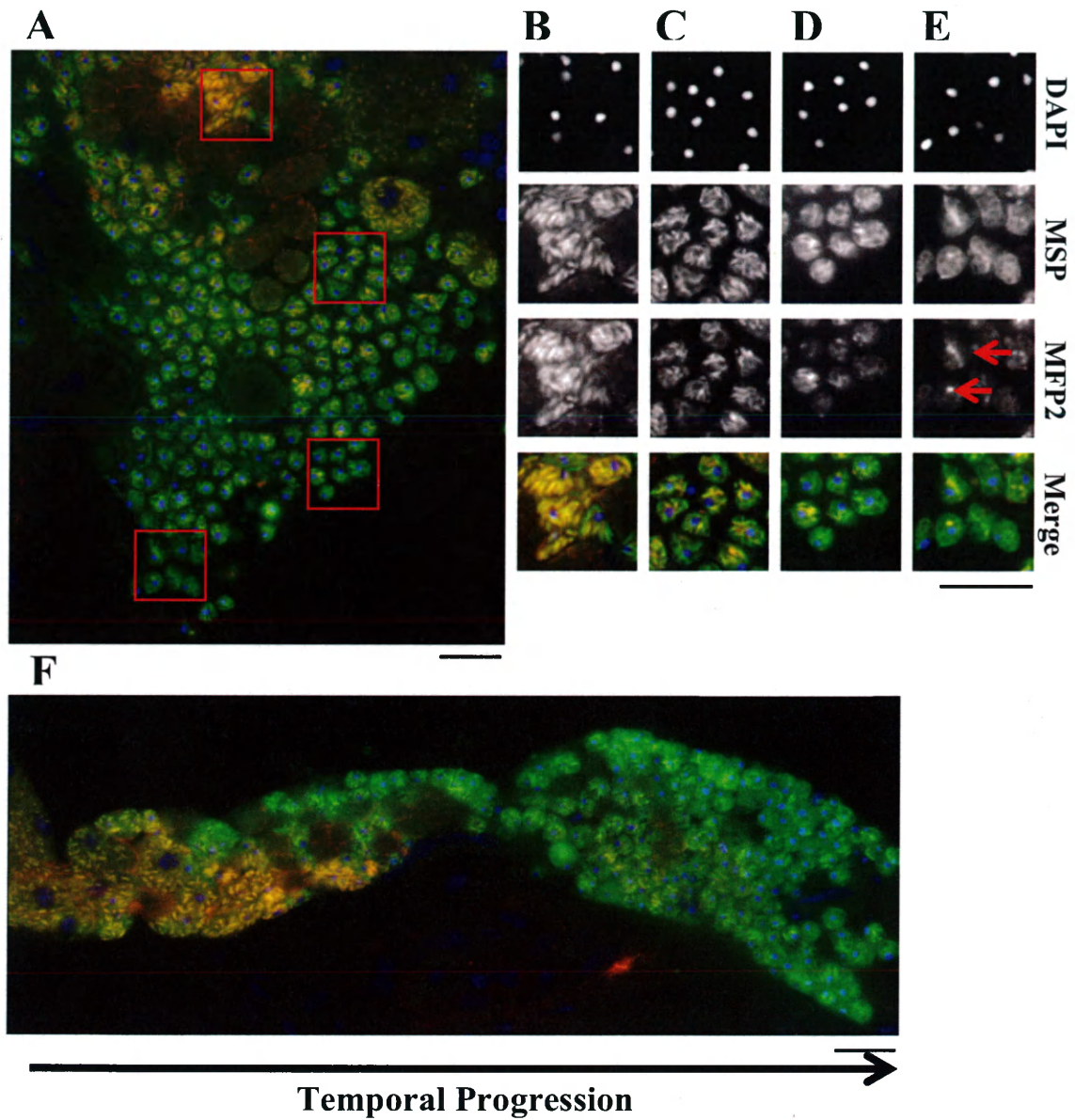
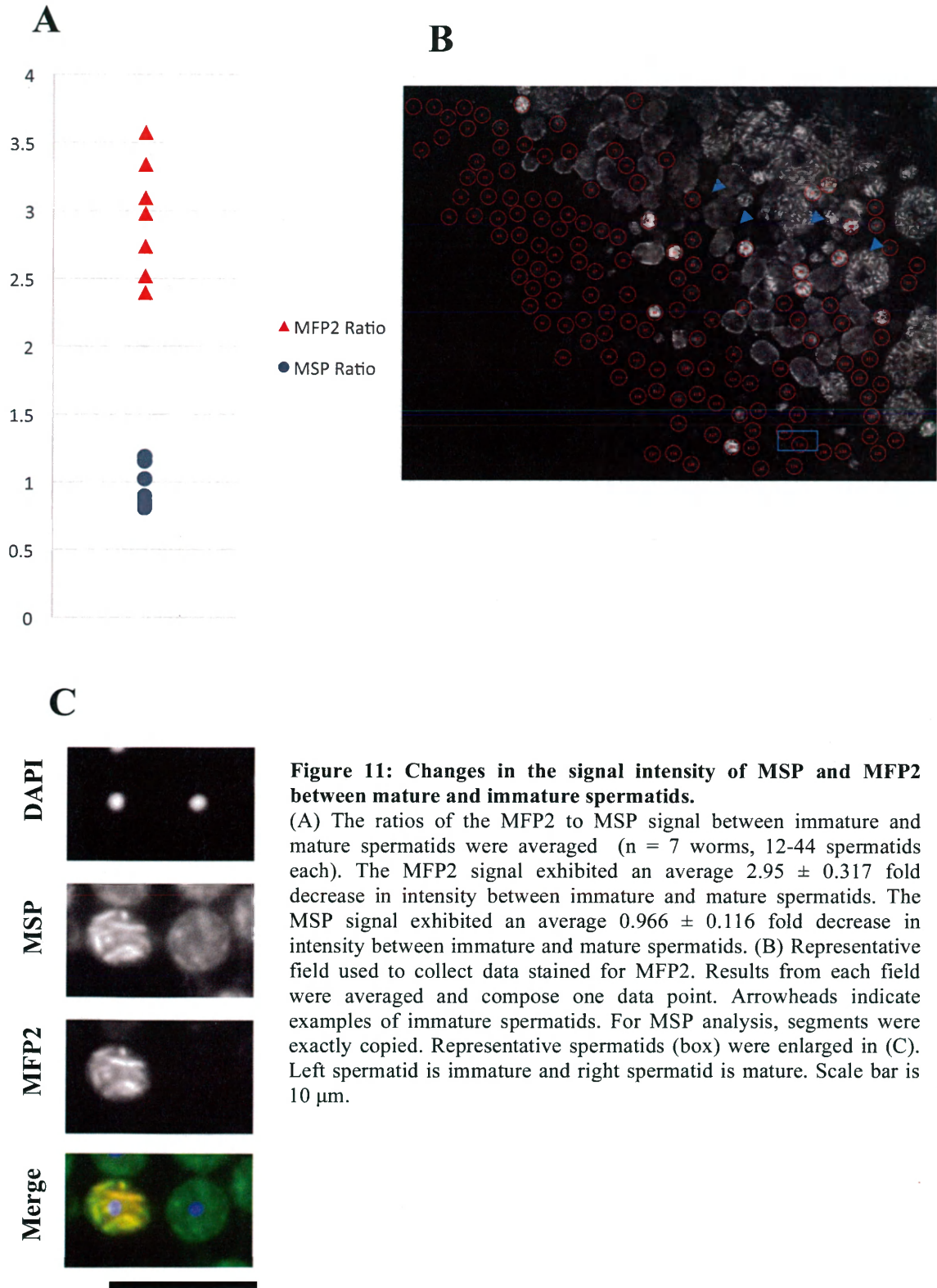


Figure 10: MFP2 and MSP localization in *fer-6 (hc6)* mutants.

(A) MFP2 and MSP colocalize in *fer-6* mutants. Representative cells are boxed in red and offset in (B-E). (B) MFP2 appears to be normal in immature spermatids (arrows). (C-E) MFP2 colocalizes with MSP in persistent FB structures but the MFP2 to MSP signal ratio appears to drop. Bright spots of MFP2 seem to remain (arrows) (F) This change in signal strength appears to occur temporally; spermatids produced



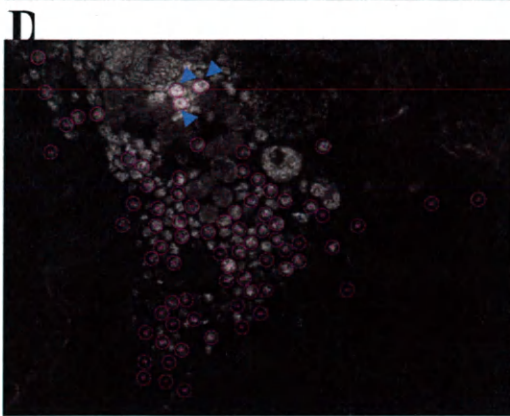
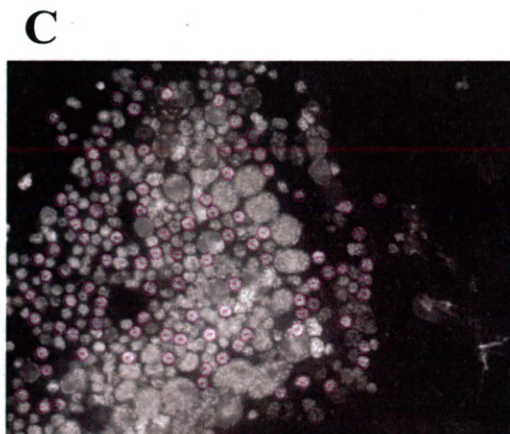
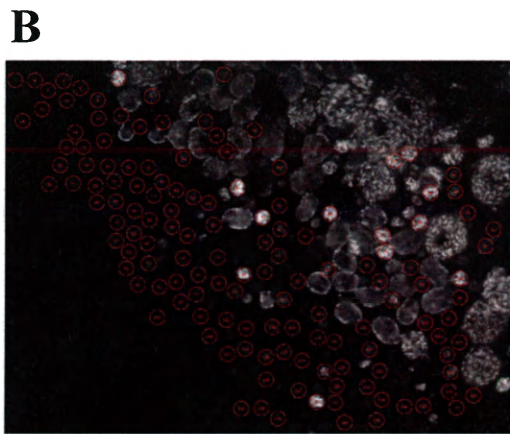
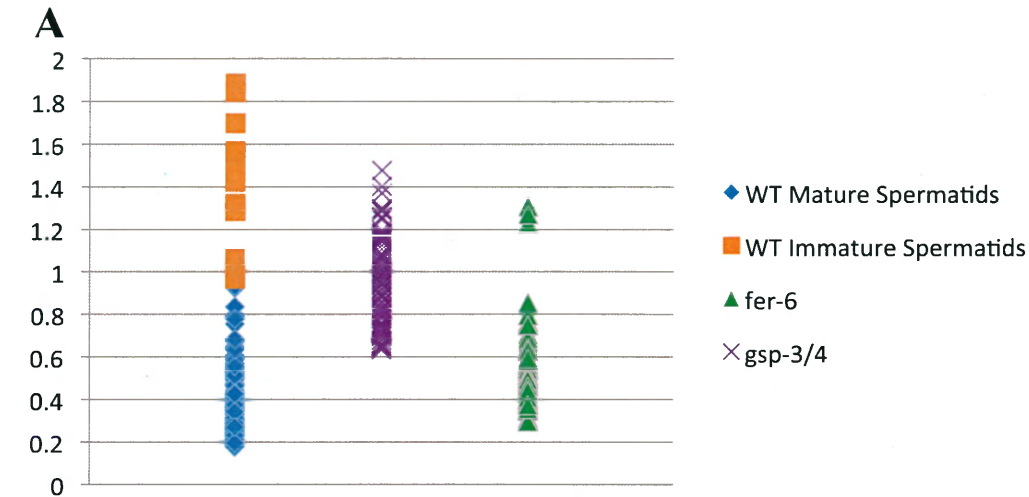


Figure 12: Comparison of MFP2 to MSP ratios in WT, *gsp-3/4* and *fer-6* mutants.

(A) The average MFP2 to MSP ratio was calculated for individual spermatids in WT, *fer-6* and *gsp-3/4*. Points represent individual spermatids from (B) WT, (C) *gsp-3/4*, (D) *fer-6* fields used to collect data and stained with MFP2. For MSP analysis, segments were exactly copied. WT exhibits a bimodal distribution, representing immature and mature spermatids. *gsp-3/4* mutant spermatids contain a range of values. *fer-6* mutant spermatids contain a bimodal distribution corresponding to recently budded spermatids. (D) Arrow heads in *fer-6* mutants point to the three highest data points in *fer-6* and are recently budded spermatids.

Table 1A: Phosida predicted S/T phospho-sites		
Position	Prediction	Score
8	S	>0.85
16	S	>0.9
57	S	>0.75
86	S	>0.75
115	S	>0.8
126	T	>0.9
136	T	>0.7
142	S	>0.8
146	T	>0.85
147	T	>0.8
155	T	>0.6
160	T	>0.7
170	T	>0.9
190	S	>0.85
202	T	>0.85
204	T	>0.8
225	S	>0.85
228	S	>0.95
229	S	>0.95
233	T	>0.65
251	S	>0.85
256	T	>0.6
261	S	>0.75
273	S	>0.85
277	S	>0.95
278	S	>0.95
281	T	>0.8
282	T	>0.75
288	S	>0.8
308	T	>0.7
313	S	>0.85
324	T	>0.75

Table 1B: NetPhos 2.0 predicted S/T/Y phospho-sites			
Position	Prediction	Score	Context
8	S	0.512	AKEDSWAFQ
32	Y	0.696	QNNQYVALW
84	Y	0.966	YKGDYNSLG
147	T	0.846	NAGTTEKYE
150	Y	0.879	TTEKYEGGA
184	Y	0.735	YDLRYGDNF
229	S	0.728	SYPSAGKT
261	S	0.548	VPEASCMGL
267	Y	0.62	MGLEYKWMP
277	S	0.911	SEGKSSGWT
278	S	0.695	EGKSSGWTT
313	S	0.63	IEKASAGYG

Table 2A and 2B: Predicted Phospho-sites on MFP2

(1A) Predicted phospho-sites on S/T residues from Phosida. "Score" represents the precision interval at which the given result was obtained. High precision intervals decrease the likelihood of false positives, but increase the likelihood of false negatives. Intervals set to ≥ 0.5 , are predicted to capture all phospho-sites in a protein, but also produce a number of false negatives. (1B) Predicted phospho-sites on S/T/Y residues from NetPhos 2.0. Score is based on a relative scale ranging from 0-1, higher scores represent sites that are more likely to be actual phospho-sites. Phospho-sites predicted by both programs are highlighted in yellow.

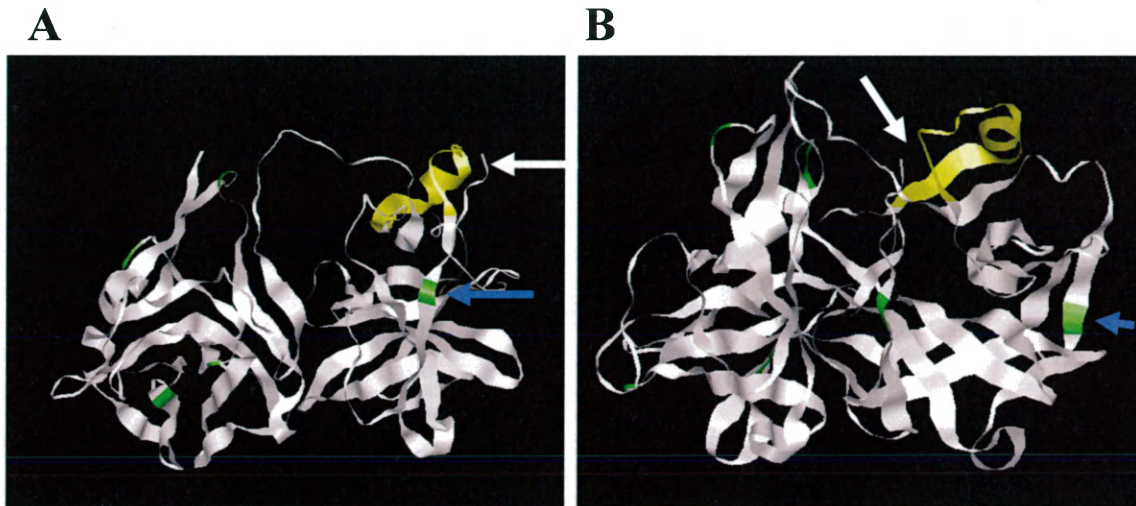


Figure 13: A visualization of predicted phospo-sites in relation to the antibody binding site
 Two different views of the I-TASSER model of *C. elegans* MFP2. Predicted phospho-sites that were identified by both NetPhos 2.0 and Phosida (green) are shown in relation to the antibody binding site (yellow) show that most sites do not appear near the binding site. The closest site, Ser8 (blue arrow) may interact, though it is not directly adjacent. C-termini are indicated by a white arrow.

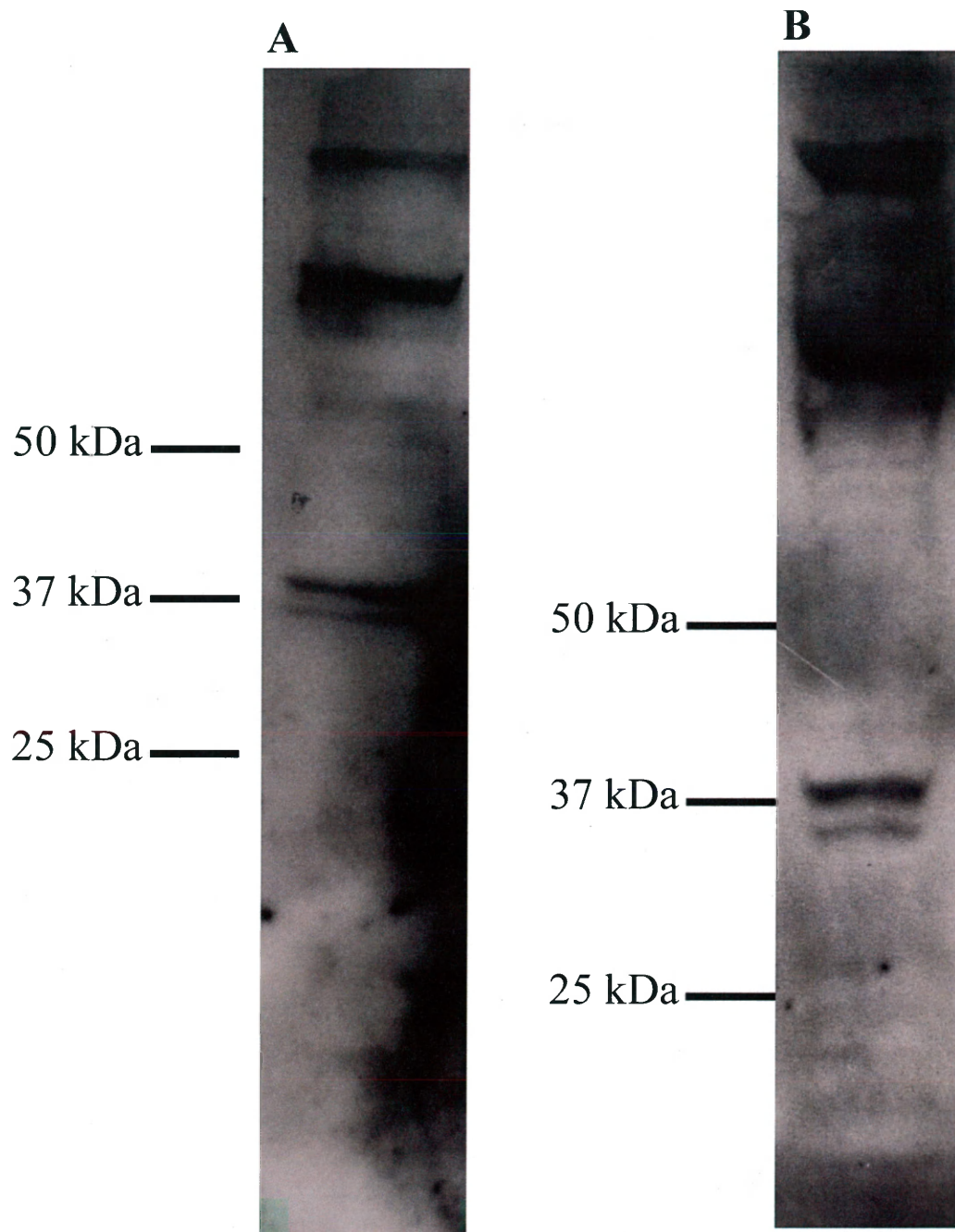


Figure 14: Western blots of MFP2.

(A) Western blots of MFP2 in *fem-3 (gf)* on Any kDa gels worms reveal that MFP2 migrates as a doublet at ~37 kDa. (B) Using a 10% gels allows increased visualization of the doublet on western blots.

z

Chapter 2: FB Defects in Different Alleles of *spe-26*, a Kelch-Like Protein

Introduction

Spermatogenesis is a highly dynamic process that involves the coordination of multiple cellular events. Over the course of spermatogenesis, a diploid spermatocyte divides meiotically to produce haploid spermatids, spermatids jettison unnecessary proteins, and cells activate to become motile cells capable of oocyte fertilization (Chu & Shakes, 2013). Each of these processes requires a specific complement of proteins whose activity must be regulated spatially and temporally.

During mammalian spermatogenesis, protein regulation is partially achieved by temporally separating the meiotic division from spermiogenesis (Kimmins et al., 2004). Throughout the meiotic progression, mammals transcribe and translate a variety of proteins required for spermatogenesis, including a wide variety of both sperm specific proteins and meiotic specific proteins (Kimmins et al., 2004). Then, following the meiotic divisions, spermatids prepare for spermiogenesis by undergoing a second burst of transcription and translation that produces proteins that shape and remodel the spherical, haploid cells into motile, fertilization-component cells (Kimmins et al., 2004). In addition, during this latter process, any unnecessary proteins and structures, including the ER and Golgi apparatus, are jettisoned into a residual body structure. Lastly, these processes precede, and slightly overlap with, hypercondensation of sperm chromatin mediated by the progressive replacement of histones with, first, transition proteins, and then, protamines (Sassone-Corsi, 2002).

In the nematode *C. elegans*, however, there is no secondary burst of transcription and translation. Instead, transcription stops in late prophase of meiosis I. Consequently, all proteins required for spermatogenesis are produced early on; any proteins that only

function after the completion of the meiotic divisions must be rendered functionally inert (Kulkarni et al., 2012). One of these proteins is a highly abundant, nematode-specific cytoskeletal protein called Major Sperm Protein (MSP) (Kulkarni et al., 2012; Messina, 2012). Although MSP is present throughout spermatogenesis, its primary function is as a motility protein in spermatozoa where its polymerization dynamics drive the extension and retraction of a pseudopod (Sepsenwol et al., 1989a). Prior to localizing to the pseudopod, MSP is sequestered within Fibrous Body (FB) structures in the form of tightly packed MSP subfilaments (Roberts, Pavalko, & Ward, 1986a). In mutants in which FBs fail to form, meiosis arrests early in prophase, suggesting that FBs exist to prevent cytosolic MSP from interfering with meiosis and cytokinesis (Messina, 2012). Consequently, the regulation of FB formation, as well as FB shape and size, must be a tightly regulated process. Although the process of FB formation has been partially elucidated, the regulation of FB size and morphology has been largely unexplored.

In this study, we have characterized the perturbation of FB size and morphology in different alleles of the *spe-26* gene. The *spe-26* gene encodes a protein that belongs to the kelch superfamily, which are a group of structurally similar proteins first identified in *Drosophila melanogaster* (Adams, Kelso, & Cooley, 2000; Varkey, Jansma, Minniti, & Ward, 1993a; Xue & Cooley, 1993). Kelch-like proteins are characterized by the presence of kelch repeats that fold into a distinctive beta-propeller domain (Adams et al., 2000). Though *spe-26* is a member of this family, its specific function remains unknown, because kelch-like proteins are known to serve functions as diverse as galactose oxidases and actin organizers (Adams et al., 2000).

However, though its function is unknown, mutations in the *spe-26* gene were previously reported to cause a wide variety of defects in chromatin segregation, as well as a decrease in overall spermatid production and fertility (Varkey, Muhlrاد, Minniti, Do, & Ward, 1995). However, the effects of these mutations on FB size and morphology were largely unexplored (Varkey et al., 1995).

Here, we characterize FB abnormalities in four of the five *spe-26* alleles that were originally isolated. We show that different *spe-26* alleles exhibit allele-specific differences in their FB lengths that differ significantly from WT. In addition, we have further characterized the broader spermatogenesis defects present in *spe-26* mutants in the context of abnormal FBs. Lastly, we have identified the terminal phenotypes of *spe-26* alleles.

Results

In WT spermatogenesis, MSP and SPE-7 localization is dynamic

Spermatogenesis in *C. elegans* is an excellent developmental model because as cells progress through spermatogenesis they move proximally along the gonad. This allows visualization of all the different cell stages in spermatogenesis in a single, adult male gonad (figure 1a). Prior to entering spermatogenesis, *C. elegans* spermatocytes are maintained in a mitotic state through their interaction with the somatic distal tip cells (DTC) (Kimble & Crittenden, 2005). As cells lose contact with the DTCs, they exit mitosis and enter meiosis. Meiotic prophase in *C. elegans* is an extended process that divides the gonad into three regions. The Transition Zone is comprised of cells in Leptotene and Zygotene (Chu & Shakes, 2013). During this time, homologous chromosomes pair and assemble synaptonemal complexes. Following this, spermatocytes enter Pachytene, where crossing-over occurs and many sperm-specific proteins are produced (Chu & Shakes, 2013). After Pachytene, chromatin enters a condensation phase as spermatocytes disassemble their synaptonemal complexes (Diplotene) and enter an extended Karyosome stage (Chu & Shakes, 2013). Following Karyosome, the spermatocytes detach from the rachis of the gonadal syncytium, transition through Diakinesis, and enter Metaphase I (Chu & Shakes, 2013).

FBs assembly begins in late Pachytene and is thought to be largely completed by Metaphase I (Messina, 2012). MSP is first translated during mid Pachytene of meiotic prophase, where it initially appears to be cytosolic (figure 1B, Intro. figure 3) (Messina, 2012). The MSP accessory protein SPE-7 is first translated during late Pachytene, and initially assembles into punctate aggregates that are unassociated with MSP (Messina, 2012). During diplotene, MSP begins associating with SPE-7 and appears to polymerize

off of the centrally located SPE-7 aggregates (Messina, 2012; Roberts et al., 1986a). However, by Metaphase I, when FB formation is thought to be completed, SPE-7 has changed its pattern and is, instead, located on four points of the developed FB (Messina, 2012). Between Metaphase I and Anaphase I, SPE-7 remains in the central core of the FB but concentrates to the two ends of the elongated FBs and by Anaphase II, most SPE-7 is located on the ends of FBs (Messina, 2012). During the budding division, SPE-7 segregates to the budding spermatids but is degraded shortly after the spermatids detach from the central residual body (Messina, 2012).

spe-26 (hc140) mutants contain abnormal FBs and FB development

Recent studies of SPE-7 and MSP localization patterns during meiotic prophase have given us new insights into early stages of FB biogenesis, yet the molecular mechanisms which regulate the size and shape of the FBs remain completely unknown (Kulkarni et al., 2012; Messina, 2012; Varkey et al., 1993a). Loss-of-functions mutations in the genes that encode SPE-7, SPE-6, and SPE-44 all exhibit severe chromosome segregation defects that are thought to be exacerbated by failures in FB assembly (Messina, 2012; Varkey et al., 1993a). To investigate determine whether defects in FBs were present in other mutants with chromosomal defects, we decided to look at different alleles of the *spe-26* gene. Five *spe-26* have been identified, all of which exhibit chromosome segregation defects (Varkey et al., 1995). Of these, four are temperature sensitive alleles that are self-sterile at 25°C, and one is a non-conditional allele that is self-sterile at all temperatures. However, though each allele is sterile at 25°C, they produce different numbers of spermatids. This result suggests that the alleles are not

equally severe, even if they are equally sterile. We obtained four of the five known *spe-26* alleles and examined the morphology of their FBs. The alleles we looked at were: *hc140* (slightly ts), *hc138(ts)*, *it112(ts)* and *eb8* (non-conditional). The former three alleles are all temperature sensitive, while *eb8* is non-conditional. Based on spermatid production, *hc140* is the most severe, because it does not produce any spermatids, followed by *hc138*, and then *it112* and *eb8* which produce equivalent numbers of spermatids (Varkey et al., 1995).

To determine whether *spe-26* mutants had FB defects, we first examined the development of FBs in *hc140* by staining with MSP and SPE-7. In *hc140*, the early pattern of SPE-7 and MSP appear normal (compare figures 1 and 2). MSP and SPE-7 both appear to be translated during Pachytene, with the beginning of MSP translation occurring before SPE-7 translation. In addition, the association of MSP and SPE-7 begins at Diplotene, and, following this, SPE-7 forms four dots on the developing FB. However, by the time the cells had reached Metaphase II we observed a deviation in the length of FBs. FBs in *spe-26 (hc140)* appeared to be much larger than in WT (compare Anaphase I in figures 1 and 2). We were also intrigued by the observation that chromosome abnormalities appeared to become markedly pronounced after Metaphase I (expanded below).

All spe-26 alleles exhibit abnormal FBs, but they differ in the terminal FB length

To compare the severity of the FB phenotype between the different *spe-26* alleles and WT, we used chromatin morphology as a basis for determining when *spe-26* alleles contained FBs that were at their maximal length. This analysis was complicated by the

observation that different *spe-26* alleles have different chromosome segregation and cytokinesis defects; in the more severe alleles, many, or most, of the cells fail to undergo cytokinesis after the first and second meiotic divisions, instead arresting as large cells with multiple chromatin masses. In spite of this, all of the different *spe-26* alleles successfully produce cells with hyper-condensed chromatin normally characteristic of spermatids that have completed the post-meiotic, chromatin-remodeling phase of the spermatogenesis program and formed mature, haploid chromatin masses (Figure 3). Because hypercondensed chromatin is usually associated with post-meiotic cells that have completed translation and jettisoned their ribosomes into the residual body, we reasoned that FBs were likely to have reached their maximal length in these cells (Shakes et al., 2009b). Consequently, we looked at FBs in each of the different alleles when their chromatin exhibited the rounded, hypercondensed appearance of mature “haploid” chromatin masses, although, in the case of *hc140* and *eb8*, these cells often contained multiple chromatin masses (figure 3). We compared these FBs to those in WT cells just before or just after budding, when the chromatin is similarly condensed. We observed that FB lengths appeared to be consistent for each allele but varied between alleles, and hypothesized that this effect might correlated with the severity of each alleles. In addition, somewhat to our surprise we did not see any noticeable effects on the short-axis of the FB; the FBs did not appear to be any wider, though we do not have quantitative data to measure this effect. Instead, FB abnormalities appeared to be limited to changes in length.

Although FBs appeared longer than in WT, we wanted to quantify this effect. We hypothesized that FB length might correlate with spermatid production and that alleles

that produced fewer spermatids might produce longer FBs. To test this hypothesis we measured FB lengths in each of the alleles using the above chromatin criteria to identify cells with what we hypothesized contained FBs at their maximal length (figure 4). Because FBs are not symmetrical in three dimensions, it was possible that we would measure FBs and get a value that was too short if the FBs we measured were angled out of the plane of the image. To minimize this effect, we used FB morphology to only measure the subset of FBs that appeared to be in the plane of the image. The results of this analysis showed significant differences in FB length between each allele. FBs were progressively longer between WT, *hc138*, *it112*, *hc140* and *eb8*. In addition, though *it112* and *hc138* had average FB lengths that were close, their lengths were still significantly different from one another to the $P < 0.01$. Although we hypothesized that FB length might inversely correlate with spermatid production, this was not precisely the case. There was a rough relationship to the extent that *it112* and *hc138* have significantly shorter FBs than *hc140*, and both produce spermatids. However, based on spermatid production, *eb8* mutants were predicted to have FBs equivalent to *it112*, they, instead, contained FBs that were longer than any others we had observed.

The phenotype of spe-26 alleles reveals abnormal MSP and SPE-7 patterns

Although we had determined that early FB development in *spe-26* mutants proceeded normally, and became abnormal later on, we also wanted to determine if there were abnormalities in the SPE-7 pattern during the meiotic divisions. In all of the alleles, we observed abnormal SPE-7 structures. Unlike WT SPE-7, which persists for only a short time at the end of meiosis, and ultimately localizes exclusively to the ends of FBs,

we observed much larger SPE-7 structures in some *spe-26* spermatids (figure 5A-B). These SPE-7 aggregates were much larger than the aggregates that SPE-7 typically forms independently during late-Pachytene in WT. In some cases, they appeared as irregular, globular structures. However, we also observed spikier structures. Based on the immunofluorescence pattern of MSP, these structures appeared to be distinct from MSP. However, we hypothesize that some of these structures may actually be forming on top of polymerized MSP that is masked by a large amount of cytosolic MSP. Furthermore, it was unclear how persistent these SPE-7 structures were. In some cases, we observed a spermatid with large amounts of persistent SPE-7 directly adjacent to spermatids without any SPE-7, suggesting that either SPE-7 only persists for a short time, or that it persists in some cells but not others (figure 5B). Lastly, in several preparations, we also observed SPE-7 structures in the most proximal region of the gonad (data not shown), suggesting that these structures may be quite stable.

In addition to the larger aggregates, which were present in the spermatids of all alleles, we also observed a second abnormal SPE-7 pattern in *eb8* and *hc140* that occurred earlier in spermatogenesis and was not present in the other alleles (figure 5C). These SPE-7 aggregates occurred earlier in meiosis, were smaller and more closely resembled previously observed SPE-7 patterns in *spe-10* mutants and *spe-6* (*hc49*) mutants. Both of these mutants contain punctate aggregates of varying size that resemble pre-FB assemblages (Messina, 2012). It was unclear, however, to what extent the SPE-7 aggregates existed independently of FBs. Some of these structures clearly localized to the FBs, albeit along a longer stretch of the FB. Some of them, though, may have been independent of MSP.

In addition, to the presence of SPE-7 aggregates, we also observed a second, consistent terminal phenotype that was present in all the alleles. In many multinucleate cells, we found places where the MSP had become cytosolic (figure 6A-C). In some of these cells, cytosolic MSP was accompanied by strands of polymerized MSP and hypercondensed chromatin (figure 6a). In other areas, however, we observed pools of MSP with an abnormal number of chromatin masses, sometimes as many as a dozen or more. These chromatin masses stained less intensely with DAPI and often appeared “doughnut shaped” (Figure 6B-C). Lastly, we observed that cells with diffuse MSP were sometimes found surrounding other cells that did not appear to have completely cytosolic MSP (Figure 6B). Because the pools of MSP were never accompanied by polymerized MSP or fully condensed chromatin, we hypothesize that these are later-stage cells. Lastly, we observed a subset of visibly lysed cells that appeared to have cytosolic MSP and weakly staining chromatin (Figure 6C).

Because of these results, we hypothesized that the cytosolic MSP and weakly staining chromatin was associated with either cell fusion events or partial or full lysis. To distinguish between these two possibilities, we used a combination of DIC and epifluorescence microscopy to examine cells stained with the fluorescent DNA dye, Hoechst. In the gonad of multiple *spe-26* alleles, we found instances of decondensed chromatin in intact cells (figure 6D-F). However, we also found instances of weakly stained chromatin in tissue that had lysed. In these cases, we saw pieces of plasma membrane spreading outwards, and contacting or surrounding intact cells which were immediately adjacent to the lysed aggregates. We believe these to be analogous to the MSP pools that were observed using immunofluorescence. Lastly, we also observed rings

and punctate masses that stained with Hoechst but did not contain any membrane. We believe these to be the remains of cells that had lysed and had time for their cellular contents to leak away. If this is indeed the case, then this is the terminal phenotype for many of the cells in *spe-26* mutants.

spe-26 mutants exhibit a variety number of defects, including, but not limited to FB defects.

In order to more fully characterize the *spe-26* alleles, we attempted to analyze their temporal progression. Because the phenotypes sorted into two basic classes (*it112* and *hc138*) and (*hc140* and *eb8*), we focused our analysis on two alleles, *it112* and *eb8*. Although, as has been previously noted, *spe-26* alleles have normal early FB development, the sizes of the FBs become unmistakably too large in *it112* by the end of Anaphase I (figure 7a). In some cases, however, we observed abnormally large FBs by Metaphase I, suggesting that there is heterogeneity in the population early in spermatogenesis. In addition, we also observed abnormal cytokinesis in many cells after Anaphase I. However, it is unclear how many of these defects were due to errors in chromatin condensation, and how many were due to errors in microtubule or actin dynamics.

After Anaphase I, the population of cells becomes even more heterogeneous because there are a wide variety of different phenotypes. While in most cases, for instance, we observed that the first cytokinesis event occurred, some cells appeared to enter Metaphase II without undergoing cytokinesis. In addition, during Anaphase II, we also observed a number of different phenotypes. Typically, during this stage FBs align

with their tips pointed towards the poles. In many cells, however, they appeared disorganized. Following Anaphase II, we also observed a number of different types of spermatids. Some spermatids contained persistent SPE-7 structures, while some did not. Spermatids also varied in the orientation of their FBs within the cell. However, we consistently found hypercondensed chromatin in Anaphase II and budding spermatids, illustrating that mechanisms for hypercondensation of the chromatin (part of the spermatogenesis pathway) do not appear to be perturbed in *it112*.

We also identified a variety of what we hypothesize are terminal phenotypes (figure 7B). In many cells, multiple chromatin masses were present, some of which contained cytosolic MSP. In addition, we observed that weakly staining chromatin was always found in cells with cytosolic MSP, though the reverse was not true. This provided further evidence that decreases in chromatin staining are associated with later-staged cells.

When we performed a similar analysis on *eb8*, we found different effects than in *it112*. In *eb8*, like all the other *spe-26* alleles, the early MSP and SPE-7 pattern appeared normal. However, by Metaphase I FBs had become noticeably longer than in WT (figure 8A). In addition, similar to *it112*, following Metaphase I, the population of cells became heterogeneous, with cells apparently progressing through multiple, parallel paths. Unlike *it112*, the chromatin segregation defects in *eb8* were significantly worse. It was relatively rare to find Metaphase I cells that appeared to have undergone correct cytokinesis. In cells that did progress through Metaphase II, we observed that, like *it112*, the mechanisms for chromatin hypercondensation appeared intact.

In *eb8*, the terminal phenotypes of different cells were worse; many more cells contained multiple chromatin masses. In addition, cells with multiple chromatin masses frequently contained frequently contained chromosomal bridges that were indicative of errors in chromosome segregation, potentially due to the presence of multiple centrosomes in each cell. In the few spermatids that did form, SPE-7 appeared to form the same persistent structures as in *it112*. Lastly, in contrast to spermatids, many of the cells with chromatin morphology indicative of earlier-staged cells appeared to have lower than normal SPE-7 levels.

Discussion and Future Directions

SPE-26 is a kelch-like protein that is currently represented by five mutant alleles that were previously described as having a variety of chromatin segregation defects (Varkey et al., 1995). In this chapter of the thesis, we used combination of immunofluorescence, DIC and image analysis software to examine FB defects in four of the five *spe-26* alleles that were previously characterized, and have attempted to place these FB defects in the context of broader chromatin segregation defects. We determined that all four of these *spe-26* alleles exhibit abnormally large FBs relative to WT, with different degrees of severity. In addition, we examined the terminal phenotype of cells and determined that, in some cells, MSP becomes cytosolic. In addition, we also determined that the large, cellular aggregates with multiple chromatin masses that contained cytosolic MSP were, in fact, cells that had lysed. Furthering our study of the terminal phenotype of *spe-26* alleles, we discovered a novel SPE-7 pattern that was another shared commonality in all of the alleles. These SPE-7 structures were abnormally large and found in some, though not all, spermatids. Lastly, we investigated the chromatin segregation defects that occurred in *spe-26* mutants and determined that *it112* and *hc138* had relatively minor chromatin segregation defects, while *eb8* and *hc140* had more severe defects, oftentimes containing chromatin bridges.

FB morphology is altered in spe-26 mutants

In WT *C. elegans* spermatocytes, FBs development is clearly a coordinated process. The translation of MSP, SPE-7 and their association with one another are consistent and predictable. However, although mutants have been identified that do not form FBs, our work is the first to characterize a class of mutants with noticeable, and

predictable, defects in FB morphology. Prior to this work, one possibility was that FB size was under physical constraints that prevented them from growing beyond a certain length. Our work has ruled out this possibility, because we have shown that FB length is not physically constrained. However, our work also suggests that FB width does not appear to change, no matter how long FBs grow. This suggests that, although FB length is not constrained, the width may be regulated in some fashion.

FBs are composed of MSP subfilaments packed together in a paracrystalline form (Roberts et al., 1986a). Consequently, the determinants of FB width and length are fundamentally different properties of the FB. Width is, apparently, determined by the number of subfilaments packed across the cross-sectional area of the FB. Conversely, length is determined by the number of MSP dimers that incorporate into the growing FB. Consequently, one possibility is that the width of the FB requires the creation of new nucleation sites along the short axis of the FB and that these nucleation sites are determined by a process that remains unperturbed in *spe-26* mutants. Given its putative role as a FB nucleator, SPE-7 is a potential candidate for this role.

One of the unanswered questions about FBs in *spe-26* mutants is how they are associated with the golgi-derived MOs. In WT, the MO surrounds and encapsulates the FB with the head of the MO located along the long axis of the FB (Roberts et al., 1986a). Consequently, it seems likely that larger FBs would either induce deformations of the MO, or, alternatively, that the membrane itself would be unable to completely surround the FB. Either situation would be an intriguing result, because it would either imply that MOs are more labile than previously thought, or, if they do not surround developing FBs, then it would mean that FB formation does not require the MO to be stable once it has

completed growing. Lastly, because FBs are hypothesized to grow from both ends, MO heads are predicted to still be centrally located on the larger FBs (Roberts et al., 1986a). Consequently, further experiments will involve studying MO localization and morphology in *spe-26* mutants.

The terminal phenotype in spe-26 mutants often involves abnormal MSP and SPE-7 patterns

In addition to abnormal FBs, we also identified two categories of abnormal SPE-7 patterns that occurred in all of the *spe-26* mutants. Previous studies of SPE-7 have shown that it is capable of assembling into larger aggregates in mutants that do not undergo a budding division (Messina, 2012). Our studies have identified an additional localization pattern. In some, but not all, *spe-26* spermatids, we observed SPE-7 forming misshapen aggregates that sometimes appeared to be strand-like. In addition, we typically found *spe-26* spermatids with these structures in proximal regions of the gonad, which would contain the oldest cells (data not shown). Based on these data, we have concluded that, in *spe-26* mutants, SPE-7 is capable of persisting for longer than in WT cells, though it remains unclear whether SPE-7 is completely persistent in these cells, or whether there is heterogeneity in the spermatid population. Because the nature of this particular SPE-7 containing structure is not understood, it is difficult to interpret this data. One possibility is that SPE-7 persists specifically in *spe-26* spermatids that have undergone abnormal budding divisions; perhaps proteins that stabilize SPE-7, and are normally segregated to the residual body, remain in the spermatids. Alternatively, factors that normally work to destabilize and degrade SPE-7 in budding spermatids could, instead, be missegregated to

the residual body. One hypothesis would be that SPE-7 persists in some spermatids because proteasomes are not correctly segregated to spermatids. An easy way to test this hypothesis would be to use immunofluorescence to stain for proteasomes in spermatids and determine whether they missegregate in *spe-26* mutants.

In addition to SPE-7 abnormalities, we also determined that, in some, or all, cases FBs breakdown correctly and MSP becomes cytosolic. When we examined cells using immunofluorescence, we observed three different subpopulations of cells with diffuse MSP. In some cases, cytosolic MSP was present in mono- or bi-nucleate cells with mature, hypercondensed, seemingly haploid chromatin masses. In other cases, however, cytosolic MSP was present in the presence of multiple chromatin masses, but it was unclear, using immunofluorescence, where the cell boundaries were. These cells were characterized by DAPI-faint chromatin masses. Lastly, we observed some cells with both weak MSP labeling and DAPI-faint chromatin. Together our DIC and immunofluorescence studies suggest a model in which FB breakdown occurs in terminal cells and is followed by chromatin degradation and, ultimately, cell lysis.

There are three models that would explain that these temporal events. In one model, FB breakdown is not directly connected to cell lysis. Instead, the mechanisms that induce FB breakdown are the same mechanisms that induce FB breakdown in WT. In this model, FB breakdown occurs because the cells have stopped dividing, and then, because the cells have abnormal protein complements, they begin to lyse, which could be due to misregulation of proteases or osmotic regulators. In a second model, abnormal cellular complements and protein misregulation induce both FB breakdown and cell lysis. In the third model, FB breakdown somehow induces cell lysis.

One way to test these models would involve staining *spe-26* alleles for proteins that are known FB regulators, such as GSP-3/4, which is required for FB breakdown. If GSP-3/4 segregation were normal, it would provide support for the hypothesis that FB breakdown is analogous to WT cells.

All spe-26 alleles are characterized by FB defects

The paper that first characterized problems that were observed in each of the *spe-26* alleles focused primarily on defects in MTs, chromatin segregation, fertility and spermatid production. Of these defects, the authors only characterized allele-specific differences in fertility and spermatid production. However, our work has shown that, in addition to differences in spermatid production and fertility, different alleles of the *spe-26* gene also exhibit differences in FB length. Our initial hypothesis was that defects in FB length would inversely correlate with spermatid production. Our data did not support this hypothesis. Instead, we observed the longest FBs in *eb8*, which has spermatid production equivalent to *it112*. Consequently, this data suggests that defects in *spe-26* mutants cannot be attributed completely to defects in FB length.

Two other possibilities remain, however, that would explain the defects we observed. In one model, SPE-26 is required for diverse cellular functions, including regulating proper FB length. In this case, the large FBs in *spe-26* spermatocytes do not contribute to the other observed phenotypic defects. In a second model, the various phenotypic defects may arise independently but abnormalities such as large FBs interfere with other cellular processes and further exacerbate the various mutant defects. In the latter model, FBs might cause problems with microtubule attachment, which would be

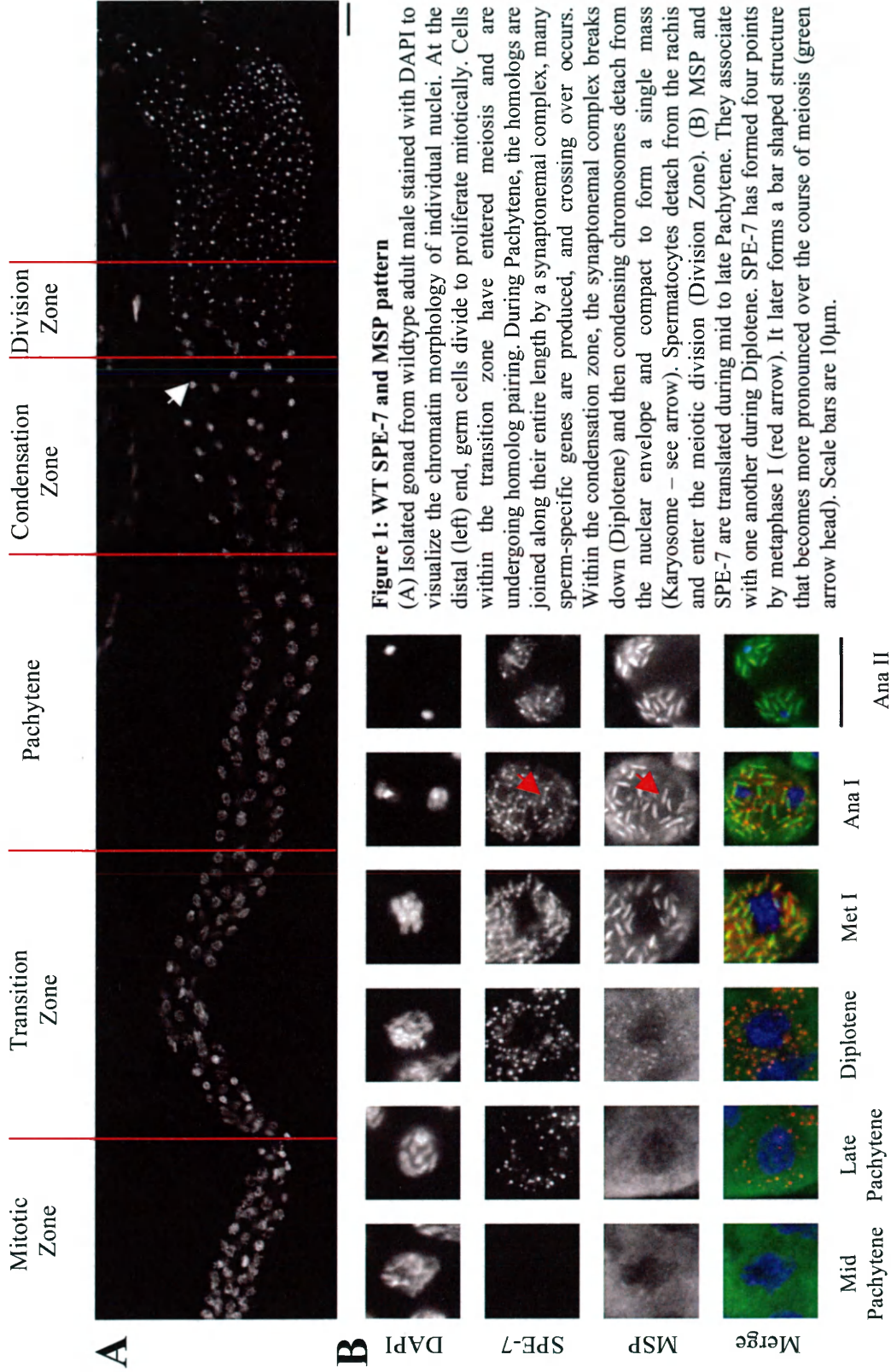
more pronounced in smaller cells and might explain the plethora of defects in Anaphase II that were observed in *it112* and *hc138*. Alternatively, larger FBs could make it more difficult to undergo cytokinesis correctly, because they protrude too far. To test these different hypotheses, we intend to future explore the nature of MT defects that were observed in the original paper and determine whether MTs appear to be influenced by FBs. In addition, we also intend to look to at actin defects that might explain problems with cytokinesis.

A core unanswered question that underlies this study, however, is the nature of the *SPE-26* protein. Although it has been identified as kelch-like protein, its precise function remains unknown and cannot be inferred because of the diversity of this protein superfamily. Kelch-like proteins have been identified which operate in processes as diverse as actin organization to galactose metabolism (Adams et al., 2000).

Consequently, one of the next steps in the study of these mutants will be to determine the WT localization of SPE-26 using immunofluorescence. Absent direct localization evidence, we can propose several functions for SPE-26 that would fit with the observed phenotypes. One possibility is that SPE-26 is directly or indirectly involved in transcription or translation. For instance, if SPE-26 were involved in chromatin condensation processes, then mutants would have abnormal transcript levels and affect a variety of cellular processes. In this model, mutants might synthesize too much MSP, resulting in large FBs. A second possibility is that SPE-26 is involved in actin dynamics related to spermatocytes detaching from the gonadal syncytium. In this scenario, SPE-26 would function similarly to KEL in *Drosophila*, which organizes the actin associated with oocyte ring canals (Robinson & Cooley, 1997; Xue & Cooley, 1993). Defects in this

structure could result in late budding from the gonadal syncytium, potentially delaying entry into the meiotic division phase and prolonging transcription and translation.

Figures



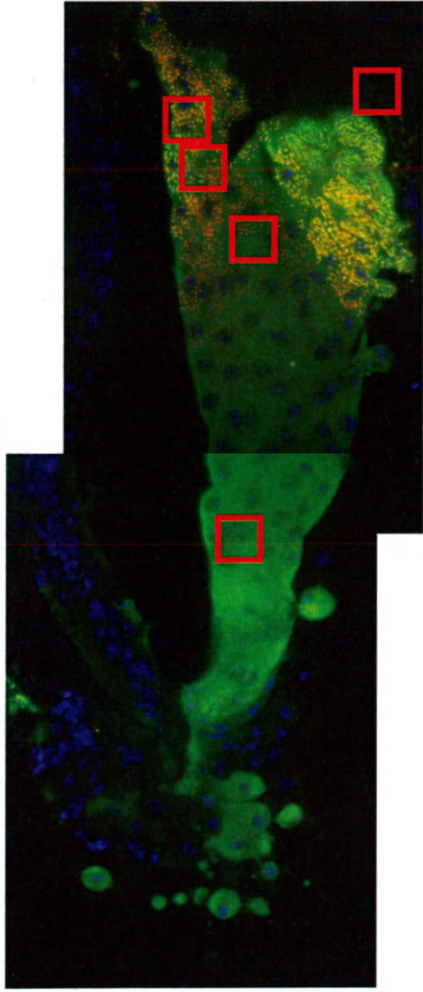
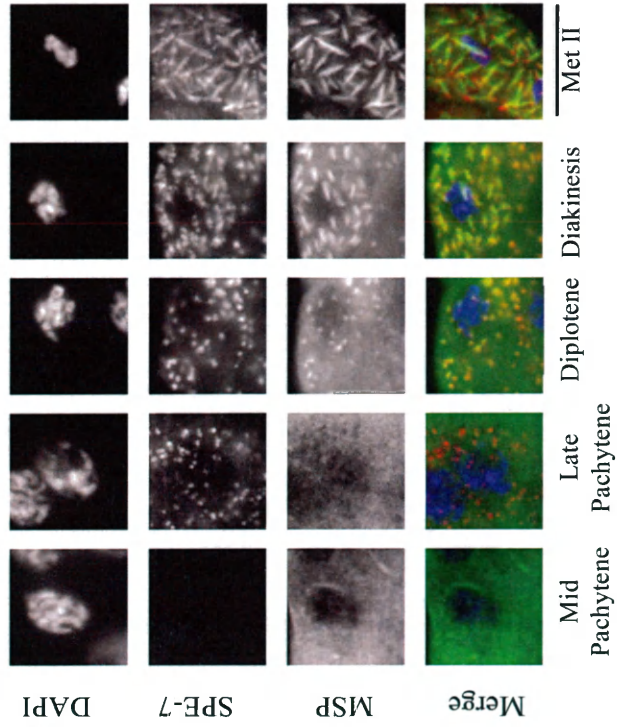


Figure 2: SPE-7 and MSP pattern in *spe-26(hc140)*

(A) Whole gonad stained for MSP (green), SPE-7 (red) and DAPI (blue) in *spe-26 (hc140)*. MSP turn on appears typical. (B) Enlarged cells from (A - red boxes). Early SPE-7 and MSP patterns in *spe-26 (hc140)* appear normal, but become markedly abnormal by Anaphase I.



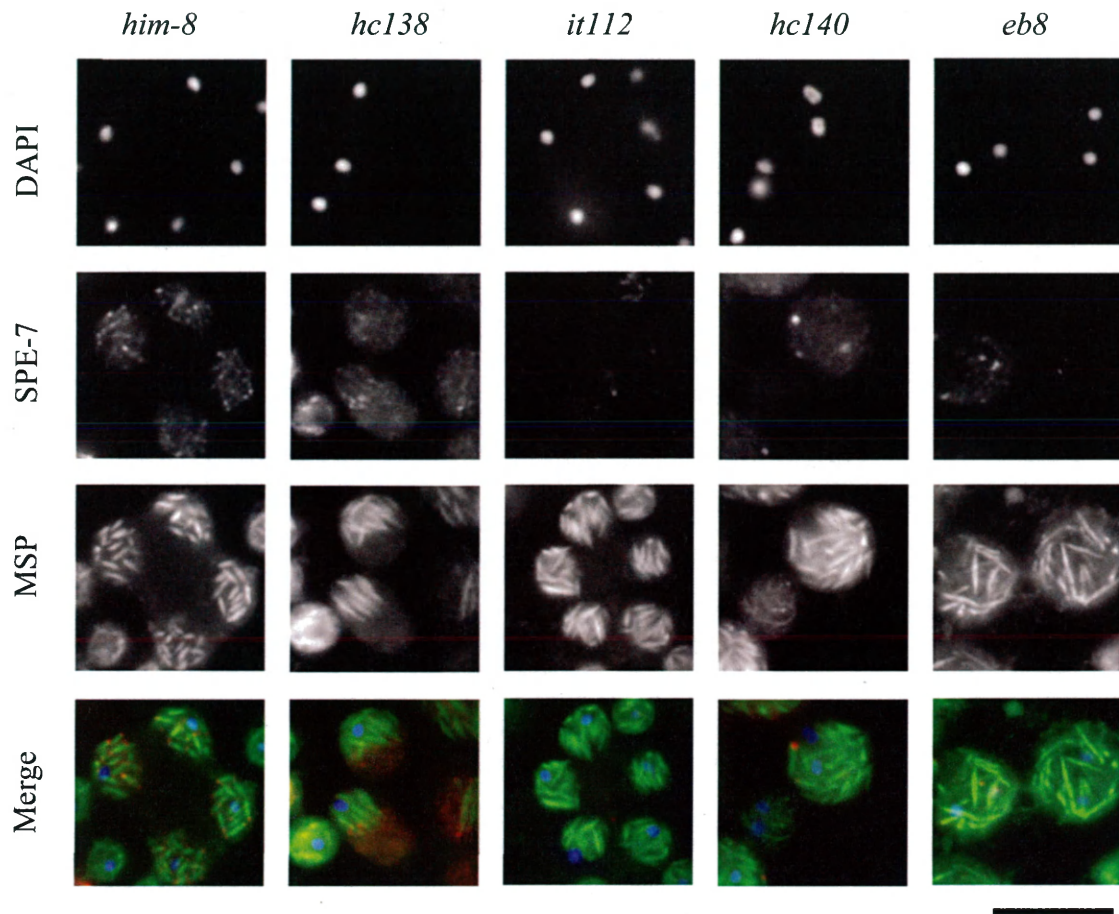


Figure 3: Comparison of maximally sized FBs in different *spe-26* alleles
MSP (green) and SPE-7 (red) labeled in each of the four *spe-26* alleles to visualize FB morphology. Images are of cells with FBs at the maximal size that was observed in each allele. Scale bars are 10 μ m.

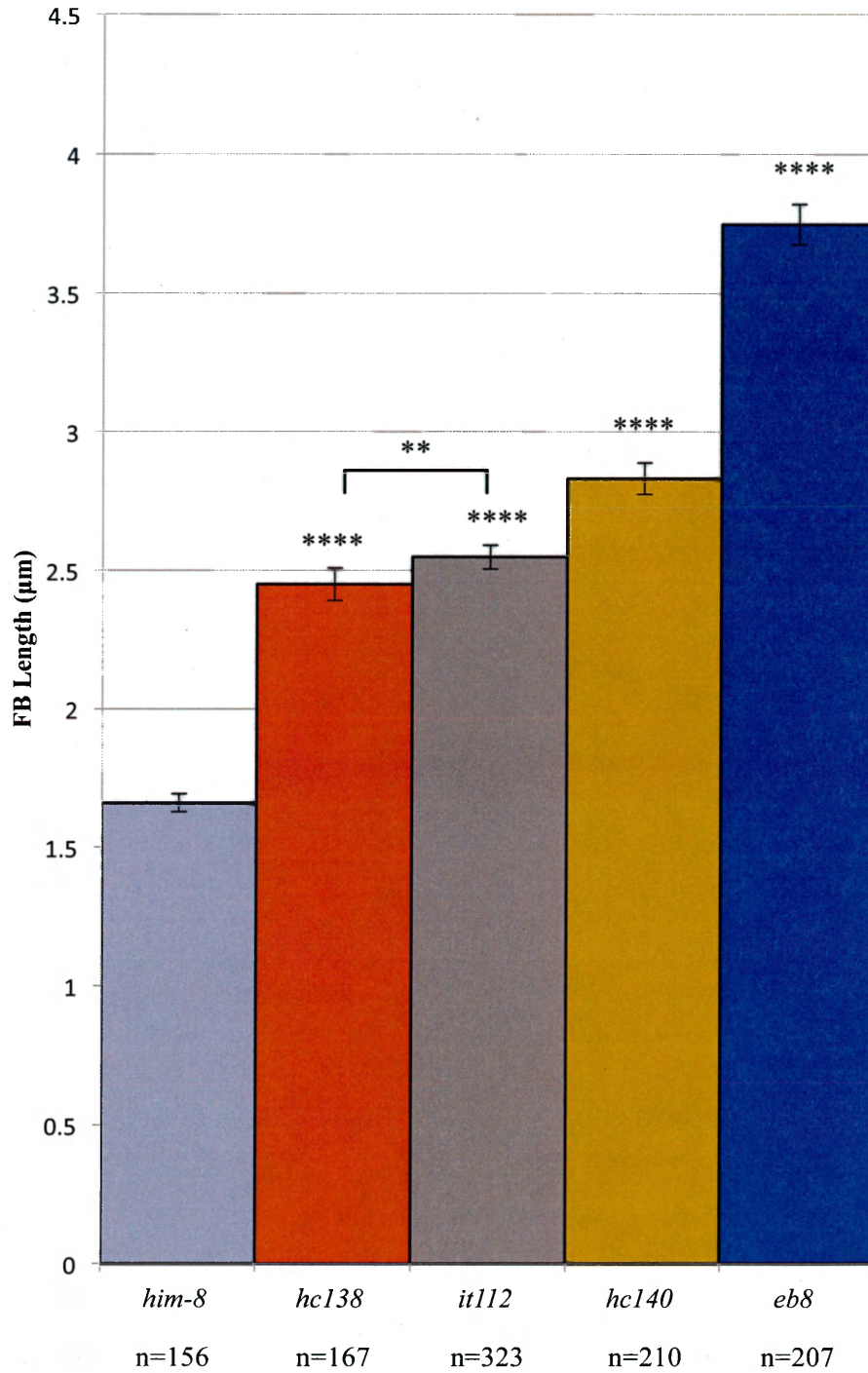


Figure 4: A comparison of average FB length between WT and *spe-26* alleles. FBs were measured in WT and *spe-26* alleles. n-values refer to the number of FBs measured. FBs were measured from 7-13 worms. Statistical significance was calculated using an unpaired, two-tailed t-test. Error bars correspond to the 95% confidence interval. When compared to WT and each other, all alleles are significant to $P < 0.0001$, except when comparing *it112* and *hc138* which are significant to $P < 0.01$. $P < 0.05$ (*); $P < 0.01$ (**); $P < 0.001$ (***) ; $P < 0.0001$ (****)

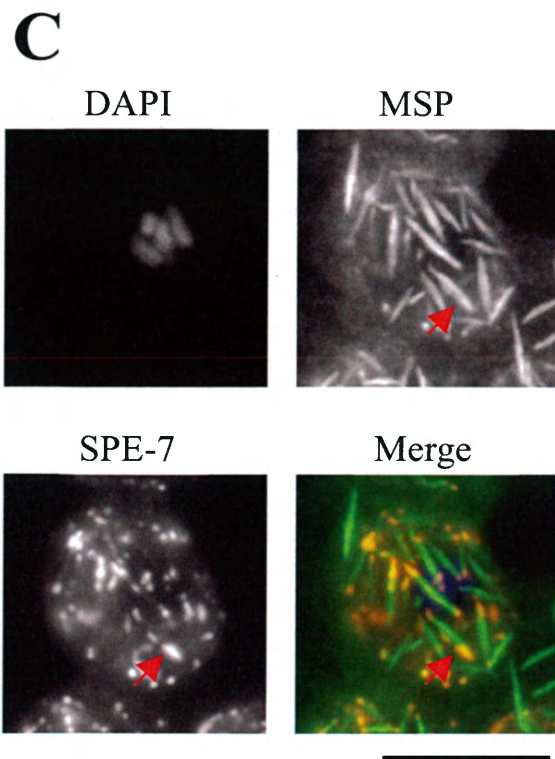
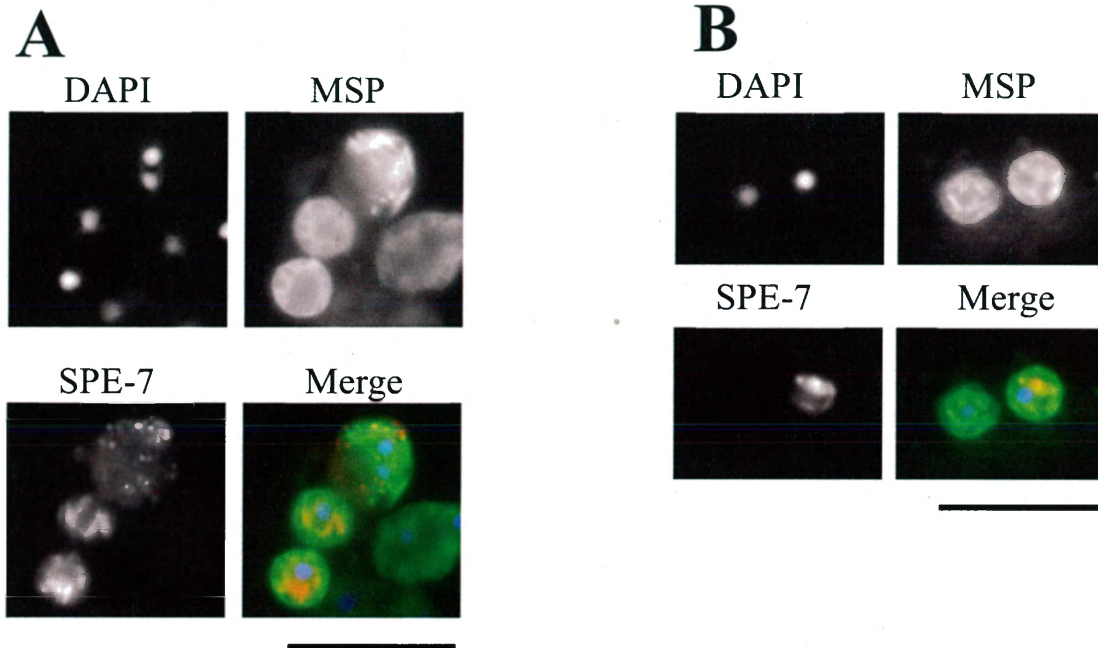


Figure 5: Visualization of novel SPE-7 patterns in *spe-26* mutants

(A) Cells from *spe-26 (it112)* labeled with SPE-7 (red), MSP (green) and DAPI (blue) that contain persistent SPE-7 structures. These structures were observed in all alleles (data not shown). (B) *spe-26 (it112)* spermatids. SPE-7 structures are not observed in every spermatid. (D) Arrested spermatocytes in *spe-26 (eb8)* mutants. SPE-7 appears to form larger but variably sized masses (arrows) that sometimes coat FBs. Similar patterns were observed in *spe-26 (hc140)* (data not shown). Scale bars are 10µm.

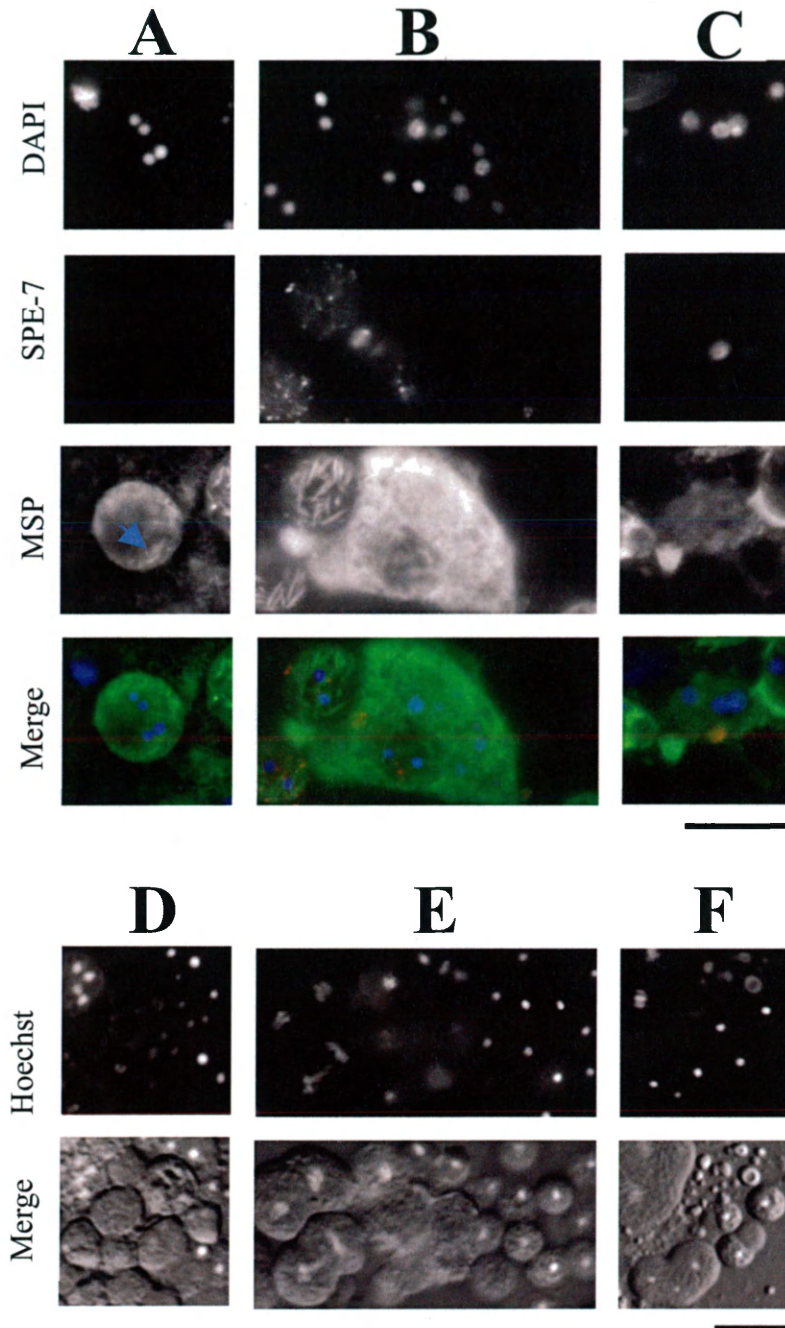
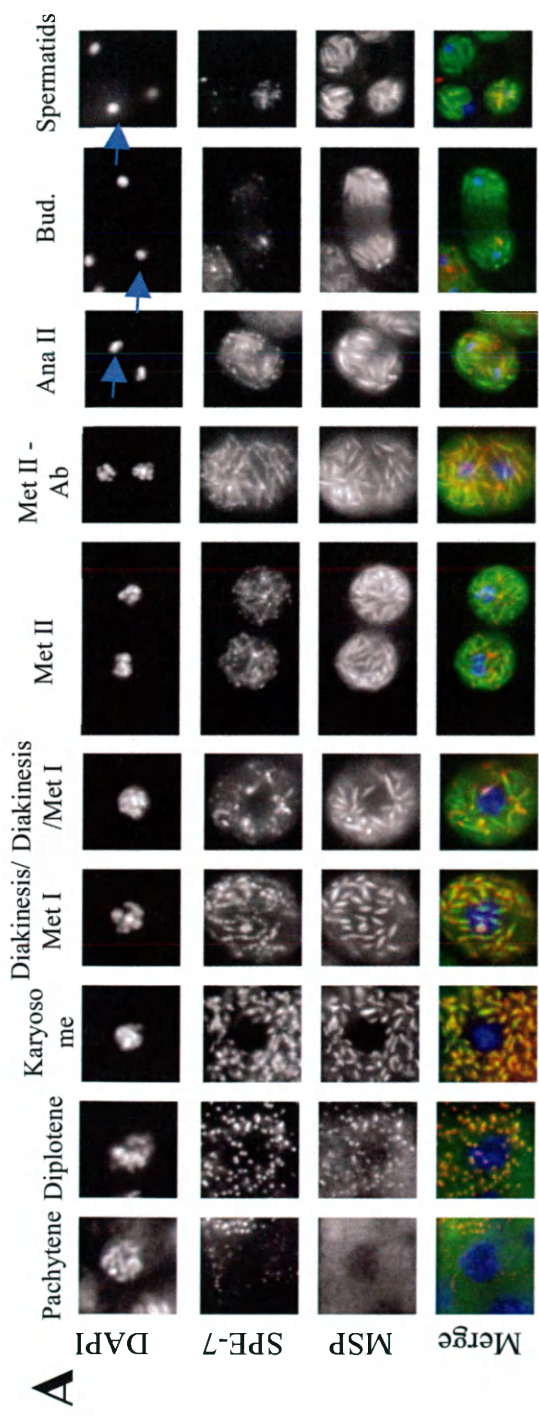


Figure 6: Terminal phenotype in *spe-26* mutants

(A) Cells with cytosolic MSP (green), no SPE-7 (red) and condensed chromatin (blue) were found in all alleles. Strands of polymerized MSP can also be seen (arrow) (B-C) Diffuse MSP patches with multiple chromatin masses (D) DIC images of intact cells with decondensed chromatin. (E) Lysed cells that weakly stain with Hoechst and likely correspond to the cells seen in (B). (F) Decondensed chromatin without a cell membrane (arrows). Scale bars are 10 μm



B

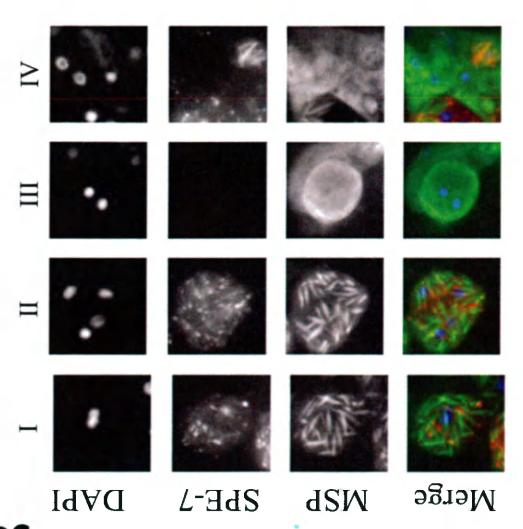


Figure 7: Spermatogenesis in *spe-26 (tit112)*
 (A) Panel of progressive stages in spermatogenesis in *spe-26 (tit112)*. Pachytene, Diplotene and Karyosome seem relatively unperturbed. By Diakinesis or Metaphase I, FBs have grown longer than in WT. Some cells transition from Anaphase I to Metaphase II with normal cytokinesis, but some exhibit incomplete cytokinesis (see Met II - Ab). Chromatin condensation events that occur during and following Anaphase II appear unperturbed (blue arrows). FBs in some Anaphase II cells appear to be disorganized. Lastly, FB orientation in spermatids was inconsistent. (B) Terminal phenotypes that result from abnormal meiotic divisions. In some cases, cells with multiple chromatin masses are observed (I-IV). Ring-shaped chromatin was also common and always co-occurred with cytosolic MSP IV).

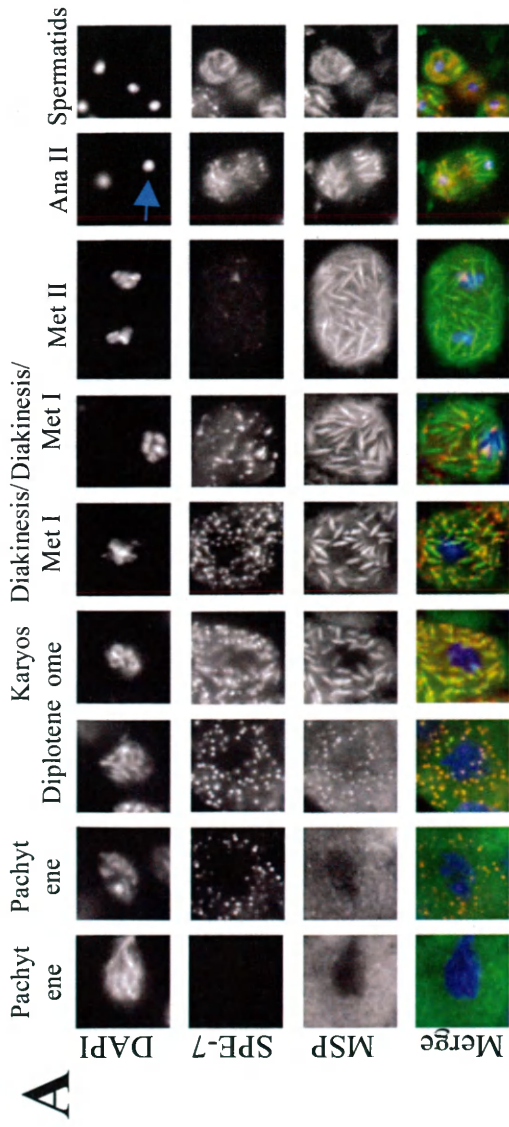
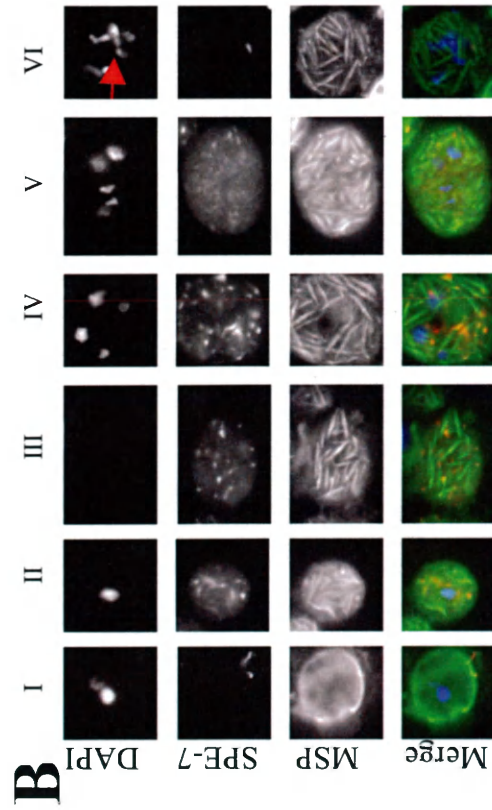


Figure 8: Spermatogenesis in *spe-26 (eb8)*
 (A) Panel of progressive stages in spermatogenesis in *spe-26 (it112)*. Pachytene, Diplotene seem relatively unperturbed. Karyosome nuclei appear less decondensed than in WT. By Diakinesis or Metaphase I, FBs have grown longer than WT. Cells rarely transition to Metaphase II with correct cytokinesis. Sometimes, the SPE-7 pattern was unusually dim by Metaphase II. In some cells, Anaphase II appears relatively normal with correctly hypercondensed chromatin (blue arrows).
 (B) Terminal phenotypes that result from abnormal meiotic divisions are more severe than *spe-26 (it112)*. Abnormally large cells with single or double chromatin masses are common (I, II). In some cases (III), anucleate cells are observed. Multiple chromatin masses with abnormal morphology are common (IV, V). Chromatin bridges are also present in many cells (VI, red arrow)



References

- Adams, J., Kelso, R., & Cooley, L. (2000). The kelch repeat superfamily of proteins: Propellers of cell function. *Trends in Cell Biology*, *10*(1), 17-24. doi:S0962-8924(99)01673-6 [pii]
- Blom, N., Gammeltoft, S., & Brunak, S. (1999). Sequence and structure-based prediction of eukaryotic protein phosphorylation sites. *Journal of Molecular Biology*, *294*(5), 1351-1362. doi:10.1006/jmbi.1999.3310
- Brenner, S. (1974). The genetics of caenorhabditis elegans. *Genetics*, *77*(1), 71-94.
- Buttery, S. M., Ekman, G. C., Seavy, M., Stewart, M., & Roberts, T. M. (2003a). Dissection of the ascaris sperm motility machinery identifies key proteins involved in major sperm protein-based amoeboid locomotion. *Molecular Biology of the Cell*, *14*(12), 5082-5088. doi:10.1091/mbc.E03-04-0246 [doi]
- Chatterjee, I., Richmond, A., Putiri, E., Shakes, D. C., & Singson, A. (2005). The caenorhabditis elegans spe-38 gene encodes a novel four-pass integral membrane protein required for sperm function at fertilization. *Development (Cambridge, England)*, *132*(12), 2795-2808. doi:132/12/2795 [pii]
- Chu, D. S., Liu, H., Nix, P., Wu, T. F., Ralston, E. J., Yates, J. R., 3rd, & Meyer, B. J. (2006). Sperm chromatin proteomics identifies evolutionarily conserved fertility factors. *Nature*, *443*(7107), 101-105. doi:nature05050 [pii]
- Chu, D. S., & Shakes, D. C. (2013). Spermatogenesis. *Advances in Experimental Medicine and Biology*, *757*, 171-203. doi:10.1007/978-1-4614-4015-4_7

- Church, D. L., Guan, K. L., & Lambie, E. J. (1995). Three genes of the MAP kinase cascade, mek-2, mpk-1/sur-1 and let-60 ras, are required for meiotic cell cycle progression in *Caenorhabditis elegans*. *Development (Cambridge, England)*, *121*(8), 2525-2535.
- del Castillo-Olivares, A., & Smith, H. E. (2008). Critical contact residues that mediate polymerization of nematode major sperm protein. *Journal of Cellular Biochemistry*, *104*(2), 477-487. doi:10.1002/jcb.21636
- Dyson, H. J., & Wright, P. E. (2005). Intrinsically unstructured proteins and their functions. *Nature Reviews. Molecular Cell Biology*, *6*(3), 197-208.
- Gnad, F., Ren, S., Cox, J., Olsen, J., Macek, B., Oroshi, M., & Mann, M. (2007). PHOSIDA (phosphorylation site database): Management, structural and evolutionary investigation, and prediction of phosphosites. *Genome Biology*, *8*(11), R250.
- Govin, J., Caron, C., Lestrat, C., Rousseaux, S., & Khochbin, S. (2004). The role of histones in chromatin remodelling during mammalian spermiogenesis. *European Journal of Biochemistry / FEBS*, *271*(17), 3459-3469. doi:10.1111/j.1432-1033.2004.04266.x [doi]
- Grant, R. P., Buttery, S. M., Ekman, G. C., Roberts, T. M., & Stewart, M. (2005a). Structure of MFP2 and its function in enhancing MSP polymerization in *Ascaris* sperm amoeboid motility. *Journal of Molecular Biology*, *347*(3), 583-595. doi:S0022-2836(05)00099-9 [pii]
- Haaf, A., Butler, P. J., Kent, H. M., Fearnley, I. M., Roberts, T. M., Neuhaus, D., & Stewart, M. (1996). The motile major sperm protein (MSP) from *Ascaris suum* is a symmetric dimer in solution. *Journal of Molecular Biology*, *260*(2), 251-260. doi:S0022283696903964 [pii]
- Kimble, J., & Crittenden, S. L. (2005). Germline proliferation and its control. *WormBook : The Online Review of C.Elegans Biology*, , 1-14. doi:10.1895/wormbook.1.13.1 [doi]

- Kimmins, S., Kotaja, N., Davidson, I., & Sassone-Corsi, P. (2004). Testis-specific transcription mechanisms promoting male germ-cell differentiation. *Reproduction (Cambridge, England)*, *128*(1), 5-12. doi:10.1530/rep.1.00170 [doi]
- King, K. L., Stewart, M., & Roberts, T. M. (1994). Supramolecular assemblies of the ascaris suum major sperm protein (MSP) associated with amoeboid cell motility. *Journal of Cell Science*, *107 (Pt 10)*(Pt 10), 2941-2949.
- Kiontke, K., & Fitch, D. H. (2005). The phylogenetic relationships of caenorhabditis and other rhabditids. *WormBook : The Online Review of C.Elegans Biology*, , 1-11. doi:10.1895/wormbook.1.11.1 [doi]
- Kosinski, M., McDonald, K., Schwartz, J., Yamamoto, I., & Greenstein, D. (2005a). C. elegans sperm bud vesicles to deliver a meiotic maturation signal to distant oocytes. *Development (Cambridge, England)*, *132*(15), 3357-3369. doi:dev.01916 [pii]
- Kulkarni, M., Shakes, D. C., Guevel, K., & Smith, H. E. (2012). SPE-44 implements sperm cell fate. *PLoS Genetics*, *8*(4), e1002678. doi:10.1371/journal.pgen.1002678 [doi]
- LeClaire, L. L., 3rd, Stewart, M., & Roberts, T. M. (2003). A 48 kDa integral membrane phosphoprotein orchestrates the cytoskeletal dynamics that generate amoeboid cell motility in ascaris sperm. *Journal of Cell Science*, *116*(Pt 13), 2655-2663. doi:10.1242/jcs.00469 [doi]
- L'Hernault, S. W. (2006). Spermatogenesis. *WormBook : The Online Review of C.Elegans Biology*, , 1-14. doi:10.1895/wormbook.1.85.1 [doi]
- Messina, K. (2012). *SPE-7, A novel regulator of MSP assembly in C. elegans Spermatocytes*. (Unpublished Biology M.S.). College of William and Mary,

Miller, M. A., Nguyen, V. Q., Lee, M., Kosinski, M., Schedl, T., Caprioli, R. M., & Greenstein, D. (2001). A sperm cytoskeletal protein that signals oocyte meiotic maturation and ovulation. *Science*, *291*(5511), 2144-2147. doi:10.1126/science.1057586

Muhlrad, P. J., & Ward, S. (2002). Spermiogenesis initiation in caenorhabditis elegans involves a casein kinase 1 encoded by the spe-6 gene. *Genetics*, *161*(1), 143-155.

Nishimura, H., & L'Hernault, S. W. (2010a). Spermatogenesis-defective (spe) mutants of the nematode caenorhabditis elegans provide clues to solve the puzzle of male germline functions during reproduction. *Developmental Dynamics : An Official Publication of the American Association of Anatomists*, *239*(5), 1502-1514. doi:10.1002/dvdy.22271 [doi]

Omary, M. B., Ku, N. O., Tao, G. Z., Toivola, D. M., & Liao, J. (2006). "Heads and tails" of intermediate filament phosphorylation: Multiple sites and functional insights. *Trends in Biochemical Sciences*, *31*(7), 383-394. doi:S0968-0004(06)00142-3 [pii]

Pollard, T. D., Blanchoin, L., & Mullins, R. D. (2000). Molecular mechanisms controlling actin filament dynamics in nonmuscle cells. *Annual Review of Biophysics and Biomolecular Structure*, *29*, 545-576. doi:29/1/545 [pii]

Presler, M. (2010). *A novel C. elegans gene interfaces cell cycle and development in spermatogenesis*. (Unpublished Biology B.S. with Honors). College of William and Mary,

Revenu, C., Athman, R., Robine, S., & Louvard, D. (2004). The co-workers of actin filaments: From cell structures to signals. *Nature Reviews.Molecular Cell Biology*, *5*(8), 635-646. doi:10.1038/nrm1437 [doi]

- Roberts, T. M., Pavalko, F. M., & Ward, S. (1986a). Membrane and cytoplasmic proteins are transported in the same organelle complex during nematode spermatogenesis. *The Journal of Cell Biology*, *102*(5), 1787-1796. doi:10.1083/jcb.102.5.1787
- Robinson, D. N., & Cooley, L. (1997). Drosophila kelch is an oligomeric ring canal actin organizer. *The Journal of Cell Biology*, *138*(4), 799-810.
- Rodriguez, M. A., LeClaire, L. L., 3rd, & Roberts, T. M. (2005). Preparing to move: Assembly of the MSP amoeboid motility apparatus during spermiogenesis in ascaris. *Cell Motility and the Cytoskeleton*, *60*(4), 191-199. doi:10.1002/cm.20058 [doi]
- Roy, A., Kucukural, A., & Zhang, Y. (2010). I-TASSER: A unified platform for automated protein structure and function prediction. *Nature Protocols*, *5*(4), 725-738. doi:10.1038/nprot.2010.5 [doi]
- Sassone-Corsi, P. (2002). Unique chromatin remodeling and transcriptional regulation in spermatogenesis. *Science (New York, N.Y.)*, *296*(5576), 2176-2178. doi:10.1126/science.1070963 [doi]
- Scott, A. L. (1996). Nematode sperm. *Parasitology Today (Personal Ed.)*, *12*(11), 425-430. doi:0169475896100636 [pii]
- Sepsenwol, S., Ris, H., & Roberts, T. M. (1989a). A unique cytoskeleton associated with crawling in the amoeboid sperm of the nematode, ascaris suum. *The Journal of Cell Biology*, *108*(1), 55-66.
- Shakes, D. C., & Ward, S. (1989). Initiation of spermiogenesis in *C. elegans*: A pharmacological and genetic analysis. *Developmental Biology*, *134*(1), 189-200. doi:0012-1606(89)90088-2 [pii]

- Shakes, D. C., Wu, J. C., Sadler, P. L., Laprade, K., Moore, L. L., Noritake, A., & Chu, D. S. (2009a). Spermatogenesis-specific features of the meiotic program in *caenorhabditis elegans*. *PLoS Genetics*, *5*(8), e1000611. doi:10.1371/journal.pgen.1000611 [doi]
- Stanfield, G. M., & Villeneuve, A. M. (2006). Regulation of sperm activation by SWM-1 is required for reproductive success of *C. elegans* males. *Current Biology : CB*, *16*(3), 252-263. doi:S0960-9822(06)01024-4 [pii]
- Varkey, J. P., Jansma, P. L., Minniti, A. N., & Ward, S. (1993a). The *caenorhabditis elegans* spe-6 gene is required for major sperm protein assembly and shows second site non-complementation with an unlinked deficiency. *Genetics*, *133*(1), 79-86.
- Varkey, J. P., Muhlrud, P. J., Minniti, A. N., Do, B., & Ward, S. (1995). The *caenorhabditis elegans* spe-26 gene is necessary to form spermatids and encodes a protein similar to the actin-associated proteins kelch and scruin. *Genes & Development*, *9*(9), 1074-1086.
- Ward, S., Argon, Y., & Nelson, G. A. (1981). Sperm morphogenesis in wild-type and fertilization-defective mutants of *caenorhabditis elegans*. *The Journal of Cell Biology*, *91*(1), 26-44.
- Wu, J. C., Go, A. C., Samson, M., Cintra, T., Mirsoian, S., Wu, T. F., . . . Chu, D. S. (2012). Sperm development and motility are regulated by PP1 phosphatases in *caenorhabditis elegans*. *Genetics*, *190*(1), 143-157. doi:10.1534/genetics.111.135376 [doi]
- Xue, F., & Cooley, L. (1993). Kelch encodes a component of intercellular bridges in *drosophila* egg chambers. *Cell*, *72*(5), 681-693. doi:0092-8674(93)90397-9 [pii]
- Yi, K., Buttery, S. M., Stewart, M., & Roberts, T. M. (2007a). A ser/thr kinase required for membrane-associated assembly of the major sperm protein motility apparatus in the

amoeboid sperm of ascaris. *Molecular Biology of the Cell*, 18(5), 1816-1825. doi:E06-08-0741 [pii]

Yi, K., Wang, X., Emmett, M. R., Marshall, A. G., Stewart, M., & Roberts, T. M. (2009a).

Dephosphorylation of major sperm protein (MSP) fiber protein 3 by protein phosphatase 2A during cell body retraction in the MSP-based amoeboid motility of ascaris sperm. *Molecular Biology of the Cell*, 20(14), 3200-3208. doi:10.1091/mbc.E09-03-0240

Yi, K., Buttery, S. M., Stewart, M., & Roberts, T. M. (2007b). A ser/thr kinase required for

membrane-associated assembly of the major sperm protein motility apparatus in the amoeboid sperm of ascaris. *Molecular Biology of the Cell*, 18(5), 1816-1825.

doi:10.1091/mbc.E06-08-0741

Zhang, Y. (2008). I-TASSER server for protein 3D structure prediction. *BMC Bioinformatics*,

9(1), 40.